CAPITAL UNIVERSITY OF SCIENCE AND TECHNOLOGY, ISLAMABAD

Organic Dye Based Opto-Electronic Devices and Sensors

by

Noshin Fatima

A thesis submitted in partial fulfillment for the
degree of Doctor of Philosophy

in the

Faculty of Engineering
Department of Electrical Engineering

2018

Organic Dye Based Opto-Electronic Devices and Sensors

By

Noshin Fatima

(DEE151007)

Dr. Hüseyin Derin

Department of Physics, Adnan Menderes University, Aydin, Turkey

Dr. Hong Meng

School of Advanced Materials, Peking University, Shenzhen, China

Dr. M. Mansoor Ahmed

(Thesis Supervisor)

Dr. Khasan S. Karimov

(Thesis Co-Supervisor)

Dr. Noor Muhammad Khan

(Head, Department of Electrical Engineering)

Dr. Imtiaz Ahmed Taj

(Dean, Faculty of Engineering)

DEPARTMENT OF ELECTRICAL ENGINEERING

CAPITAL UNIVERSITY OF SCIENCE AND TECHNOLOGY

ISLAMABAD

2018

Copyright © 2018 by Ms. Noshin Fatima

To my Beloved Family and Respected Supervisors

CERTIFICATE OF APPROVAL

This is to certify that the research work presented in the thesis, entitled "**Organic Dye Based Opto-Electronic Devices and Sensors**" was conducted under the supervision of **Dr. Muhammad Mansoor Ahmed**. No part of this thesis has been submitted anywhere else for any other degree. This thesis is submitted to the **Department of Electrical Engineering, Capital University of Science and Technology** in partial fulfillment of the requirements for the degree of Doctor in Philosophy in the field of **Electrical Engineering**. The open defence of the thesis was conducted on **April 18, 2018**.

Student Name: Ms. Noshin Fatima (DEE151007)

The Examining Committee unanimously agrees to award PhD degree in the mentioned field.

Examination Committee :

(a)	External Examiner 1:	Dr. Ashraf Ali Professor GIK Institute, Topi
(b)	External Examiner 2:	Dr. Arshad Saleem Bhatti Professor CIIT, Islamabad
(c)	Internal Examiner :	Dr. Muhammad Ashraf Associate Professor CUST, Islamabad

Supervisor Name : Dr. Muhammad Mansoor Ahmed
Professor
CUST, Islamabad

Name of HoD : Dr. Noor Muhammad Khan
Professor
CUST, Islamabad

Name of Dean : Dr. Imtiaz Ahmad Taj
Professor
CUST, Islamabad

PLAGIARISM UNDERTAKING

I solemnly declare that research work presented in the thesis titled **"Organic Dye Based Opto-Electronic Devices and Sensors"** is solely my research work with no significant contribution from any other person. Small contribution/ help wherever taken has been duly acknowledged and that complete thesis has been written by me.

I understand the zero tolerance policy of the HEC and Capital University of Science and Technology towards plagiarism. Therefore, I as an author of the above titled thesis declare that no portion of my thesis has been plagiarized and any material used as reference is properly referred/ cited.

I undertake that if I am found guilty of any formal plagiarism in the above titled thesis even after award of PhD Degree, the University reserves the right to withdraw/ revoke my PhD degree and that HEC and the University have the right to publish my name on the HEC/ University Website on which names of students are placed who submitted plagiarized thesis.

Noshin

(Ms. Noshin Fatima)

Dated: 18   April, 2018   Registration No. DEE151007

AUTHOR'S DECLARATION

I, **Ms. Noshin Fatima (Registration No. DEE-151007)**, hereby state that my PhD thesis titled, **'Organic Dye Based Opto-Electronic Devices and Sensors'** is my own work and has not been submitted previously by me for taking any degree from Capital University of Science and Technology, Islamabad or anywhere else in the country/ world.

At any time, if my statement is found to be incorrect even after my graduation, the University has the right to withdraw my PhD Degree.

(Ms. Noshin Fatima)

Dated: 18 April, 2018

Registration No : DEE151007

List of Publications

It is certified that following publication(s) have been made out of the research work that has been carried out for this thesis:-

Journal Papers

1. **N. Fatima**, M. M. Ahmed and Kh S. Karimov, "Effects of humidity and temperature on orange dye based organic field effect transistors fabricated at different gravity," *Journal of Electronic Materials*, pp. 1-7, 2017.

2. **N. Fatima**, M. M. Ahmed, Kh. S. Karimov, Z. Ahmad and F. F. Muhammad, "Optical sensors based on the NiPc-CoPc composite films deposited by drop casting and under the action of centrifugal force," *Chinese Physics B*, vol. 26, pp. 060704, 2017.

3. **N. Fatima**, F. Aziz, Z. Ahmad, M. A. Najeeb, M. I. Azmeer, Kh S. Karimov, M. M. Ahmed, S. Bashir, R. A. Shakoor, and K. Sulaiman, "Compositional engineering of the pi-conjugated small molecular VOPcPhO: Alq$_3$ complex to boost humidity sensing," *RSC Advances*, vol. 7, pp. 25621-25621, 2017.

4. Q. Zafar, **N. Fatima**, Kh. S. Karimov, M. M. Ahmed, and K. Sulaiman, "Realizing broad-bandwidth visible wavelength photodiode based on solution processed ZnPc/PC$_{71}$BM dyad," *RSC Advances*, vol. 7, pp. 131-136, 2017.

5. Kh. S. Karimov, Z. Ahmad, **N. Fatima**, M. M. Ahmad and M. Abid, "Effect of humidity on copper phthalocyanine films deposited at different gravity conditions," *Pigment and Resin Technology*, vol. 46, pp. 64-70, 2017.

6. Kh. S. Karimov, M. M. Ahmed, **N. Fatima**, M. Saleem, M. M. Tahir, S. A. Moiz, Kh. M. Akhmedov, M. Zahid, S. Z. Abbas, and A. Rashid, "Nickel phthalocyanine based organic photo transistor: effect of semiconductor film thickness," *The European Physical Journal Applied Physics*, vol. 72, pp. 20202, 2015.

Conference Proceedings

1. **N. Fatima**, M. M. Ahmed, Kh. S. Karimov, Kh. M. Akhmedov, "Humidity effect on organic semiconductor NiPc films deposited at different gravity conditions," *Materials Science and Engineering*, vol. 164, pp. 012035, 2016.

2. **N. Fatima**, M. M. Ahmed and Kh S. Karimov, "Effect of heating on the impedance of NiPc based organic field effect transistor," *Proceedings of the 2016 International Conference on Industrial Engineering and Operations Management*, pp. 2667-2674, Kuala Lumpur, Malaysia, 2016.

Ms. Noshin Fatima

(DEE151007)

Acknowledgements

All praise to Almighty ALLAH who has been bestowing me with his great bounties and enabled me to complete my dissertation.

I would like to express my gratitude to my supervisor Prof. Dr. Muhammad Mansoor Ahmed, Vice-Chancellor, Capital University of Science and Technology (CUST), Islamabad, and co-supervisor Prof. Dr. Khasan Sanginovich Karimov, Ghulam Ishaq Khan Institute of Science and Technology (GIKI), Swabi, who have supported me throughout my topic selection, experimental work, paper and thesis writing with patience and knowledge whilst allowing me in the laboratory to work in Pakistan as well as in Malaysia. I attribute the level of my PhD degree to their encouragement and efforts. Without them, this research work would not have been completed. I am very much competent due to their support from initial to final stage, and every day they make several discussions and explain things in practical way, which deepen my knowledge.

I would like to thank my family for their discussion, effective comments, financial and moral support, and they are always a source of motivation for me. I would not have reached this stage but with the prayers, love, and moral support of my parents.

Thanks to Dr. Khula Sulaman for allowing me to do my research at Malaya University, Malaysia. I would also like to thank FMSC and FEE departments for allowing me to do research work at GIKI, Swabi, Pakistan. Thanks are also due to Dr. Fakhra Aziz, Dr. Qayyum Zafar, Dr. Zubair Ahmed, Dr. Mansoor Ani, Dr. Tahseen Amin Khan Qasuria, Mr. Umair Rafique and all other well-wishers for their support.

Abstract

Organic semiconductors have been the subject of intense scientific investigation for the past 50 years. Applications of these materials include chemical, physical and biological sensors, electronic, and photonic devices. Low cost production of these devices is possible by using thermal evaporation, centrifugation, spin coating and drop casting technologies. This thesis describes fabrication and characterization of organic semiconductor sensors for temperature, humidity and light measurements using novel organic materials. Different types of commercially available organic dyes have been used as active materials to fabricate sensors.

In the first part of the thesis, humidity sensors have been fabricated using CuPc/NiPc thin films deposited by drop casting and centrifugation. Another type of humidity sensor based on VOPcPhO, Alq_3 and their composites have also been fabricated by spin coating technique, wherein organic films have been grown over a substrate having pre-fabricated aluminum electrodes. Optimum ratio of VOPcPhO and Alq_3 has been identified to achieve best capacitive and resistive response of the sensor.

In the second part, optical sensors from composite films of NiPc:CoPc (1:1) have been fabricated by drop casting and centrifugation on a ceramic alumina substrate having surface-type interdigitated Ag electrodes. Variation in impedance and capacitance w.r.t. illumination have been measured. Another type of optical sensors based on organic photodiodes (OPDs), using composite $ZnPc:PC_{71}BM$ dye, have been fabricated and characterized. The optimum ratio of $ZnPc:PC_{71}BM$ (1:0.8) has been determined by detecting photocurrent density with respect to varied illumination levels of impinging light at different reverse biased conditions of the optical sensors. Moreover, the light to dark current density ratio (J_{ph}/J_d) of the devices has been evaluated along with the transient photo-current density response to assess their sensitivity.

In the third part, organic field effect transistors (OFETs) functioning as temperature/humidity senors (referred to as multi-functional sensors) have been fabricated

using orange dye (OD) and its composite OD:sugar at positive (+1 g) and negative (-1 g) gravities by drop casting. It has been observed that in drop casting method, properties of OFET sensors are dependent upon gravity as well as solution composition employed for OFETs channel definition.

Additionally, OFETs have been fabricated by depositing NiPc of varying thickness (100-300 nm) and semi-transparent thin films of aluminum in sequence by vacuum evaporation on a glass substrate having silver source and drain electrodes. It has been observed that the drain current of OFETs increases with increase in radiation intensity, and the OFETs having 200 nm thick NiPc film, exhibited better performance compared to 100 nm and 300 nm thick films. For temperature evaluation, it has been noticed that the reduction in the impedance is higher when thickness of the film is decreased. It has also been demonstrated that for improved performance, as a temperature sensor, the OFET channel film should be $\sim$100 nm.

Contents

List of Figures

List of Tables

Abbreviations

A	Acceptor
AFM	Atomic force microscopy
Al	Aluminium
Alq$_3$	Tris-(8-hydroxyquinoline)aluminum
CDs	Compact discs
CNTs	Carbon nanotubes
CoPc	Cobalt phthalocyanine
CuPc	Copper phthalocyanine
D	Donner
DI	De-ionized
EA	Electron affinity
FESEM	Field emission scanning electron microscope
GaAs	Gallium arsenide
Ge	Germanium
HOMO	Highly occupied molecular orbital
IE	Ionization energy
ITO	Indium tin oxide
I-V	Current-voltage
J-V	Density-voltage
LiF	Lithium fluoride
LUMO	Lowest unoccupied molecular orbital
M-S	Metal-semiconductor
MTR	Multiple trapping and thermal release
NiPc	Nickel phthalocyanine

NIR	Near-infrared
OD	Orange dye 25
OFET	Organic field fffect transistor
OMCs	Organic molecular crystals
OPD	Organic photo diode
OSC	Optically stimulated current
Pc	Phthalocyanine
PC$_{71}$BM	[6,6]-Phenyl-C$_{71}$−Butyric-acid Methyl ester
PDT	Photodynamic therapy
PEDOT	Poly(3,4-Ethylene Di-Oxy Thiophene)
PIA	Photo-induced absorption
PL	Photo luminescence
PSS	Poly styrene sulfonate
PVD	Physical vapor deposition
SCLC	Space charge limited current
SEM	Scanning electron microscopy
Si	Silicon
SMU	Source measure unit
TCLC	Trapped charge limited current
TCNQ	Tetra cyanoquinodimethane
TOF	Time-of-flight
TSC, TSL	Thermally stimulated current and luminescence
UV-Vis	Ultraviolet visible Spectroscopy
VOPcPhO	Vanadyl 2,9,16,23-tetraphenoxy-29H,31H-Phthalocyanine
ZnPc	Zinc phthalocyanine

Symbols

A_{eff}	Effective device area
a, b, γ	Fitting parameter
a_{eff}	Available channel
a_0	Ratio between DOS and concentration of traps
C	Capacitance
C_H	Capacitance under humid condition
C_n	Capacitance at normal conditions
d	Film thickness
d_m	Distance
E	Irradiation of the incident light
E_C	Conduction band energy
$E_{F_m}, E_{F_{SC}}$	Energy required to free an electron from metal's and semiconductor's fermi level
E_g	Energy gap
E_i, E_j	Energy states i and j
E_t	Energy difference between delocalized band edge and trap level
E_V	Valance band energy
F	Electric field
f	Fermi function
g	Gravity
g_m	Trans-conductance
H	Humidity
H_0	Initial humidity

I_1, I_2	Light on independent current source 1 and 2
I_3	Dependent current source
I_D	Drain current
I_{dd}, I_{di}	Drain current under dark and illumination conditions
I_{ph}	Drain current generated by light irradiation
J	Current density
J_d, J_{ph}	Dark and light current density
k	Boltzmann constant
N_n	Concentration of water molecules at normal condition
N_0	Pre-exponential factor
n	Free charge density
n_i	Carrier concentration
P	Optical power incident on the channel of the device
q	Electronic charge
qV_i	Work function difference between metal and semiconductor
qV_n	Fermi level difference between metal and semiconductor
$q\phi_{b_n}$	Barrier height
$q\phi_m, q\phi_{SC}$	Work function of metal and semiconductor
$q\chi$	Electron affinity
R	Resistance
R_{ij}	Distance between energy states i and j
R_0	Initial resistance
R_{res}	Responsivity
r	Radius
$r_{on/off}$	Ratio of photo (on) and dark (off) currents
S	Sensitivity
S_C, S_Z	Capacitance and impedance sensitivity
T	Temperature
V	Applied voltage
V_{bi}	Built-in potential
V_{DS}	Drain-to-source voltage

V_F, V_R	Forward and reverse bias voltages
Z	Impedance
α	Acceleration
α	Polarization
$\alpha_{dip}, \alpha_e, \alpha_i, \alpha_{tr}$	Dipole, electronic, ionic and transfer polarizabilities
β	Exponential factor
ε	Permittivity
ε_0	Permittivity of free space
ν_0	Electron-coupling term constant
μ	Mobility
μ_d	Drift mobility
μ_0	Mobility in the delocalized band
θ	Trapping factor
$\Delta C, \Delta R$	Changes in capacitance and resistance
ΔE	Activation energy
$\Delta RH, \Delta T, \Delta Z$	Change in relative humidity, temperature and impedance
ω	Angular velocity/circular frequency

Chapter 1

Introduction

In this chapter, an overview of organic semiconductor dyes is presented to show their promising potential for organic electronic industry to get reliable and reproducible sensors and transistors. An outline of the organic semiconductor dye materials is given along with their deposition techniques and electrical properties. Inspiration, motivation and intentions of the presented effort and the framework of the dissertation is also discussed.

1.1 Organic Semiconductors

The materials whose electrical conductivities and resistivities are sandwiched between insulators and metals are termed as semiconductors. The resistivity and conductivity of these materials can be altered extensively by varying their conditions such as, contamination level, such as, humidity, temperature and optical excitation. For the production of electronic devices, this tunability is of the at most importance [1, 2]. The organic semiconductor technology has attained more interest in recent years due to its low cost, light weight, elasticity and no high temperature process of fabrication. While there have been incredible advancements during the last era in organic electronics, still there is work to be done in the field of different sensing technologies, which is a back-bone of every equipment.

1.2   Organic Semiconductor Based Devices

Organic semiconductor materials offer many advantages, some of which are: low fabrication cost, wide area applications, and novel functionalities (humidity, heat, optical, biological and chemical sensing, etc.) all of which are rare in inorganic semiconductors. The impressive and extended progress of organic semiconductors during the last two decades has attracted a lot of attention in the field of electronics. Particular organic semiconductor devices such as organic light emitting diode (OLED) and displays centered on OLEDs have already been commercialized [3]. While other devices like organic semiconductor based sensors, diodes and organic thin film transistors (OTFTs) are on the border of commercialization.

On the basis of materials, semiconductors can be categorized into two diverse sets, such as organic semiconductors and inorganic semiconductors. The supreme recognized inorganic semiconductors include germanium (Ge), silicon (Si) and gallium arsenide (GaAs), which are repeatedly used in the electronic industries due to their exciting electrical and structural properties [4, 5].

On the other hand, organic semiconductor materials can be synthesized and the electrical and physical properties of these materials, e.g. cheap price, ease of processing, mechanical flexibility and multiplicity are desired for chemical synthesis [6, 7]. Numerous organic dyes are insulators but still, there is a huge quantity of dyes whose properties are parallel to semiconductors and metals. The arena of organic electronics is comparatively a novel multidimensional exploration field, which comprises a series of observational and theoretical focus regarding electronic devices prepared from carbon based materials [8].

One of the major differences between inorganic and organic semiconductors is the charge transport mechanism. In case of inorganic semiconductor, electrons move in wide bands as delocalized plane waves with very limited scattering, due to which they have relatively high mobility compared to the organic semiconductors, where charge transport is based on carriers hopping between localized states and electrons undergoing a lot of scattering. Accordingly, this results in a very low

mobility and conductivity of the organic semiconductors. The greatest significance of organic semiconductor over inorganic semiconductor materials is that the latter offers a relative easy processing along with low cost [9].

1.3   Fabrication Technologies

Organic semiconductor dye materials have numerous benefits in electronic device fabrication. They are relatively non-toxic and do not need high temperature during fabrication, which makes them easy to handle. Both flexible and rigid substrates can be used for fabrication of electronic devices. Some additional key advantages of organic materials are that they are comparatively uncomplicated and require simple thin film technology. Thus, devices fabricated using organic semiconductor dyes are cheap and allow batch fabrication [10]. Common techniques involved in the fabrication of organic devices are: spin coating; centrifugation; paste deposition and drop casting.

In this thesis, it has been tried to engage simple possible fabrication technologies to get the devices fabricated; keeping in view that their should be no compromise on the device quality and reproducibility. Different types of devices are fabricated, which include:

(a) two terminal sensors such that both the terminals are ohmic;

(b) two terminal device such that the device is an organic diode; and

(c) three terminal device such that the device is a transistor.

The above mentioned devices are fabricated by using different organic materials and simple fabrication techniques as summarized in Table 1.1. These sensors are categorized in three classes: (a) humidity sensors; (b) light sensors and (c) temperature sensors. These devices are fabricated under normal gravity (1 g) as well as at high gravity (70 g). Some of the devices are also fabricated at negative

TABLE 1.1: Summary of fabricated devices.

Organic Dye	Fabrication Technique	Gravity	Device Type	Sensitivity
CuPc	Drop-casting, Centrifuge	1 g, 70 g	Sensor	Humidity
NiPc	Drop-casting, Centrifuge	1 g, 70 g	Sensor	Humidity
VoPcPHO	Spin-coating	1 g	Sensor	Humidity
NiPc-CoPc	Drop-casting, Centrifuge	1 g, 70 g	Sensor	Light
ZnPc	Spin-coating	1 g	Sensor	Light
OD	Drop-casting	+1 g, -1 g	Transistor	Humidity, Temp.
NiPc	Thermal Evaporation	1 g	Transistor	Light, Temp.

gravity (-1 g). This means that the organic substance is applied to the substrate while the substrate was looking downward. Under such conditions, the properties and the thickness of the films shall be determined by the gravitational forces. By employing such simple techniques, the aim was to enhance the sensitivity of the sensors and to show that the device characteristics can be improved by changing the fabrication methodologies.

1.4   Motivation

Recently, there has been an increased interest in the demand of flexible, light weight and small sized electronic devices [7]. This is possible only with innovative materials, such as dyes, which allow batch fabrication of devices therefore, ensuring cost effectiveness. Moreover, they are light weight and flexible thus, can meet the requirements of today's high-tech electronic industry. These are the main reasons that has made dye-based organic semiconductor technology more provoking and interesting. Just by altering the external parameters during chemical synthesis and level of doping in the production of electronic devices, dye-based organic semiconductors can be tuned to have desired characteristics. Majority of organic dye materials offer high absorption coefficient in wide spectrum and also exhibit high photo-electromagnetic sensitivity even at low radiation intensities [11]. Moreover, the deposition of dyes thin films by vacuum sublimation is a relatively easy process. Its purification is simple and economical because, sublimation of these materials

occur at relatively low temperatures (400-600 °C). Thus, their use in electronic industry would be an economical choice for device fabrication. A good knowledge about the electrical characteristics of dye-based organic semiconductors would be a prerequisite requirement to exploit their potential use in electronic industry.

Organic materials, which are synthesized in laboratories can have good optical absorbtion and (semi)conducting properties ranging from nano materials to azo dyes [12]. Among them, the organic dyes, and phthalocynines are the most commonly used semiconductors, as they are easily accessible. Due to this reason, it has been decided to investigate the potential use of dye based organic semiconductor for making humidity, temperature and light sensitive devices. Composites of organic dyes with Alq$_3$, sugar, etc. are also investigated by involving different fabrication techniques, such as centrifugation, spin coating and drop casting.

Organic dyes, in principle, are carbon-based composites developed for dyeing or coloring in material trade. These organic colors can either be naturally or unnaturally manufactured. In this thesis, Orange dye 25 (OD), Copper Phthalocyanine (CuPc), Nickel Phthalocyanine (NiPc), Vanadyl 2, 9, 16, 23-tetraphenoxy-29H, 31H-Phthalocyanine (VOPcPhO), Cobalt Phthalocyanine (CoPc), Zinc Phthalocyanine (ZnPc) and their composites are used to fabricate a variety of electronic devices. These are commonly accessible dye materials and their applications on substrate to fabricate a device is quite easy. The devices, which can be achieved by employing these materials will therefore be a lot cheaper compare to their inorganic counterparts.

Literature on humidity, temperature and light dependent electrical characterization of dye based devices provide very little or no details of devices fabricated at different gravity conditions [13]. So, in this work, efforts are made to explain in detail, effects of gravity on the characteristics of organic devices.

The dissertation aims to investigate humidity, temperature and light sensitive electrical characterizations, which include impedance, capacitance, current and voltage measurements of organic sensors. Sensors, diodes and transistors are fabricated by using different types of fabrication technologies in order to find their

reliability for industrial applications. Industrial demands desire that such sensors should be simple in their structure and they should be cost efficient as far as their fabrication is concerned. Furthermore, they should exhibit good sensitivity and their response to a time varying ambient condition should also be very efficient. It is expected that this research will provide a technology to fabricate efficient and cost effective sensors by exploiting dye-based organic semiconductors. Owing to this fact, numerous dye-based materials and their composites are considered for sensors fabrication.

1.5   Outline of the Dissertation

This thesis reports the fabrication and characterization of organic semiconductor dye based humidity, temperature and optical sensors. Some of which are deposited at normal gravity and others are at different gravity conditions with variant frequencies, substrates and techniques. The work in this dissertation is organized as follows:

Chapter 2: This chapter deals with the history of organic electronics with special reference to organic dyes. It deliberates on the old times of diverse classes of organic semiconductor dye materials and their consumption in sensor, diode and transistor equipments; deposition techniques and their operational standards. Theoretical background, charge transport process, traps distribution and space charge limited current model are also discussed.

Chapter 3: In this chapter, fabrication techniques and experimental setups, which have been employed in this research are discussed. As far as fabrication of an electronic gadget is concerned, the main aim is to get a reliable device capable of translating a physical change into an electrical signal with a high precision. Since, reproducibility of a device is mainly dependent on the conditions in which it is fabricated, it is therefore discussed in this chapter that substrate cleaning prior to the device fabrication is of vital importance. Furthermore, fabrication techniques used in organic thin film deposition, for example, drop casting,

high vacuum thermal evaporation, spin coating and centrifugation methods are explained with sufficient detail.

Chapter 4: In this chapter, humidity sensors based on CuPc are fabricated and characterized. The sensors are fabricated by drop casting and centrifugation techniques under different gravity conditions, such as $1g$ and $70g$. Impedance and capacitance- measurement with respect to relative humidity are presented. A plausible explanation related to capacitance/impedance changes is prescribed.

Chapter 5: In this chapter, humidity sensors fabricated on NiPc using various techniques are discussed in detail. Characteristics achieved due to difference in physical morphology and electrical parameters like, impedance, capacitance sensitivities of NiPc humidity sensors are discussed in detail.

Chapter 6: In this chapter, humidity sensors based on VoPcPhO and its composites with Alq$_3$ are fabricated by using spin coating and annealing methods at different temperatures and frequencies. Physical and electrical parameters, such as impedance, capacitance and resistance are discussed in detail. Sensitivities variation with respect to ambient environment are also discussed in detail in this chapter along with the response and recovery times of the fabricated devices.

Chapter 7: In this chapter, the effect of illumination on the impedance and capacitance of the NiPc-CoPc composite sensors have been investigated. The sensors are fabricated by drop casting and under centrifugal force, and the detail on the fabrication methods, and graphical results are discussed.

Chapter 8: In this chapter, the visible wavelength photodiode (ITO/ PEDOT:PSS /ZnPc: PC$_{71}$BM /LiF /Al) is fabricated and characterized by facile, eco-benign and low power thermal evaporation budget fabrication techniques. The electrical characterization of the photodiode are carried out by measuring the photocurrent density-voltage relationship in response to varied illumination levels of incident light. Significantly improved sensing parameters such as responsivity, and switching time between stable dark and illuminated states are observed. An improved

model is presented to simulate the characteristics of photodiode and the results are compared with its counterparts.

Chapter 9: This chapter presents the fabrication of multifunctional organic field effect transistors (OFETs) using 3-[ethyl[4-[(4-nitrophenyl)azo]phenyl]amino]prop- -anenitrile, usually known as Orange-Dye 25 (OD) and its composite with sugar. The study investigated heat- and humidity-dependent electrical characteristics of the fabricated devices. Fabrication is carried out from the aqueous solution of the materials using different gravity conditions, i.e. positive gravity ($+1g$) and negative gravity ($-1g$). It is demonstrated that devices fabricated using OD at $-1g$ are more sensitive than those fabricated at $+1g$. Moreover, OFETs fabricated at $-1g$ using OD:sugar offered capacitance-temperature sensitivity much higher than devices fabricated at $+1g$. It is also been shown that in drop casting method, properties of OFETs are dependent upon gravity as well as solution composition employed for channel definition.

Chapter 10: In this chapter, NiPc based OFETs with Al-NiPc Schottky junctions are fabricated and their electrical characteristics are investigated under filament light illumination and temperature. An equivalent circuit of OFET has been developed where gate-source and gate-drain junctions are represented by independent current sources, and source-drain channel by a dependent current source. It is shown that the performance of the device depends on the channel thickness. Effects of heating on the impedance of NiPc based OFETs are investigated and it is shown that the transistors exhibited high temperature dependency. It is also demonstrated that the transistors fabricated using NiPc films can be used as multi-functional sensors to evaluate light and temperature variations.

Chapter 11: In the final chapter, conclusion of the thesis is presented and extension to this research in the form of future work is presented.

Chapter 2

Literature Review and Organic Semiconductors Fundamentals

2.1 Organic Semiconductors

Electronic devices have sensitive layers, which are based on either organic or inorganic materials. Some of the advantages of organic over inorganic materials are their light weight, low density, flexible substrates (plastic, paper, rubber, cloths), easy processing, simple fabrication, low temperature processing, and low cost [14–18]. Organic materials are based on carbon elements, e.g. monomers, dyes, and polymers. Key benefit associated with organic semiconductor materials is ease of deposition, such as drop casting, spin coating, centrifugal deposition, etc. These methods are frequently employed to deposit organic semiconductors thin layers on an appropriate substrate. These deposition techniques are not expensive and they also do not require high temperature processing. Thus, modest compared to other deposition techniques used in inorganic semiconductor industry. Keeping in view these facts sooner rather than later, it is expected that organic electronics would replace inorganic devices.

Organic semiconductors are typically assembled from π-conjugate bonds, in which electrons move through π-electron cloud either by tunneling or hopping mechanism

to define conduction [19]. Like inorganic semiconductors, organic semiconductors can also be doped to modify their conductivity. Doping in organic semiconductors can either be done by adding an electron to the conduction band to increase its electron conductivity or by creating a vacancy in the valence band to increase hole conductivity.

Organic semiconductors can be classified as:

 (i) **Single Molecule:** Single molecule organic semiconductors are defined by relatively small molecules typically with a non-repeating structure and are called monomers.

 (ii) **Short Chain (Oligomers):** An oligomer consists of a limited number of monomer units.

(iii) **Long Chain (Polymers):** A polymer molecule consists of linked chain of monomers, which are typically connected by a covalent bond.

Mostly, polymers have carbon atoms in combination with other elements like Ni, O, H, Si, Cl, etc. Many techniques are in practice to grow single organic molecular crystals (OMCs), such as: a) vapor phase deposition; b) solution based growth; c) Czochralski and d) Bridgman method. Despite the fact that OMCs have better electrical performance, thin films grown using various quick deposition techniques (e.g. spin coating) are widely used to manufacture electronic devices [20–22].

Organic semiconductors offer numerous advantages over their counterparts and few of them are listed below:

 (i) Thin films of organic semiconductors can easily be deposited.

 (ii) Organic semiconductors are relatively more sensitive to external agents.

(iii) They offer less cost because of large scale fabrication.

(iv) Have high absorption coefficient.

(v) Flexible devices can be fabricated by employing organic semiconductors.

In this chapter, a literature review and fundamentals of organic semiconductor devices are discussed. History of organic semiconductor devices, their junctions/contacts, charge injection, trapping and conduction mechanisms involved in organic semiconductor devices are discussed in detail. Modern organic semiconductor devices, their current state of technology and use in the industry is presented. Possibility of organic semiconductor to substitute inorganic electronics in the near future is assessed. Novel organic materials involved in the fabrication of sensors, transistors and diodes are explored. At the end, the current trend of technology is summarized.

2.2 Organic Semiconductor Based Electronic Devices

Initially, organic materials were considered as insulators, which was proved wrong after the observation of photoconductivity in anthracene. Anthracene was known to be the first photoconductive organic material as reported in Ref. [23–25]. In 1960's, basic phenomena of charge carrier transport and optical excitation was observed in organic molecular crystal [26]. Followed by the discovery of conducting polymers in 1970's, as a result of a laboratory accident, for which the group involved was awarded Nobel Prize in the year 2000 [26, 27]. As a result of these revelations, researchers and scientists started working with great enthusiasm to synthesize polymers and doped organic materials [28]. By the end of 1990's, carbon-based semiconductor devices entered into commercialization phase and by then, organic light emitting diodes (OLEDs) were available in abendent [3]. In the 20th century, enhancement of organic materials conductivity attracted interest of researchers and analysts to investigate the potential use of organic materials for electronic devices to supplement conventional inorganic electronics [29, 30]. A growth history of organic semiconductor technology is summarized in Table 2.1.

TABLE 2.1: History of organic semiconductor (OS) materials and devices.

Year	Development	Reference
Before 1941	Organic materials were considered as insulators.	–
1941-46	Initial interest in OS; π-electron transfer.	[28, 31]
1948	Observation of weak electric conductance in Dyes.	[32]
1950	Organic semiconductor introduced.	[33]
1955	Electroluminescence response in organic solids.	[34]
1970	Organic thin film by vacuum evaporation.	[35]
1970	Field effect phenomena in organic semiconductor.	[36]
1976	Metallic conductivity in polyacetylene.	[29]
1983	First polyacetylene based OFET.	[37]
1983	Photovoltaic effect in organic semiconductors.	[38]
1987	First polythiophene based OTFT.	[39]
1987	Fabrication of first OLED.	[40]
1947-97	Research to improve charge carrier mobility.	[41]
2000	Successful synthesis of conductive polymers.	[42]
2000-09	Commercialization of organic sensors.	[43]
2010-2017	Commercialization of organic transistors, diodes.	[44–56]

2.3   Metal-Semiconductor Junction

Metal semiconductor (M-S) junction is formed when metal is brought in contact with a semiconductor. Following are the main properties of an ideal M-S contact [57]:

(i) There should be no interfacial layer between the semiconductor and the metal.

(ii) Metal and semiconductor should not intermix; their boundaries should be sharp and distinct.

(iii) Interface should be free from surface charges.

F. Braun, in 1874, reported formation of junction in M-S diode [58], and the same explained in 1938 by Schottky and Mott. [59]. In a Schottky junction with the application of external potential, there is a change in the barrier height. This change

is observed only towards the organic semiconductor side because of the presence of depletion inside the organic material. A variation in the applied potential generates a current, which is non-linear in nature, thus, an asymmetric current-voltage $(I - V)$ characteristics are observed. On the other hand, if the contact formed by the metal organic semiconductor is an ohmic contact then the observed characteristics, by varying the applied potential, shall be linear in nature, which implies that there is no depletion caused by the contacting metal. The nature of the contact whether ohmic or Schottky will depend upon the properties of the chosen metal, especially its work function with respect to the organic semiconductor. However, under usual conditions, metal organic semiconductor contacts are Schotkky. To have an ohmic M-S contact, specific metals are required such that with the application of a nominal external potential carriers available in the organic film or in the metal can flow comfortably without experiencing any barrier [60]. There are two basic processes, which are involved in defining the M-S junction properties:

(i) Charge carriers injection from either side of the junction.

(ii) Charge flow mechanism and life time of the injected carriers.

Based on the above mentioned processes, the electrical response of a junction can be explained for a given device.

2.3.1   Schottky Contacts

As discussed before, whenever a metal is brought in contact with an organic semiconductor, under usual condition, it gives a Schotkky contact. This is so, because there are normally surface states, which cause pinning of energy levels at the surface of a semiconductor and are mainly responsible in generating a non-ohmic contact. On the other hand, if the fabrication is taking place in a highly clean environment, it can be assumed that the organic semiconductor is free from surface states and junction properties and nature should be determined by the difference of

M-S work function. Surface states free semiconductor also allows to have improved junction characteristics by improving the target organic semiconductor properties.

A Schottky contact can be achieved by choosing an appropriate metal having a work function lower than the organic semiconductor's work function. Energy band diagram identifies the potential barrier between the chosen metal and the semiconductor permitting the carriers to flow from the semiconductor to the metal. Energy band diagram, shown in Fig. 2.1(a), is sketched by assuming that there are no surface states and prior to the contact formation, the metal was at a finite distance from the semiconductor. Further, it is assumed that the organic material is an *n*-type semiconductor therefore, the Fermi level is closer to the conduction band and falls in the upper half of bandgap, E_g.

Conductivity of an *n*-semiconductor can be determined by the energy gap given by $\Delta E = E_C - E_{F_{SC}}$ [61]. In Fig. 2.1(a), E_V represents valence band energy, E_C is the lower energy level of conduction band, $q\phi_{SC}$ is the energy level required to move an electron from $E_{F_{SC}}$ to the free space; whereas, $q\chi$ is the energy level required to release an electron from the conduction band to the free space. Figure 2.1 also shows that $q\phi_m$ represents energy required to move an electron from the metal conduction band to the free space referred to as metal work function [61].

When the metal is brought in contact with the semiconductor by making distance zero, there would be a modification in the band diagram and same is shown in Fig. 2.1(b). Under such circumstances, if a carrier tries to move from the semiconductor to the metal, it will experience a barrier represented by $qV_i = q(\phi_m - \phi_{SC})$ [61] as shown in Fig. 2.1(b). On the other hand, if the carrier is trying to move from the metal to the semiconductor, it will see a barrier having height $q\phi_{B_n} = q(\phi_m - \chi)$ as shown in Fig. 2.1(b). The presence of a barrier at M-S interface is responsible for the generation of non-linear $I - V$ characteristics of the device, and the contact is known as a Schotkky contact. A development history of M-S contact is given in Table 2.2.
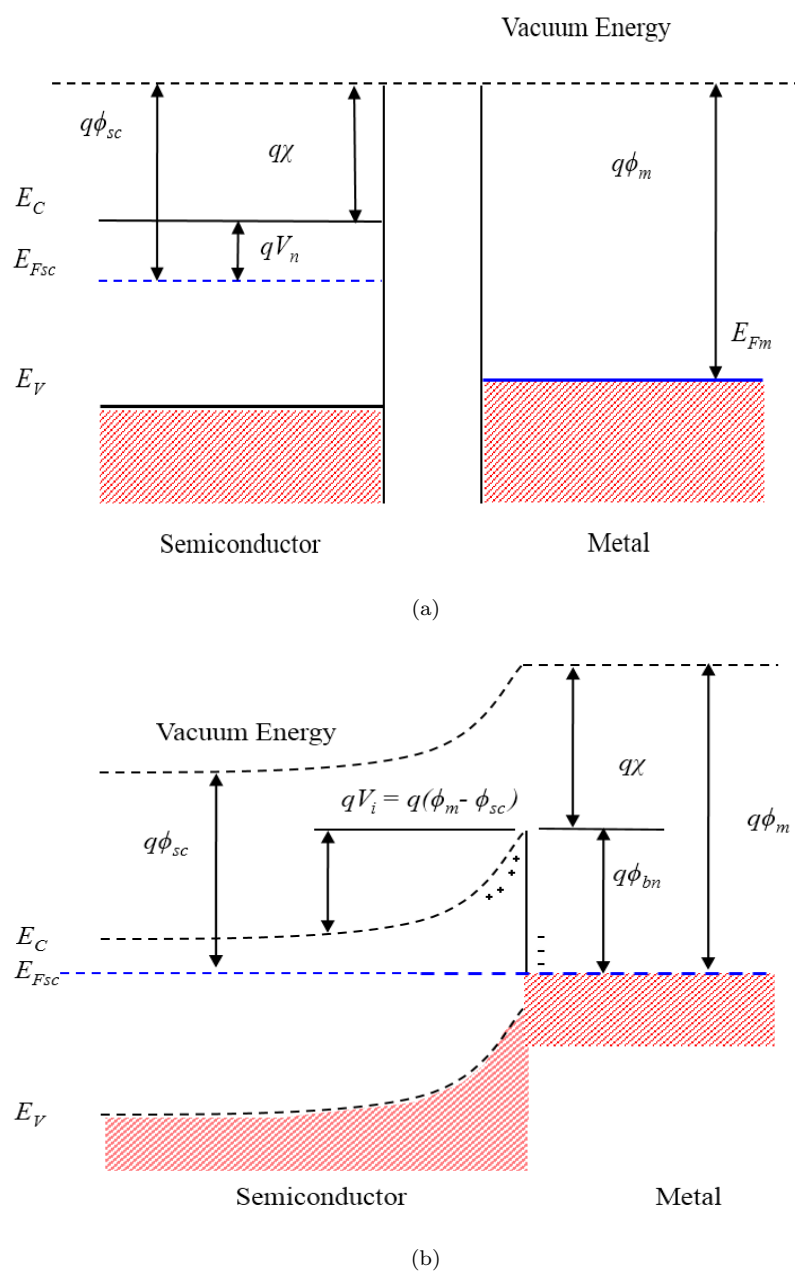
FIGURE 2.1: Energy band diagram showing metal and *n*-type semiconductor (a) before contact and (b) formation of Schottky barrier when a metal is brought in contact to an organic semiconductor [61].

TABLE 2.2: History of Metal-Semiconductor (M-S) contacts.

Year	Development	Reference
Before 1874	There was no concept of M-S contact rectification.	–
1874	Discovery of rectification property in M-S contacts.	[58]
1904	M-S diodes concept was proposed.	[62]
1906	First patent was granted on point-contact rectifier.	[63]
1926	First M-S diode fabricated.	[64]
1938	Schottky and ohmic junctions were introduced.	[59]
1947	Introduction of surface states and rectification.	[65]
1965	Tungsten-Semiconductor Schottky barrier diodes.	[66]
1978	GaAs based Schottky barrier solar cell.	[67]
1980	Interfacial layer theory of Schottky barrier diodes.	[68]
1993	Ohmic contacts to GaAs: fundamental discussion.	[69]
2000	Fermi-level pinning in Schottky contact.	[70]
2001	GaAs Schottky contacts based photodetectors.	[71]
2003	Schottky nanocontacts.	[72]
2008	Patent on nitride-based transistors with ohmic contacts.	[73]
2012	Ohmic contacts formed in graphene FETs.	[74]
2015-2016	Flexible M-S based: sensors, diodes and FET.	[75, 76]

2.3.2 Effects of Interface States

In an actual device, periodic nature of a semiconductor crystal is disturbed at the interface, and there are a large number of states created within E_g known as interface states/traps. Their energy values are between E_V and E_C, and they act as electron taps, if their energy levels are below the Fermi level.

Figure 2.2(a) shows that there is a high density of energy states inside E_g of the semiconductor, which can potentially trap a charge carrier whenever it will try to move from E_V to E_C. Usually, these states are found in those atoms/molecules, which are closer to the surface and generate dangling bonds. Electrons inside the semiconductor materials get trapped in these interface states, creating a depletion region as shown in Fig. 2.2(a). It can also be seen from the figure that energy band curvature $q\phi_0 = E_{F_{SC}} - E_V$ is present at the semiconductor surface, which offers a barrier to the follow of carriers trying to cross the junction.

Figure 2.2(b) shows energy band diagram of the semiconductor after making contact with the metal. Some of the trapped electrons from the surface state, which are above the Fermi level, get themselves transferred to the metal, enhancing the potential barrier. The new height represented by $q\phi_b$ is shown in Fig. 2.2(b). So, in general, it can be said that the presence of surface states at M-S interface creates a negative impact on the device characteristics. They will trap and de-trap the carriers and the time such consumed shall influence the device characteristics.

(a)

(b)
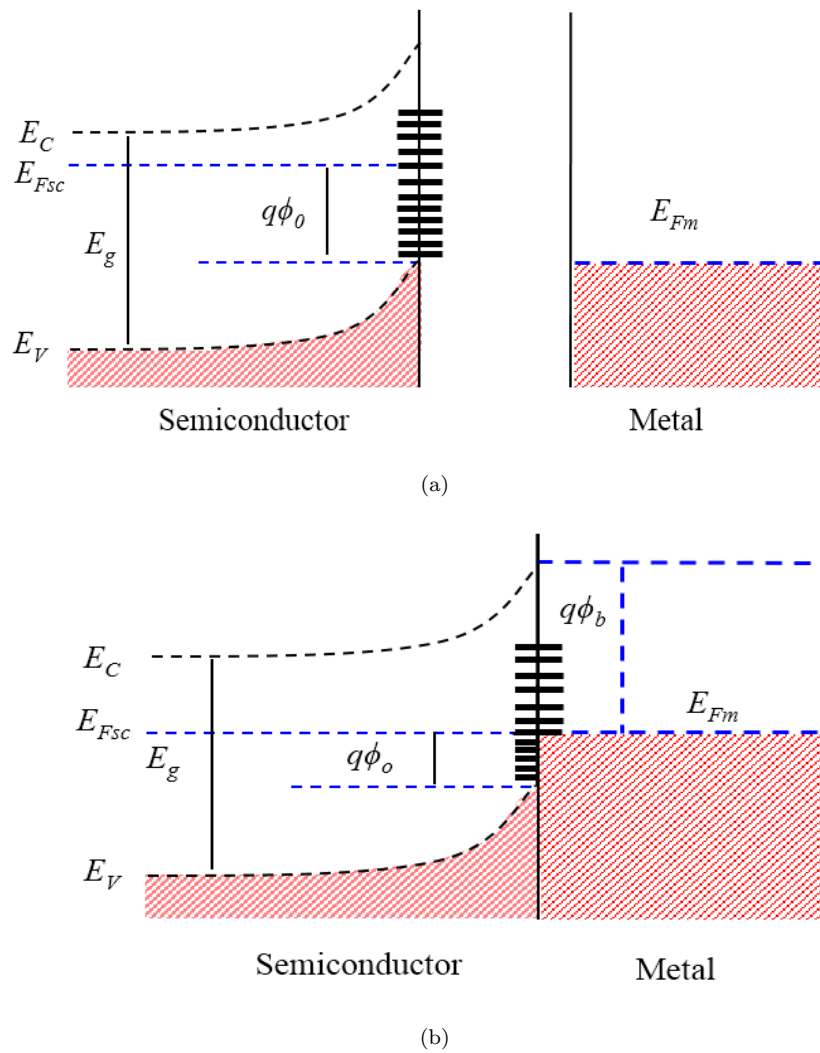
FIGURE 2.2: Energy band diagram in the presence of interface states (a) before and (b) after contact with the metal [61].

2.3.3 Depletion Layer

Depletion layer defined by an M-S contact is an insulated region in a semiconductor from where the carriers are swept away by a diffusion process. Figure 2.3 shows energy band diagram of metal/n-type semiconductor under thermal equilibrium, forward biased and reverse biased conditions. Forward biasing is achieved by applying an appropriate potential to a M-S junction. This will cause a reduction in the built-in depletion and the system under such conditions can be represented by a band diagram shown in Fig. 2.3(b). Since the barrier, from the metal to the semiconductor, represented by $q\phi_{bn}$, is maintaining its height therefore, very few electrons will drift towards the semiconductor; whereas, there is a reduction in the barrier height from the semiconductor to the metal represented by qV_{bi}-V_F. It would be therefore, easy for carriers to move from the semiconductor to the metal and the observed current will be a positive current. In case of reverse biasing, as shown in Fig. 2.3(c), the Fermi level of the metal is raised w.r.t the semiconductor, resulting into an increase in semiconductor potential. This extends the length of the depletion region, and the barrier it offers to the flow of carriers from the semiconductor to the metal will be relatively higher than its equilibrium value and is represented by $qV_{bi} + V_R$ [61]. Under such conditions, no current will flow and the device under ideal behavior will act as an open circuit. In summary, one can say that the presence of depletion at M-S junction will determine its electrical response, and it plays a very crucial role in defining the quality and characteristics of a semiconductor device.

2.3.4 Ohmic Contact

A M-S contact, which offers a negligible resistance, including the contact and the bulk resistance of the semiconductor is referred to as ohmic contact [77, 78]. This type of contact is non-rectifying and has a linear $I - V$ curve in both directions. The quality of an ohmic contact is determined by the specific contact resistance of the device and a good ohmic contact would be the one, which should offer
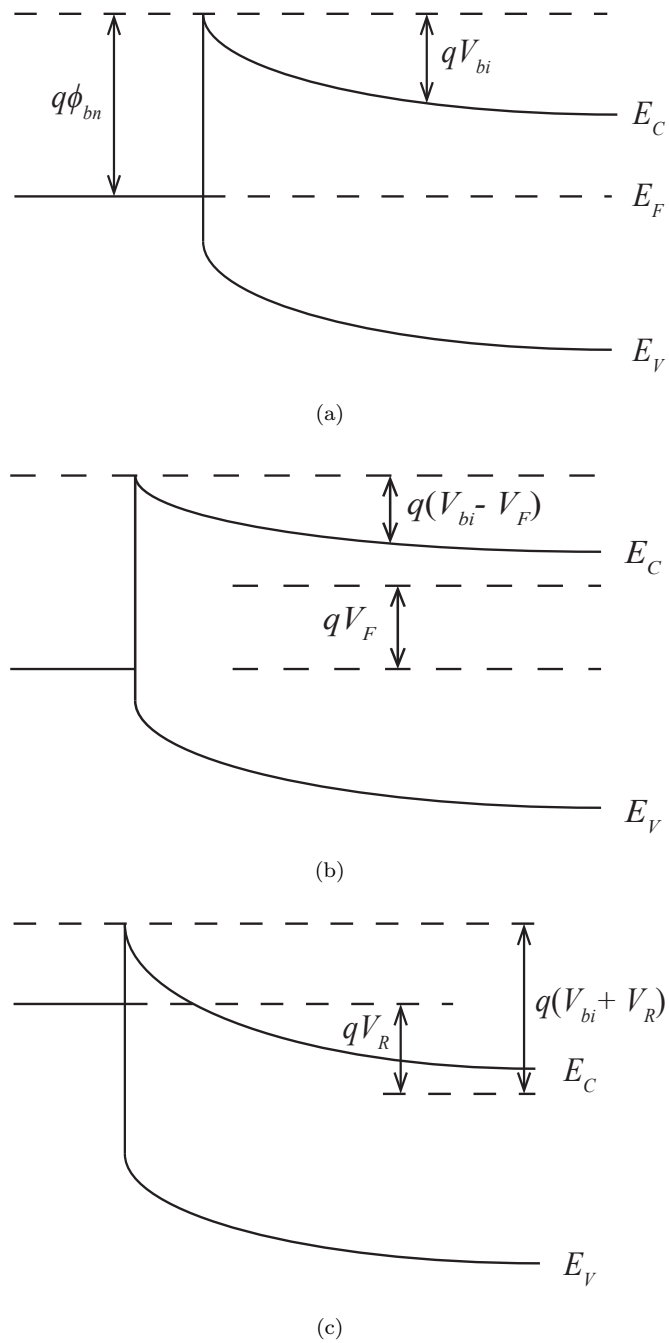
Figure 2.3: Energy band diagrams of a metal-semiconductor interface under different conditions: (a) thermal equilibrium; (b) forward bias; and (c) reverse bias [61].

specific contact resistance in the range of 0.5-1 Ω/mm. Since there are surface states, normally present on the exposed surface of a semiconductor therefore, under ordinary conditions, it would be very hard to get an ideal ohmic contact. For a good quality ohmic contact, extra precautionary measures are required to clean the surface of the semiconductor before depositing the ohmic metal.

Assuming that there are no surface states present on the surface of a semiconductor, the formation of an ohmic contact will be dependent upon the work function of the chosen metal. The metal should be chosen such that free electrons from the metal should move to the semiconductor thus, creating an M-S interface having barrier $\sim$0.01 eV. A barrier with such a small height will offer practically no resistance to the flow of carriers from either side of the junction, and the characteristics of the junction will be linear in nature. A contact of such characteristics is referred to as an ohmic contact. In order to reduce the ohmic contact resistance, it is a convention in semiconductor industry that a contact layer having relatively higher doping than the channel is also deposited, which offers dual benefits: a) to reduce the contact resistance and b) to off-set upto some extent the bulk resistance of the semiconductor. In a nutshell, one can say that in order to have a comfortable communication of a semiconductor device with exterior world, ohmic contacts are required, and an ohmic contact of good quality will play a significant role in determining the performance of the device.

2.4   Charge Injection and Transport

Efficiency of an organic semiconductor device depends upon its charge transport. It is a well known fact that organic semiconductors have small bandwidth and wide E_g. Usually, the gap between the HOMO-LUMO is in the range of 1-4 eV [79]. With such a large gap, it might be expected that the organic materials would have very low conductivity. But, practically they offer better conduction because of large number of energy states available inside E_g, which allows transportation of charges. Charge movement, under the influence of external applied voltage, in

an organic semiconductor device can be divided into three different processes and the detail of which is given below.

2.4.1 Charge Injection

In an organic semiconductor device, one of the mechanism, which is responsible for the flow of current is described by the process called as charge injection. In an M-S junction, carriers can be injected into the barrier and the carriers ought to be injected must overcome the potential offered by the barrier. Charges to be injected from the metal to the organic semiconductor should overcome the barriers offered by the M-S interface while observing it from the metal side. The quality of the M-S interface plays an important role in determining the device efficiency in terms of carriers injection. It is an established norm that charge injection from the electrodes to the device is limited by the properties of M-S interface. This implies interface barrier height; interface doping; electrode material; interfacial morphology and interface doping profile. Furthermore, carriers injection is influenced by the presence of dipoles, atomic diffusion process and chemical reactions, which are commonly observed at the interface of the device [80–82].

Another process of carrier injection across M-S interface is referred to as thermionic emission. In thermionic emission, energetic carriers climb over the barrier either by absorbing thermal energy from the ambient or from the channel field. This emission would be high if the barrier height is relatively small [77, 78]. There are other mechanisms, which can also be observed in organic semiconductor devices, responsible in defining the current flow in these devices and comply to the definition of charge injection. One such injection is known as quantum mechanical tunneling. In the presence of quantum mechanical tunneling, the injection of carriers take place through the barrier and thus, the presence of potential barrier becomes insignificant. So, it can be said that in the presence of quantum mechanical tunneling, the device will not exhibit charge flow under thermionic emission process. Injection limited models have conventionally been described either under

thermionic emission or by tunneling mechanism [77, 83]. Various analytical models and Monte Carlo simulations are available by involving thermionic emission or quantum mechanical tunneling to explain injection current in organic semiconductor devices [84–86].

2.4.2   Charge Transport

Transportation of charges from exterior world to a device fabricated using organic semiconductor material plays an important role in determining the quality of the device. Charge transport depends both on the electrodes of the device as well as on the properties of bulk semiconductor material. Thus, electrodes and organic semiconductor layers collectively define charge transport properties of a device. As far as bulk organic semiconductor properties are concerned, the charge transport would be limited to mobility, doping density, trap density and layer structures, etc.

It is an established fact that the interaction between surrounding molecules in organic materials is usually weak and is known as Van der Waals interaction. This interaction results into a relatively narrow bandgap between conduction and valence bands. This allows a comfortable band to band conduction in an organic material. This can be further enhanced by improving the free charge carrier density of an organic material. In general, the charge transport mechanism in an organic material can be explained by using two different models:

  (i) Hopping transport mechanism

 (ii) Band transport mechanism.

For a typical hopping transport mechanism, mobility is thermally activated whereas, movement of charges under band transport mechanism dominates when thermal mobility of carriers is deactivated [77].

2.4.2.1 Hopping Transport

In 1980s, it was proposed that flow of current can take place by the hopping of electrons from one localized site to another. In amorphous materials, the tunneling between localized states can occur by the transportation of charges, which is assisted by the phonon, known as phonon assisted hopping mechanism. The rate of hopping can be expressed as [87]:

$$\upsilon_{ij} = \upsilon_0 f\left(E_i\right) \exp\left(\frac{2R_{ij}}{a} + \frac{E_j - E_i}{kT}\right) \tag{2.1}$$

where f is the Fermi function and υ_0 is a constant that defines electron-phonon coupling. E_i and E_j are the energy states of ith and j^{th} location, respectively. k is the Boltzmann constant, T is the temperature in Kelvin and R_{ij} is the distance between energy states.

A variable-range hopping model was developed by Mott et al. [88]. They described the electron transport at low temperature through exponential distribution of localized states. The model also predicted a thermally activated mobility of free carriers in an organic semiconductor material. Authors of Ref [89] presented a multiple trap and thermal release (MTR) model in which traps were formed by associating the high concentration of localized levels with a narrow delocalized band. When a carrier reaches near a trap, it is apprehended immediately and as a result, the next trapped carrier will get free by thermal activation. Equation (2.2) shows a relationship between drift mobility, μ_d and low field mobility, μ_0 in an organic semiconductor delocalized band

$$\mu_d = \mu_0 a_0 \exp\left(-\frac{E_t}{kT}\right) \tag{2.2}$$

where E_t is the energy difference between the delocalized band edge and the trap level and a_0 is the ratio between the effective density of states at the delocalized band edge and the concentration of traps. Equation (2.2) indicates that at higher temperature, the value of μ_d increases and for a given temperature, it also increases when there is a smaller energy difference between the delocalized band edge and

the trap level. Equation (2.2) also indicates that μ_0 is the hopping mobility, which gets effected by the material parameter defined by E_t and ambient parameters defined by kT. This indicates that the performance of an organic semiconductor device will be dependent upon: a) quality of the semiconductor layer and b) the ambient in which the device will be operated.

2.4.2.2   Band Transport

Band transport mechanism is defined as, "the occurrence of charge transport at low temperature in highly ordered molecular crystals due to charges available in delocalized states". The band transport becomes a dominating process at low temperatures, i.e. ∼25K. While considering inorganic semiconductors, it is a well-studied fact that the electronic delocalization is weak and has small bandwidth. Due to which, at room temperature, the molecular crystals mobility lies in the range of 1 to 10 cm^2(Vs)$^{-1}$ [90], which is treated as a good mobility for inorganic semiconductors. Since band transport is observed at ∼25K therefore, for commercial organic semiconductor devices, which are normally operated at room temperature (∼290K), this type of conduction is usually not observed and the device characteristics are generally determined by Eq. (2.2).

2.4.3   Charge Recombination

After carriers injection and transport, both electrons and holes can recombine to form various excited states, such as singlet excitons, triplet excitons, etc [91]. Since high trap densities usually exists in organic semiconductor materials, the charge transfer excitons in organic molecules create a flow resulting into an observable current in the device. Thus, contrary to inorganic semiconductors where electron hole recombination generally, causes a quanta of energy to be released in atmosphere. In an organic semiconductor, this recombination process generates excitons, which contributes into the flow of current [92, 93]. It is, therefore, treated as a current flow process in an organic semiconductor devices.

2.5   Electronic Traps

One of the fundamental issues in organic semiconductors is to understand the properties of electronic traps responsible to control the conduction process. In organic semiconductors, there is a significant charge trap density between HOMO and LUMO levels. The presence of traps, due to the disorder of organic semiconductors, increase localized energy states within E_g [94]. Localized space charges are formed by the charge centers created by filling of traps and by injected charge carriers [92]. Electron traps are the one, which are caused by the localized states under or near LUMO level, and hole traps are the localized states near or above HOMO level [95]. In an organic semiconductor, LUMO and HOMO can replace the conduction and the valance bands, respectively. Figure 2.4 shows Gaussian-like distribution of localized molecular orbital of individual molecules as a function of density of states (DOS) in an amorphous layer of organic semiconductor [96].

Origin of traps in an organic semiconductor may be associated with several reasons. It was reported that, apart from other factors, density of traps in an organic semiconductor also depends upon flow deposition rate as well as on substrate temperature [96]. Traps are called as charge storage sites, as they trap the charges thus, causing a reduction in number of mobile carriers [97]. Henceforth, affecting the overall conductivity of the sample.

Traps of an organic semiconductor can be detected by different experimental methods like, optically stimulated current (OSC), thermally stimulated current (TSC), thermally stimulated luminescence (TSL), photo-induced absorption (PIA), electroabsorption experiments [98], time-of-flight (TOF) techniques [99], etc. Moreover, $I-V$ characteristics of space charge limited current (SCLC) provides the data regarding the presence of traps in a given sample [100], and by impedance spectroscopy [89], one can have the details about the depth of traps and their energy distribution.
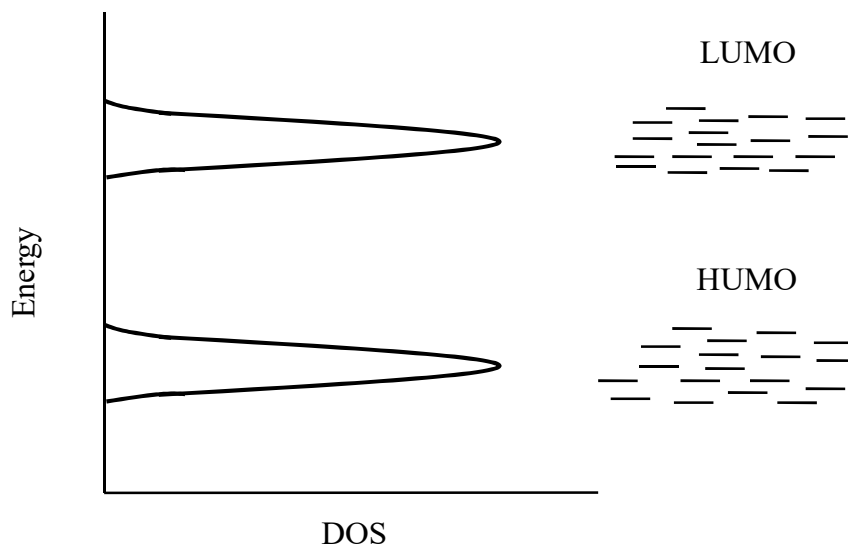
FIGURE 2.4: Distribution of HOMO and LUMO levels in amorphous organic semiconductors.

2.6   Space Charge Limited Current

Space charge limited current (SCLC) can be observed whenever sufficient number of carriers are injected in the transport layer of a device, so that the injection contact is able to provide a higher carrier density. The injected carriers will create a space charge inside the device creating a contact on the influx of more carriers and hence, the current referred to as SCLC. SCLC theory was first given by Rose [101], which was modified by Lampert [102] in 1956, who included the effects of traps, and the modified theory is known as trapped charge limited current (TCLC). In SCLC, different conduction regimes are observed by measuring $I - V$ characteristics of an organic device. The transport mechanism related to these regimes can be detected with the help of $I - V$ curves observed at various biasing.

2.6.1   Ohmic Region

At low biasing, the charge carriers are captured by the traps below the LUMO level of an organic semiconductor. This type of capturing is observed when the applied injected current density is less than the intrinsic charge density (applied electric field less than 10^4 Vcm^{-1}). For such a biasing, the current is determined

by Ohms Law (J∼V) and the region where this behavior is occurring is known as ohmic region. So, in ohmic region, current increases linearly by increasing applied voltage. The current density of the ohmic region can be written as [103, 104]:

$$J = \frac{qn\mu V}{d} \tag{2.3}$$

where n is the thermally generated free charge density, V is the applied voltage and d is the film thickness.

2.6.2 SCLC in the Presence of Shallow Traps

When biasing is increased upto a certain level, more carriers are injected into the organic thin film from the electrodes and the traps are filled. As a result, there is a rapid increase in the current due to the reduction of empty traps. At extremely high injection level, the injected current density becomes higher than the intrinsic current density, and the injected charge carriers form space charges near the organic/electrode interfaces due to low carrier mobility. An electric field inside the organic layers is also induced by these excess charges. This leads to an enhanced total internal electric field resulting in a high current density. Magnitude of current, which is dominated by injected charges, in the presence of traps can be expressed as [103, 104]:

$$J = \frac{9\mu\varepsilon\theta V^2}{8d^3} \tag{2.4}$$

where ε is the permittivity of organic semiconductor and θ is the trapping factor. Equation (2.4) shows a non-linear behaviour, which is a usual response of an organic thin film having finite thickness, d with two ohmic electrodes used for injection purpose.

2.6.3 Trap Charge Limited Current (TCLC)

In an organic semiconductor, traps are exponentially distributed in E_g defined by the finite distance in between HUMO and LUMO of an organic thin film. Some

of the injected carriers will be lost due to these traps and only a small number of charges will remain in the conduction band [101, 102, 105]. TCLC model is a modification of the SCLC model that includes trap distribution [94, 106].

In Eq. (2.4), if we assume that there are no trapping at all in a given organic semiconductor then θ will be taken as unity. In the presence of traps, θ will have a value less than unity, usually less than $E_g/2$, and this will have a significant impact in determining the magnitude of J. As evident from Eq. (2.4) that for $\theta > 1$, the magnitude of J will be relatively higher, which indicates that in the presence of traps, the current will be controlled by them and it is, therefore, known as TCLC.

2.6.4   SCLC in the Absence of Shallow Traps

In some organic devices, at high voltage, the slope of $I - V$ curve reduces after TCLC region as shown in Fig 2.5. This indicates that all the traps in the organic layer are completely filled and the current becomes SCLC having no influence of traps. In such a case, $I - V$ data exhibit a squared-law dependence ($I \sim V^2$). At that very point, conduction is trap free and it is only controlled by the space charge developed inside the device. The current density, J having no impact of traps can be expressed as [106–108]:

$$J = \frac{9\mu\varepsilon V^2}{8d^3} \tag{2.5}$$

2.7   Organic Dye Materials

Amongst the organic semiconductor materials, azo dye has attracted much interest during the past few decades due to its wide applications in electronic and opto-electronic devices [109]. Organic dyes having semiconductor properties are easily available. Electrical conductivity of organic dyes depends upon the mobility, temperature and charge carrier concentration. As discussed before, the mobility and
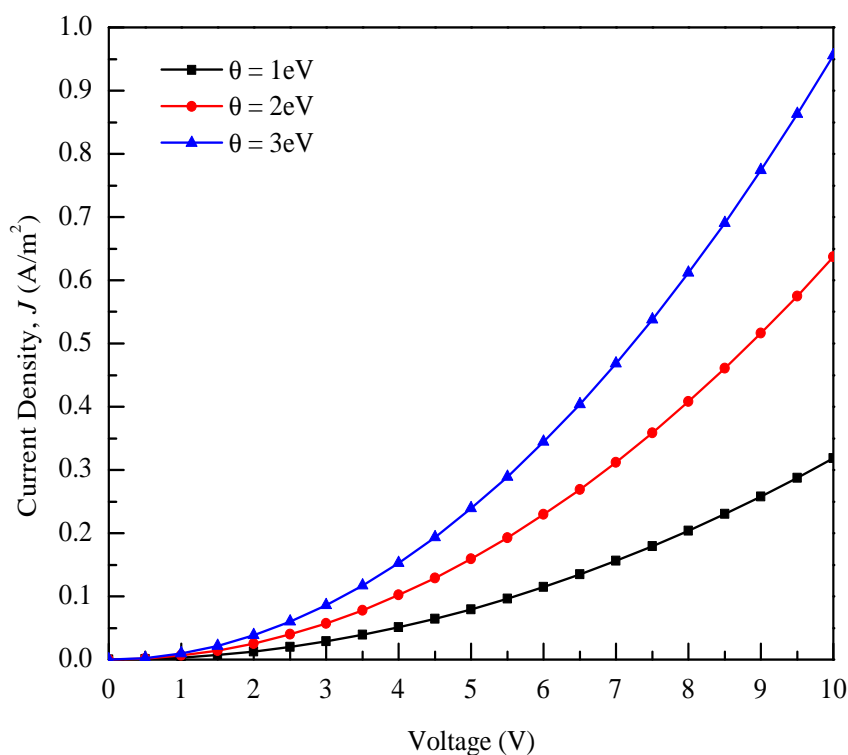
FIGURE 2.5: Space charge limited current density in the presence and absence of shallow traps.

charge carrier concentration in an organic semiconductor material, including dyes is low compared to inorganic semiconductors but still sufficient enough to use them in electronic industry.

Orange Dye (OD) and Phthylocyanine are members of azo dye family [13]. OD is a high purity p-type semiconductor and has a well defined chemical structure. It is a good water absorber, stable at normal conditions and extremely sensitive to humidity [110]. In 1907, the first unknown colour substance was found by Braun and Tcherniac after heating o-cyanobenzamide [111]. Then in 1928, Scottish dyes limited, in Grangewmouth, observed a blue impurity during the reaction of phthalic anhydride and ammonia to prepare phthalimide [112]. This impurity was later named Fe(II)Pc. This substance was most probably known as metal phthalocyanine.

Metal phthalocyanine and metal-free phthalocyanine have been known for many years. The word Phthalocyanine was first used by Professor Linstead [113], which was derived from the Greek term for naphtha (rock oil) and cyanine (dark blue).

He described a new class of organic compound, which consists of metal-free, or di-hydrogen phthalocyanine, and metal phthalocyanines and their derivatives. Phthalocyanine (Pc) is a planar aromatic macro-cyclic compound, which forms co-ordination complexes with almost 70 metals including Fe, Co, Cu, V and Ni, etc. These compounds are formed by arranging the nitrogen and carbon atoms alternatively forming four isoindole units with a cloud of 18 delocalized π-electrons [114].

Dyes are chemically and thermally stable, which makes them suitable for thin film device fabrication [115]. Since these discoveries, dyes have been widely used in a variety of applications such as inks, paints, colors and dye stuff for textiles [114, 116], and in electronic devices like, photovoltaics, LCD's, electro-chromic devices, rectifying devices, liquid crystal displays and photo diodes [114, 116–122]. Some of the dyes derivatives show liquid crystal properties at higher temperature. These properties allow their use in optical recording devices, thermal writing displays, laser printers, laser filters and infrared photography [123, 124]. Dyes are currently employed as photo-sensitizers in photodynamic therapy of cancer (PDT) [125, 126], involved in linear [127] and non-linear optics [128], used as electro [129] and biomimetic [130] catalysts, fluorescent agents [131] and light-absorbing films to coat compact discs (CDs) [132]. It is noted that electrical, optical and structural properties of dyes thin films are dependent on various parameters, such as evaporation rate, substrate temperature and post-deposition annealing [133, 134]. Use of dyes as an active material in electronic and optoelectronic devices has been reported in the literature [135–139]. These extensive studies have shown that dyes exhibit a variety of interesting optical, electrical, photoelectric, and magnetic properties in electronic devices.

2.8 Fabrication Under Gravity

Gravitational force is considered as one of the greatest factors affecting the physical and chemical properties of a material. Before centrifugal facility, gravitational

force was not viewed as an adjustable parameter [140]. High gravity fabrications received greater attention when Muller et al. [141] and Rodot et al. [142] demonstrated fabrication of $InSb_3$ and $PbTe_4$ crystals at diverse gravity conditions.

In 2001, R. V. Parfeniev et al. fabricated crystals of anisotropic semiconductor materials under varying gravity conditions [143]. They fabricated crystals from micro-gravity levels to $10g$, and demonstrated a successful growth of organic films. After that, Park et al. proposed a thin-film surface micro-machining technique to manufacture humidity and temperature sensitive devices [144]. In [145], the authors fabricated silicon heterojunctions and thin layers of poly-N-epoxypropylcarbazole with tetracyanoquinodimethane (TCNQ) impurities. The poly-N-epoxypropylcarbazole films on silicon wafers were deposited at normal temperature and at varying gravity conditions. $I - V$ attributes of the fabricated devices, as a function of temperature between 20-60 °C, were measured, such as: reverse saturation current; rectification ratio; junction resistance and threshold voltage, etc.

In 2005, OD thin films were fabricated at usual gravity conditions on Au and SnO_2 substrates. The procedure was repeated at an angular speed of 1000 rpm to get humidity sensitive sandwich type structures at room temperature. It was observed that the sensitivity of OD/Au was 5.4, while for Ga/OD/Au devices, its observed value was 5.0. These observed values were significantly better than what had been reported earlier [146]. Karimov et al. in 2008, reported a plainer construction of humidity sensors using copper phthalocyanine (CuPc) films [147]. They used capacitive property of the sample to assess the variation in ambient humidity. In 2008, organic thin films were deposited on Ni substrate by a centrifugation process at a value of gravity as high as $1107g$ [147]. In Ref. [147] thin films of p-CuPc were deposited by centrifugation and then Al layers were coated by vacuum evaporation on the grown film. Their fabricated devices exhibited rectifying characteristics. They also demonstrated that the processing technique affects the properties and the structures of the films which, eventually determine the electrical response of the sensor. In 2009, M. M. Tahir et al. fabricated organometallic sensors at high

gravity conditions by centrifugation and found an improvement in their sensitivity as a function of gravity [148].

In [149], a centrifugal atomizer technique was used to achieve SAC-305, (a led free alloy's powder) and the technique gave $\sim$11% finer grains relative to its normal growth process. Meng et al. [150] fabricated humidity sensor from OD-PANI composite layers. Sensors electric parameters such as impedance and capacitance were evaluated under varying humidity conditions ranging from 30-90%. A decrease in impedance but an increase in capacitance both in non-linear manners were observed in the fabricated sensors as a function of ambient humidity. In 2013, another humidity sensitive device based on $PEPC+NiPc+Cu_2O$ thin film was fabricated by physical vapor deposition [151]. It was noted that Ni can also be used as a metalic subsitution in Pc to fabricate humidity sensors. In 2014, a sequence of solidification of TiC-TiB_2 was invented by a combustion synthesis process at ultra-high gravity i.e, $2500g$ [152]. In 2015, R. A. Markelonis et al. deposited variety of nanoparticles on both rigid and flexible substrates by using centrifugal technique. It was observed that centrifugation technique was a simple method to fabricate uniform nanoparticle films on different substrate for chemical and optical characterization [153]. In [154], an OD based thin film resistive hygrometers were fabricated using high gravity technique and it was reported that the sensors fabricated under high gravity showed relatively better results. Because, the fabricated films offered more active area to sense the changes in the ambient humidity. In 2017, X. Yin et al. fabricated, using high gravity process, two-dimensional molybdenum disulfide nanosheets [155]. In the same year, Chani et al. fabricated and characterized the organic-inorganic (Orange Dye-Vanadium Oxide) composite based humidity sensitive devices at normal $(+1g)$ and at negative $(-1g)$ gravity [156]. It was reported that devices fabricated at negative gravity exhibited high sensitivity compared to the devices fabricated at normal gravity. The history of sensors fabrication by employing different techniques has been summarized in Table 2.3.

TABLE 2.3: Various gravity techniques for devices fabrications.

Year	Development	Reference
Before 1997	Gravitational force was not viewed as an adjustable parameter.	[140]
1982	First $InSb_3$ crystal obtained at diverse gravity.	[141]
1986	$PbTe_4$ crystal obtained at diverse gravity.	[142]
2001	Crystals of anisotropic organic semiconductor grown at $10g$.	[143]
2003	Micro-machining technique proposed.	[144]
2004	$I - V$ attributes of silicon at diverse gravities were measured.	[145]
2005	OD based humidity sensor fabricated at 1000 rpm.	[146]
2008	CuPc based capacitive device fabricated at $1107g$.	[147]
2009	Fabricated organometallic devices by centrifugation at $1650g$.	[148]
2011	Centrifugal atomizer used to get finer grainuals.	[149]
2013	Sensors were fabricated by physical vapor deposition.	[151]
2014	Centrifugation with combustion synthesis incorporated at $2500g$.	[152]
2015	Centrifugally coated graphite obtained at 5000 rpm.	[153]
2017	2-D Molybdenum disulfide nanosheet was prepared by high gravity.	[155]
2017	Humidity sensor fabricated at positive and negative gravity.	[156]

2.9   Humidity Sensitive Devices

Generally, porous thin or thick films of organic materials are used in humidity sensitive devices. In such devices, condensation of water vapors takes place in the active layer, which contains micro-pores. Due to incoming water molecules, (H_2O) doping of thin film occurs, which produces changes in the physical properties of the film. These changes are either resistive or capacitive in nature and causes variations in conductivity and/or in dielectric constant of the organic film [20, 157, 158].

Humidity, in general, is a measure of water vapor content in air or in other gases [158]. Humidity sensitive devices are usually engaged to measure relative humidity (RH), which is the ratio between the moisture content of air and the saturated moisture contained by the active layer of the sensor at identical temperature and pressure. Humidity sensitive devices have wide industrial applications, such as atmospheric humidity assessment, humidification and dehumidification of a given system, humidity adjustment in air conditioners, etc [159]. Intensive research in

semiconductor technology, especially in dyes, have made it possible to fabricate humidity sensitive devices that are highly accurate, durable, and cost effective. In a simple organic humidity sensitive device, organic film is deposited over conductive electrodes on a glass, ceramic or on a silicon substrate. In order to improve further, humidity sensitive thin film is normally covered by a porous metal electrode to avoid condensation or/and contamination.

2.10   Temperature Sensitive Devices

Temperature sensitive devices are mostly utilized as a part of industry and medicine technology. In modern industry, it is very critical to measure and control the temperature of a given system accurately. In temperature sensitive devices, usually a change in the device physical parameters, such as resistance and capacitance is observed. This change could either be linear or nonlinear w.r.t the change in the temperature. Moreover, the response of a temperature sensitive device is dependent on the quality of thin film, which translates changes in ambient temperature into impedance and/or capacitance changes. In some cases, it is also observed that the dielectric of the film is also sensitive to the changing temperature properties.

Temperature sensitive devices work on the principle of measuring the heat energy of the surrounding and then directly relating it to the molecular energy of the system. It provides the input physical parameter as an output electrical signal. According to the sensing mechanism and structure of the temperature sensitive devices, they are grouped as electronic/electrical, electromechanical and resistive/-capacitive sensitive devices [160].

2.11   Light Sensitive Devices

Dyes, such as metal phthalocyanines (MPc) are versatile organic semiconductors, which possess unique electronic absorption characteristics, high thermal stability

along with good environmental stability [161–163]. In this modern era, they can play an important role in electronic industry as light sensitive devices.

Light sensitive devices work on a simple principle in which a ray of light passes through an active thin film, while traveling, it loses energy by dissociating atoms and molecules, which exist in the matter. This happens because the energy of the photons are transferred causing physical/chemical changes in the structure of the film. This brings a change in the dielectric constant of the photo-sensitive organic film. Resultantly, all those characterization in which dielectric constant is used will also change. This allows the translation of light signal into an electrical signal and the device will be referred to as a light sensitive device.

2.12   Summary

This chapter presents a brief overview of organic semiconductor technology and its fundamentals pertaining to organic semiconductor based devices. Developmental history of organic semiconductors as a competitor of inorganic semiconductor has been reviewed. It has been established that organic semiconductors have the potential to substitute inorganic semiconductors, especially in the field of humidity, temperature and light sensitive devices. Furthermore, it has been shown, while reviewing the current state of technology, that organic semiconductors have good potential for LEDs related industry. Electrical response offered by organic semiconductor based devices is either associated with hopping or space charge limited current, the fundamentals of both the mechanisms have been discussed in the chapter.

It has also been discussed that dyes, which can be synthesized in different metallic form (CuPc, NiPc, ZnPc), are very useful organic semiconductors and can be employed to fabricate numerous sensors. Sensitivity of these devices can be further enhanced by investigating both novel design as well as novel composite of dyes.

Chapter 3

Fabrication Techniques and Experimental Setup

This chapter discusses the fabrication techniques employed in organic semiconductor industry and associated setup to characterize finished devices. A step by step procedure to fabricate organic semiconductor devices, such as transistors, diodes and sensors are discussed in detail. In the first part, techniques, such as substrate cleaning, electrodes deposition, thin film depositions, etc. are discussed. In the second part of this chapter, characterization techniques, such as surface morphology assessment, spectroscopy to determine the quality of grown films along with those techniques used to assess the electrical response of organic devices are discussed.

3.1 Substrate Cleaning

The substrate cleaning is one of the main processes to avoid contaminations. Three types of substrates are used in this research. First one was based on ceramic alumina sheet having 14 mm length and 7 mm width. It contains surface-type interdigitated silver electrodes having 0.21 mm interelectrode distance, fabricated by screen printing and followed by chemical etching. Second one was glass slides,

FIGURE 3.1: Plasma etcher used to clean substrate prior to fabrication.

and third one was indium tin oxide (25×25 mm^2, sheet resistance ∼20 Ωsq^{-1}). All of them were first cleaned and the cleaning process for the three substrates was identical. The substrates are cleaned with acetone for 10 min followed by cleaning with ethanol for another 10 min in an ultrasonic bath. Afterwards, they were washed with de-ionized (DI) water and dried with a Nitrogen (N$_2$) blower. Substrates were then processed in an oxygen plasma etcher, shown in Fig. 3.1, for 5 min under a pressure of 1 mbar, and later dried in an oven at 100°C for 1 hour.

3.2 Thermal Evaporation Technique

Thermal evaporation or vacuum evaporation is a widely used technique for thin films deposition [164]. The advantages of thermal deposition include: high quality film with low impurity concentration; high deposition rate and relatively low damage to the substrate because of the low energy of the impinging metal molecules. Following are the three basic physical steps, which were involved in the deposition of thin films using thermal evaporation technique.

(i) Physical generation of individual molecules at the source.

(ii) Transportation of these molecules as a vapor to the substrate.

(iii) Allowing the molecules to deposit on the substrate.

In thermal vacuum evaporation, a stream of molecules is generated by heating the source. The generated molecules, after leaving the source, travel as a molecular flow towards the substrate and other parts of the chamber. There they condensed but those who are deposited on the substrate give a thin layer of film. The thickness and quality of the film is determined by the evaporation rate, evaporation time and vacuum level inside the chamber. The schematic view of a thermal evaporator is shown in Fig. 3.2. The glass substrate was fastened to the sample holder facing a boat in which material, to be evaporated, was placed. In this research, molybdenum boats were used for the evaporation of Al, Ag, Au and NiPc thin films. A shadow mask might be used along the substrate surface if evaporated material patterning is desired. Once the sample was placed in the chamber, the chamber was pumped down to a base pressure of 10^{-6} mbar. Material to be evaporated was heated by a resistive heating source. Film thickness and deposition rate were monitored by a quarts crystal sensor. It is a well known fact that characteristics of a film is affected by deposition rate, pressure during deposition, thickness, angle of evaporation, temperature of the substrate and residual atmosphere. In this research work, Edward Auto 306 thermal vacuum evaporator was used for the deposition of thin films.

3.3 Drop Casting

It is usually entitled as a simple casting technique because of its inexpensiveness and modest form of thin film deposition [165, 166]. A huge area can be deposited by using this technique in a very economical way. Quality of the film attained by drop casting technique is not comparable to that of vaccuum evaporation [167]. But, it is an inexpensive and efficient way and can be employed in those areas where high
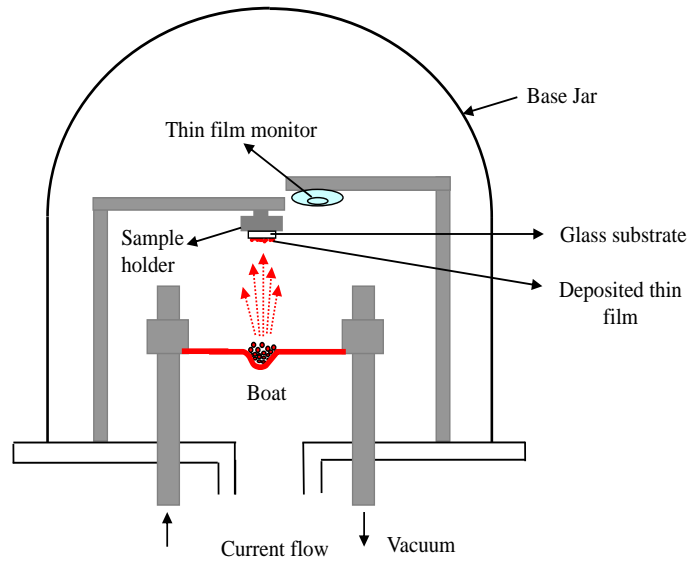
FIGURE 3.2: Thermal vacuum evaporator showing the growth of thin film using thermal evaporation process.

quality film is not a crucial requirement. In this procedure, a liquidified material dissolved in any solvent and solute can be dropped on the substrate as shown in Fig. 3.3. After the evaporation of solvent, a film will be deposited on it. So, many organic-organic or organic-inorganic materials arrangements can be formed by the selection of appropriate solute and solvent. The mixture is transferred on substrate placed on a smooth surface and then left it to dry at room temperature and pressure. In general, one can say that drop casting is a cheap, easy, simple and energy saving technique for the growth of thin films.

3.4   Spin Coating

Spin coater works on the principle of centrifugal acceleration. Spin coating relative to vacuum evaporation is simple, cheap, less time consuming and a reliable technique to get thin films of varying thickness. For deposition of thin films by spin coating, few drops of the solution are placed on the substrate, which is held on the spinner chuck by a vacuum pump. Spinner, while holding the substrate, spins at high speed and spread the solution over the entire substrate leaving behind a thin film. Final film thickness and other properties will depend on the nature of
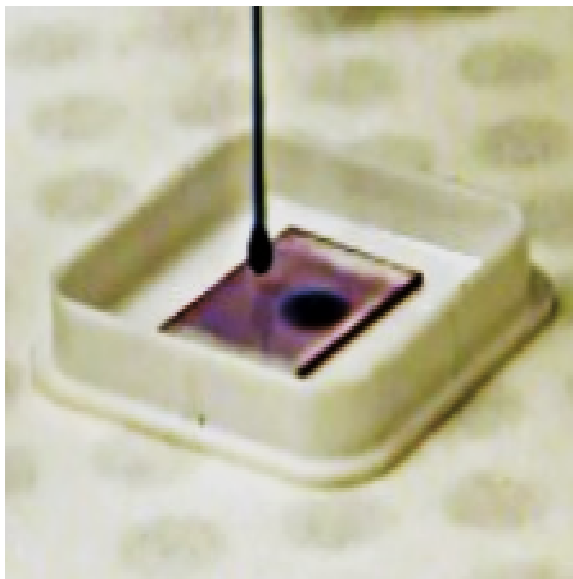
FIGURE 3.3: Drop casting process for the growth of organic thin films.

the liquid (viscosity, drying rate, solid percentage, surface tension, etc.), and the parameters selected for the spinning process, such as rotational speed and acceleration. In this work, spin coater Laurell WS-650-23NPP was used as shown in Fig. 3.4.

3.5 Centrifugal Deposition

Centrifuge is a mechanical device that uses the principle of centrifugal force. It rotates and evaporates the liquid leaving behind deposited thin film. The working principle of centrifugal machine is shown in Fig. 3.5. The acceleration, a of this process can be calculated by using the following equation.

$$a = r\omega^2 \tag{3.1}$$

where r is the radius and ω is the angular velocity.

First of all, a substrate was placed in glass tubes mounted at the arms of centrifugal machine. The diameter and length of the glass tubes were 12 mm and 95 mm, respectively. During deposition of the films, the usual speed of centrifugal machine was set at 5000 rpm. For each experiment, two symmetrically installed glass tubes

FIGURE 3.4: Spin coater (Laurell WS-650-23NPP) top view. It is used for the growth of thin film using centrifugal principle [168].
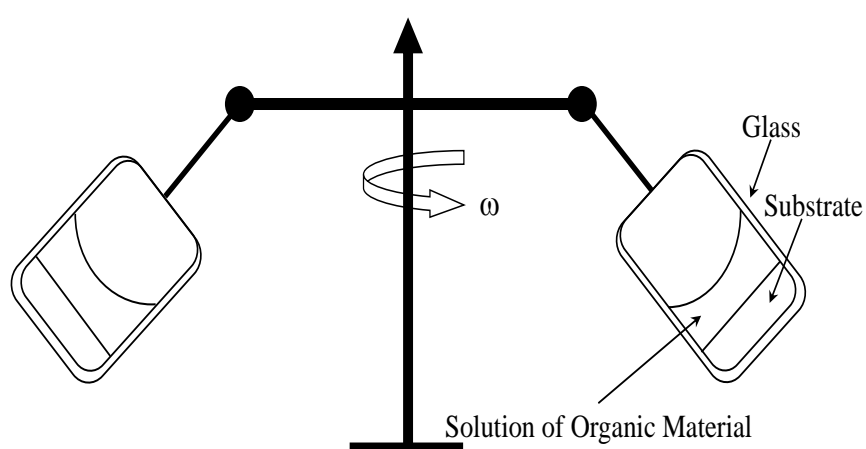
FIGURE 3.5: Working principle of centrifuge having two vessels installed with substrate and solution.

filled with the solution of equal volume were used. During centrifugation process, the solution was allowed to evaporate at room temperature and atmospheric pressure without any additional heating. The films deposition process completed in 30-50 minutes, and the thickness of the film varied between 6-12 μm.

3.6 Characterization Technique

3.6.1 Scanning Electron Microscope

Scanning electron microscope (SEM) uses an electron beam for the assessment of device external structure and surface morphology. SEM uses an electron gun from where an electron beam is radiated, which is then steered by the electromagnetic lenses as shown in Fig. 3.6. Samples are exposed in SEM by the electron beam after its acceleration by a high field inside the column of the SEM. Accelerated electrons release their energy by interacting with the sample due to scattering and random absorption. Absorbed electrons could either be lost inside the sample, or alternatively they can cause secondary electron emission. On the other hand, electrons scattered by the sample will reflect back at various angles and could be detected by a back scattered detector. Both back scattered electrons as well as secondary electrons have information about the sample, which can be detected by appropriate detectors to interpret the information about the sample under investigation. A fundamental principle of SEM is illustrated in Fig. 3.6 in which a column functioning SEM is shown. It is mandatory to have a high vacuum to allow the electrons to travel from the starting location to the targeting sample. That is why the column of SEM has been placed in a vacuum chamber as shown in Fig. 3.6. Immediately after their release, the electrons are attracted by a high voltage anode, shown in Fig. 3.6. The accelerated electrons are then focused by the two lenses shown in the figure followed by a scanning electromagnetic coil, which allows the deflection of the beam to scan the sample. The final lens before the secondary detector is used to eliminate the stigma and to make the electron prob as fine as possible. Traditionally, secondary detector is used for physical characterization
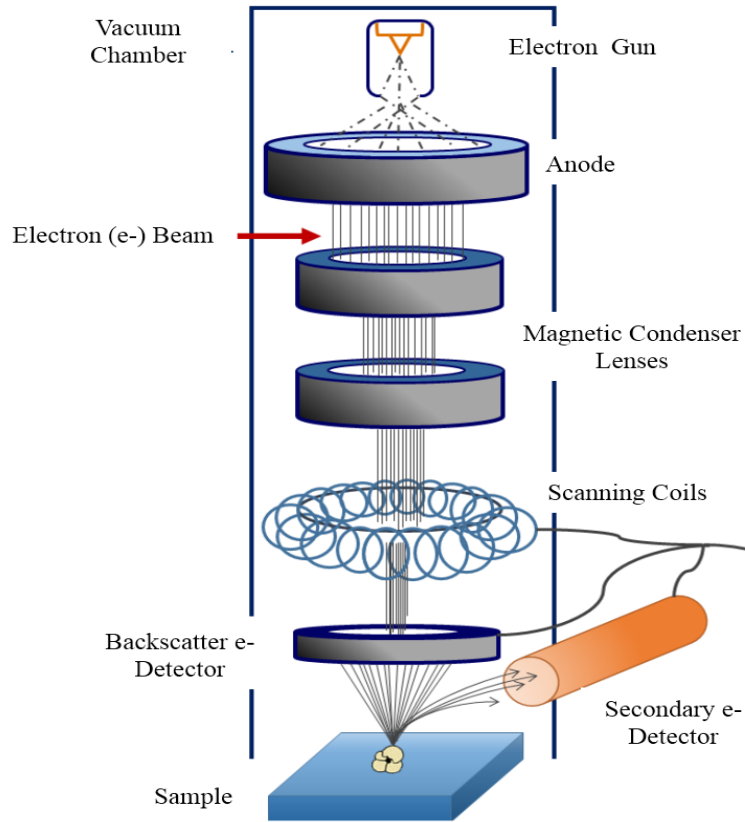
FIGURE 3.6: Fundamental principle of scanning electron microscope [169].

of the sample whereas, back scattered detector is employed when two surfaces having different contrast have to be identified. SEM with good electromagnetic lenses offer resolution as low as $\sim$1 nm. In material characterization, SEM based measurements, after good calibration, are considered to be highly reliable one. To avoid the charging of the sample, especially non-conducting thin films, a thin conducting layer is usually deposited on the sample prior to its characterization. In this study, Philips XL30 scanning electron microscope was used for microstructural analysis as shown in Fig. 3.6.

3.6.2 Atomic Force Microscope

Atomic force microscope (AFM) is one of the primary apparatuses, which can handle measurements and obtain images of samples at atomic level. The working principle of an AFM is explained in Fig. 3.7. Figure 3.7(a) shows that a laser
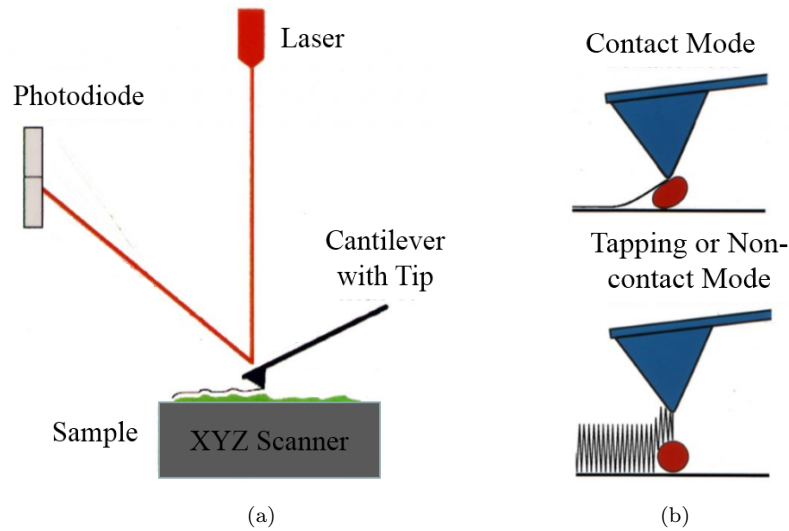
FIGURE 3.7: (a) Fundamental principle of atomic force microscope and (b) AFM image mode [170].

beam is hitting on a tip defining the cantilever and the reflection is then gathered through a detector made by photodiode. While scanning the surface, the angle of tip will vary corresponding to the variation of the surface of the sample causing the incident laser to reflect on different angles, which are then detected by the photo diodes of the installed detector. As shown in Fig. 3.7(a), AFM allows movement of sample in all the three directions, i.e. x, y and z. This results into a 3D image of the sample. Since, AFM is de-coupled from the floor vibration by using a suspension system, therefore, it allows precise 3D imaging upto atomic scale. A mechanical prob is used in AFM to collect the data, and for the collection of data there are two possibilities: in first scenario, a fine prob of AFM is getting the information of the sample by making a physical contact with it; whereas, in the second case, it is transferring the data to the detecting system by maintaining a finite distance from the surface of the sample through an electromagnetic coupling as illustrated in Fig. 3.7(b). In both the cases, whether it is a contact mode measurement or a non-contact mode measurement, the system insures that the surface morphology of the sample shall remain intact. In this research, samples were characterized using a Veeco Dimension 3000 AFM. With the help of this equipment, accurate assessment of the surface morphology, thickness and uniformity were assessed to explain the observed characteristics of various devices.

3.6.3 Ultraviolet-Visible Spectroscope

Ultraviolet-visible spectroscope (UV-Vis) uses light in the visible and its adjacent (near-UV and near-infrared-NIR) ranges. Fundamental ingredients used in the designing of the spectrophotometer are consist of: a light source; a sample holder; a prism (light wavelength separator) and a detector. Dependent upon the design and usage of a spectrophotometer, it can have either single or double beam. In case of a single beam, entire light passes through the sample cell under investigation, and based on the transmission and absorption of the light, spectra results are obtained. These results are then analyzed for the understanding of optical properties of organic semiconductor materials for its potential applicability for opto-electronics. Since, optical characterization is based on absorption or emission of a specific wavelength it is, therefore, considered a highly reliable tool for the understanding of material properties of a sample.

In case of a double-beam, first of all, the light is splitted into two beams by using a beam splitter: one is considered as reference beam; while the other is allowed to pass through the sample. The reference beam intensity is taken as 0 absorbance (or 100% transmission), and the result displayed is the ratio between the intensities of two beams. A double beam technique is efficient in terms of its utility because the data in this technique can be obtained without removing the sample. In the present study, UV-Vis-NIR spectrophotometer Shimadzu UV-3101PC was used, which is a double beam spectrophotometer and its fundamental principle is shown in Fig. 3.8.

3.6.4 Humidity/Temperature Characterization Chamber

Humidity and temperature sensitive devices (transistors, and sensors) were characterized in a chamber fitted with humidity (TECPEL 322) and temperature (FLUKE 87) gadgets. In this chamber, humidity is controlled either by dry N_2 (to decrease humidity) or by wet air (to increase humidity) to get desired humidity level within the range of 0 to 100% RH. The chamber also provided a controlled
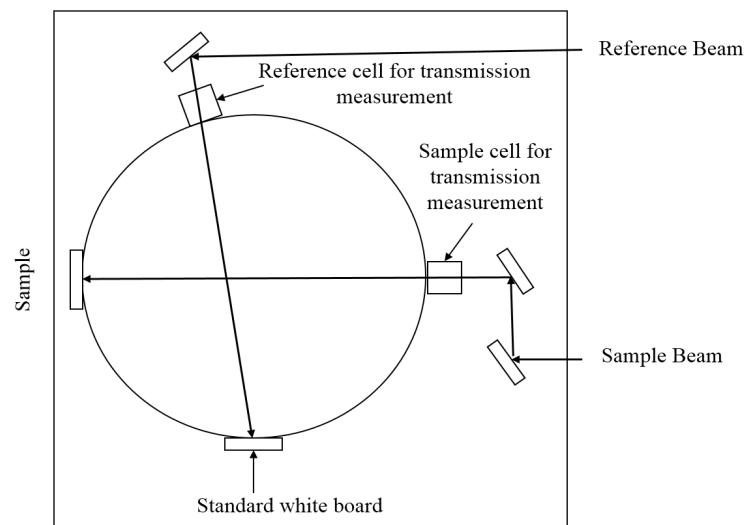
FIGURE 3.8: Fundamental principle of an ultraviolet-visible spectroscope [171].
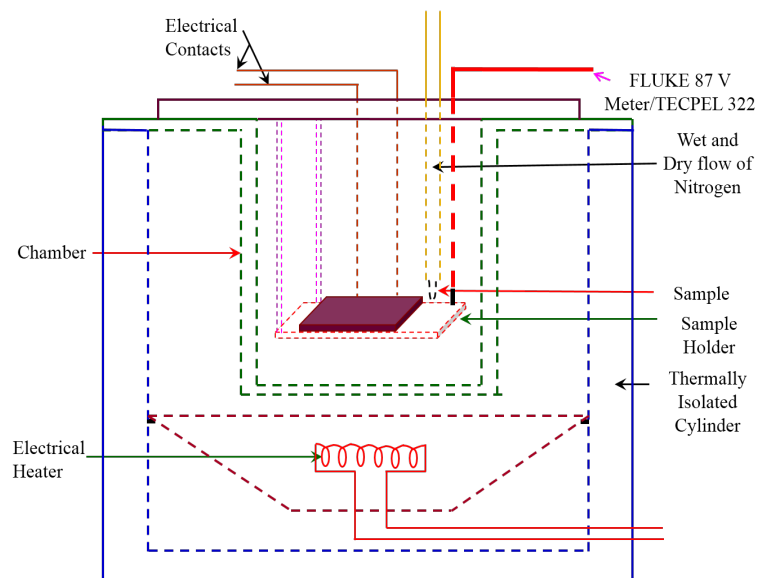
FIGURE 3.9: Humidity/temperature measurement setup.

temperature environment from 20-70 °C, which can be obtained by using an electric heater as shown in Fig. 3.9. The device under investigation was placed inside the chamber, and its impedance and capacitance variations as a function of ambient humidity and temperature were then assessed using an LCR meter (MT 4090).
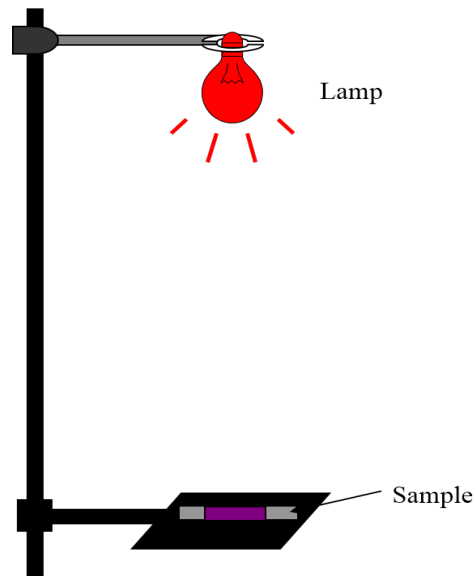
FIGURE 3.10: Optical measurement setup.

3.6.5 Light Characterization Chamber

In case of optical transistors and sensors, the samples were exposed to a filament lamp of 100 W as shown in Fig. 3.10. Different illuminations were obtained by changing the distance between sensor and lamp. The intensity of light was measured by CEM DT-1300 illumination meter.

The absorption spectra was studied to fabricate organic photo diode (OPD) by using a UV-Vis-NIR spectrophotometer (Shimadzu UV-3101PC). The photoluminescence (PL) characteristics were measured by RENISHAW inVia Raman microscope (laser wavelength ∼325 nm). Spectroscopic properties of photo active thin films were measured to asses their suitability for their potential use in organic devices. Photodiode current density-voltage ($J - V$) measurements were estimated in dark and under simulated solar light using computer interfaced Keithley 236 source measure unit (SMU), shown in Fig. 3.11(a), in combination with Oriel 67005 solar simulator, shown in Fig. 3.11(b). Laboratory assembled solar simulator using Xe and Hg(Xe) bulb sourced by NEWPORT 69907 Oriel Digital Arc Lamp Power Supply was used to generate focused light with varied illumination levels .

(a)   (b)
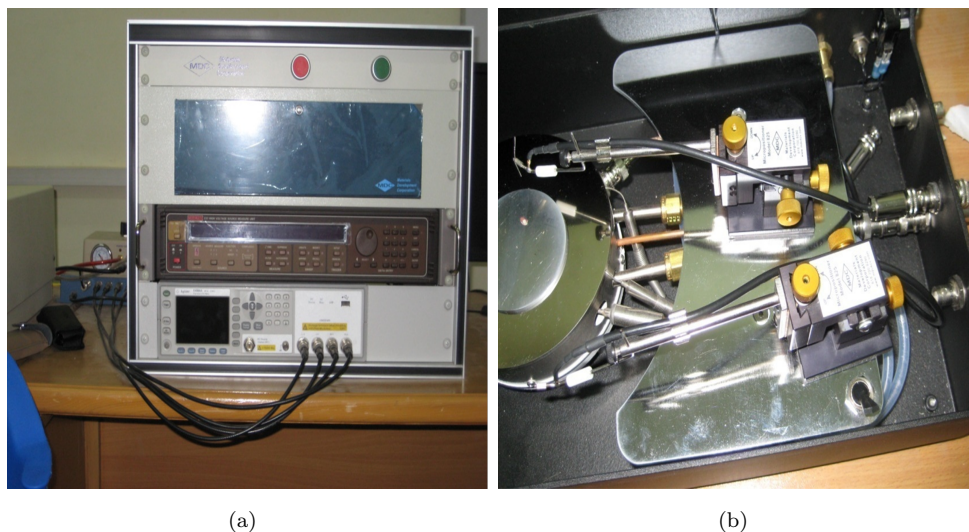
FIGURE 3.11: (a) Keithley 236 source measure unit (SMU) and (b) Oriel 67005 solar simulator.

3.7 Summary

In this chapter, fabrication techniques and experimental setups, which have been employed in this research are discussed. As far as fabrication of any electronic gadget is concern, the main aim would be to get a reliable device capable of translating a physical change into an electrical signal with a high precision. Since reproducibility of a device is mainly dependent upon the environment in which it is fabricated. It is, therefore, emphasized in this chapter that substrate cleaning prior to the device fabrication is of vital importance. The processes, which are involved in the cleaning of a substrate like: surface treatment; plasma etching and ultrasonic bath, etc. are discussed in detail. Fabrication techniques used in organic thin film deposition, for example, drop casting, high vacuum thermal evaporation, spin coating and centrifugation methods are explained with sufficient detail. Merits and demerits of each method are described, so that an appropriate method could be chosen for the fabrication of organic sensors and transistors. Techniques, which can determine the quality of a grown film like scanning electron microscopy (SEM), atomic force microscopy (AFM) and optospectroscopy are described with sufficient detail. The electrical characterization of the finished devices using $I - V$ measurement techniques have also been described in this chapter.

Chapter 4

CuPc Based Humidity Sensors

4.1 Introduction

Phthalocyanines are used as pigments and dyes in automotive paints, printing inks, blue or cyan dyes for textiles and paper industry. Due to their versatile applications, dyes have been the focus of interest in organic semiconductor and photosensitive industries as well. It is an established fact that the structures and properties of organic semiconductors are highly dependent upon their processing technology [172, 173]. Generally, organic materials have a high molecular weight, strong intramolecular but weak van der Waal's intermolecular bonding. Due to these properties, organic semiconductors are found suitable for centrifugal processing [174, 175].

The properties of devices based on metallo-phthalocyanines grown by organic molecular beam deposition (OMBD) technique were investigated by Colesniuc [176]. It was reported by Colesniuc that the conductivity of the grown films increases exponentially with temperature whilst it decreases exponentially with increasing the thickness of the films. Applications of Copper Phthalocyanine (CuPc) include photovoltaic cells, paint, ink, etc. Organic thin-film transistors were also fabricated using CuPc dye with standard vacuum evaporated method [177]. A comparative analysis of I-V characteristics in dark and under illumination showed

49

that the devices were sensitive towards visible light. Their absorption spectra exhibit photo sensitivity in the wavelength ranging from 200 nm to 850 nm. [178], reported preparation and characterization of CuPc nanocrystals embedded into the polymer host and investigated optical absorption spectra of the grown films.

A comparison of electric and optical properties of an organic semiconductor clearly demonstrates an obvious correlation between the activation energy measured by the conductivity-temperature or by the absorption spectra [179]. Similarly, the color of an organic material is dependent on its band gap or activation energy. Encouraged from these characteristics, the colorants films were fabricated especially in an unconventional environment, for example at high gravity conditions, to explore their potential use in the organic semiconductor industry.

Previously, we reported the heterojunctions fabricated under high gravity using p-type Si and thin films of poly-N-epoxypropylcarbazole (PEPC) doped with tetracyanoquinodimethane [145]. The PEPC films were grown on Si wafers at different gravity conditions (i.e., 1 g, 123 g, 277 g and 1,107 g). It was observed that the grown organic polymer films had uniform surface morphology and good adhesiveness on Si substrate. The *I-V* characteristics of the fabricated hybrid structures were evaluated as a function of temperature ranging from 20 °C to 60 °C. It was found that all the samples were p-p isotype heterojunctions. Rectification ratio, threshold voltage, reverse saturation current and junction resistance of the fabricated junctions were evaluated at different temperatures. Later on, a theoretical model has been proposed by [180] by developing a relationship that quantitatively linked the centrifugal time with centrifugal conditions to fabricate high-quality photonic crystals.

In this chapter, in continuation of our efforts pertaining to humidity and temperature sensors [181, 182], humidity-dependent electrical properties of CuPc thin films deposited at different gravity conditions (1 g and 70 g) using the centrifugation technique are presented.
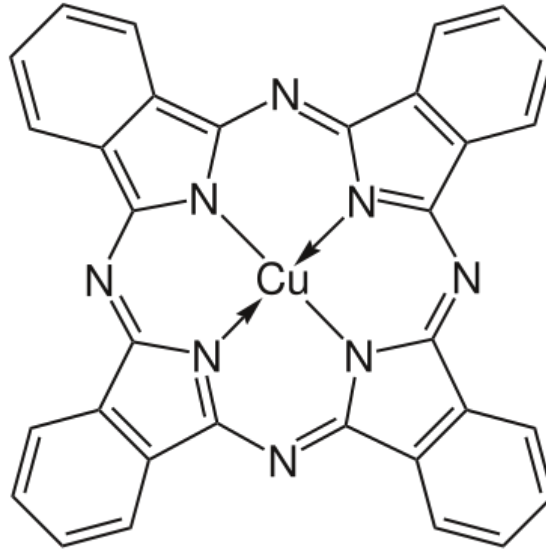
FIGURE 4.1: Molecular structure of CuPc.

4.2 Experimental

For thin film deposition, commercially produced (Aldrich) CuPc ($C_{32}H_{16}CuN_8$) powder was used. Figure 4.1 shows the molecular structure of the CuPc. Its molecular weight is 576.08, and is very stable [183]. It is a photosensitive semiconductor [184] and has broad absorption spectra in visible and partly in UV and IR wavelength regimes [185].

Thin films of CuPc were deposited from a 5 wt.% solution in benzene at normal (1 g) and at high (70 g) gravity conditions. At 1 g, the films were deposited by dropcasting whereas, at 70 g, the films were deposited using a table-top centrifugation apparatus (Model: HETTICH EBA-20 S). The acceleration, a was calculated as:

$$a = r\omega^2 \qquad (4.1)$$

where r is a radius and ω is the angular velocity.

Figure 4.2 shows a schematic diagram of the sample. A 200 nm thick copper films were deposited using the vacuum thermal evaporation technique. The CuPc powder was dissolved in benzene at room temperature. Glass substrates with pre-deposited Cu electrodes having inter-electrode spacing 30-40 μm were placed
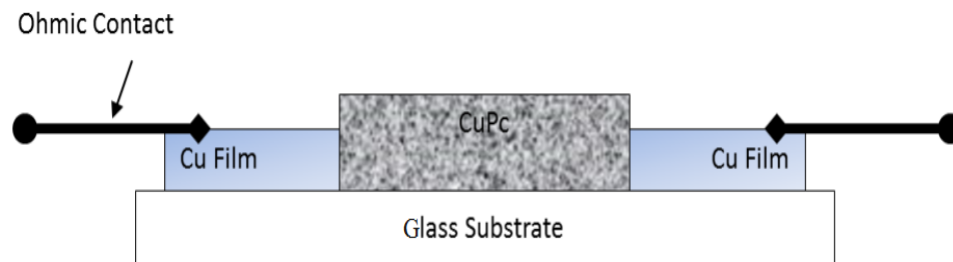
FIGURE 4.2: Schematic diagram of the sample.

inside a glass tube mounted in the centrifugal machine. The diameter and length of the glass tube were 12 mm and 95 mm, respectively. During deposition of the films, the centrifugal machine speed was set at 5000 rpm. For each experiment, two symmetrically installed glass tubes filled with the solution of equal volume of 0.5 ml were used. During centrifugation process, the solution was allowed to evaporate at room temperature and atmospheric pressure without any additional heating. The films deposition process completed in 30-50 minutes, and the thickness of the films varied from 6-12 μm. Impedance and capacitance measurements of the fabricated devices were carried out using LCR meter MT 4090 configured at 1 kHz and 1V. The in-situ humidity was measured using humidity and temperature meter TECPEL 322.

4.3   Results and Discussion

Figure 4.3 shows atomic force microscope (AFM) images of the CuPc films deposited at normal (1 g) and high (70 g) gravity conditions. The figure clearly shows that films grown at 70 g offered smoother surface morphology as compared to films grown at 1 g. Impedance-humidity and capacitance-humidity relationships for CuPc films deposited at 1 g and 70 g are shown in Fig. 4.4(a) and (b), respectively. Experimental results presented in Fig. 4.4 show that films deposited at 1 g exhibited a maximum of 45.4% (ΔZ 100% Z^{-1}) change in its impedance value, whereas in capacitance, the maximum observed change was 26.5% (ΔC100% C^{-1}). On the other hand, films deposited at 70 g showed 42.2% and 15.7% maximum change in their impedance and capacitance values, respectively.

(a)

(b)
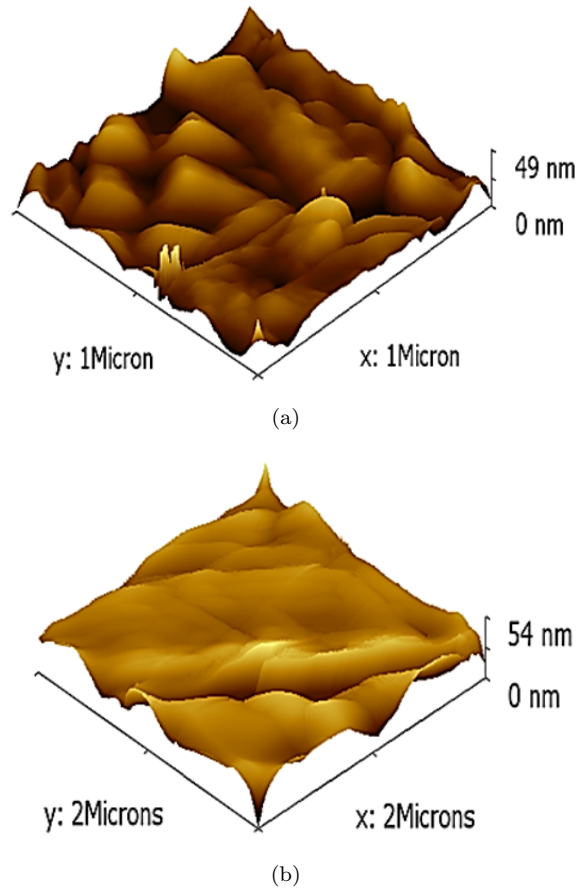
FIGURE 4.3: AFM images of the CuPc films deposited from benzene solution at: (a) 1 g; (b) 70 g.

The impedance (Z) of the samples can be represented by the parallel combination of a resistor (R) and a capacitor (C). From circuit point of view, the magnitude of Z caused by sample resistance and capacitance can be represented as [186]:

$$Z = \frac{R}{1 + j\omega RC} \tag{4.2}$$

Variation in impedance due the varying values of ambient humidity can be associated with adsorption and absorption of water molecules by the CuPc films. As a result of these processes, permittivity of the organic material increases, this in return increases the capacitance of the films, as shown in Fig. 4.4. At the same time, because of the displacement currents related to the movement of bound charges of water molecules, the resistance of the samples may decrease. Finally, as per Eq. (4.2), the impedance of the samples decreases due to the increase of the capacitance and decrease of resistance as a function of ambient humidity as
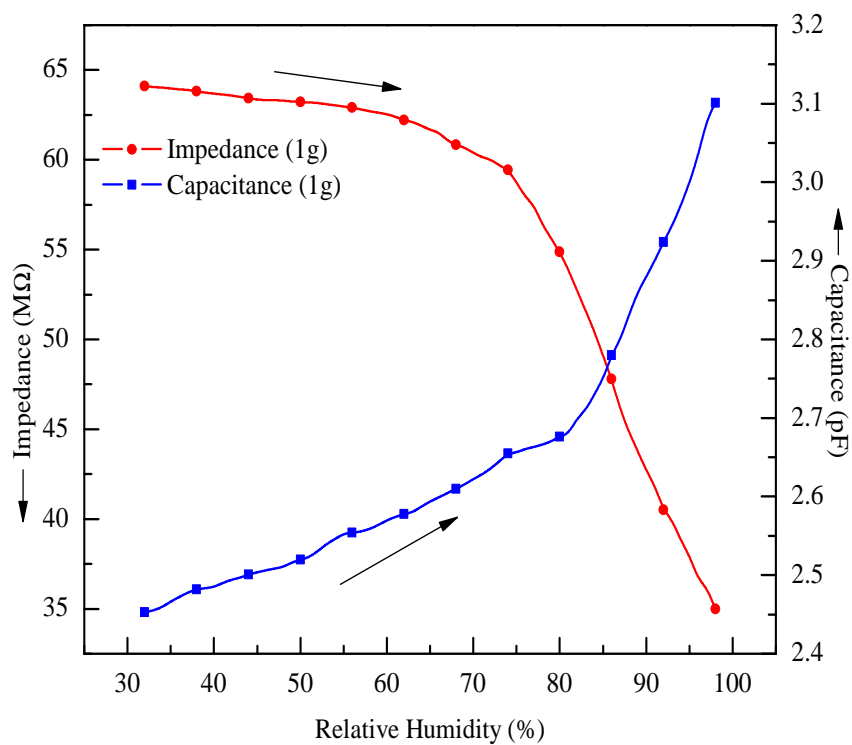
(a)
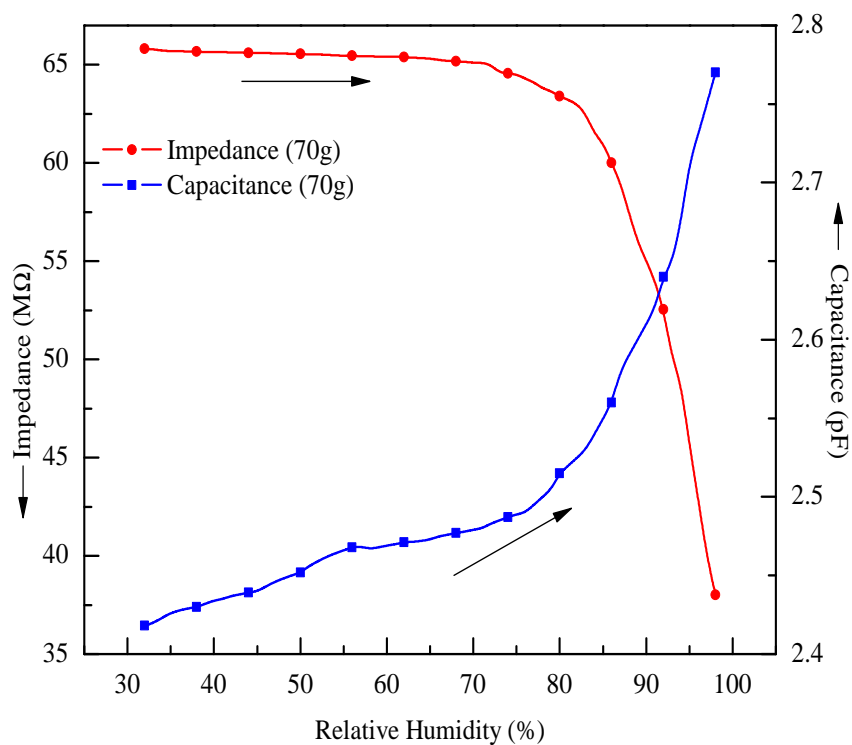
(b)

FIGURE 4.4: (a) Impedance- and capacitance-humidity relationships of CuPc films deposited at 1 *g*. (b) Impedance- and capacitance-humidity relationships of CuPc films deposited at 70 *g*.

observed experimentally.

It is a well-known fact that the value of the capacitance depends on the polarizability of the material, which has several basic sources, i.e. dipolar, α_{dip}, ionic, α_i and electronic, α_e polarizability [187]. In this case, α_{dip} seems to play a dominating role due to the presence of water dipoles absorbed by CuPc. Whereas, α_e is a universal phenomenon and arises due to the relative displacement of the orbital electrons. It is also assumed that CuPc molecules, after interacting with water molecules, may form charge-transfer complexes, which as a result originate α_i. Thus, the total polarizability, which could affect the electrical response of CuPc films would be the sum of all the three components discussed hitherto.

It is assumed that the dielectric permittivity of the CuPc increases due to adsorption and absorption of water molecules, which have higher dielectric permittivity value. The absorption takes place by the diffusion process through the surface of the CuPc films. This increases the capacitance value of the sample. Further, the presence of displacement current caused by the water molecules could also be a source of increased capacitance and decreased resistance values. Moreover, there is also a possibility of CuPc films doping by the absorbed water molecules, which as a result, will increase the polarizability as well as concentration of free charges. Both the processes in return, will enhance the capacitance on one hand and decrease the resistance of the sample on the other hand [188]. For organic semiconductor humidity sensors, impedance-humidity and capacitance-humidity characteristics were simulated by [189]. Their simulation was based on Clausius-Mosotti relationship [187].

$$\frac{\varepsilon - 1}{\varepsilon + 2} = \frac{N_n \alpha_n}{3\varepsilon_0} \tag{4.3}$$

where ε is relative permittivity, N_n is the concentration of water molecules at normal conditions, α_n is the polarizability of dye film due to absorption of water molecules at usual conditions and ε_0 is the permittivity of free space. Considering the proportionality of capacitance with permittivity, we can use the expression
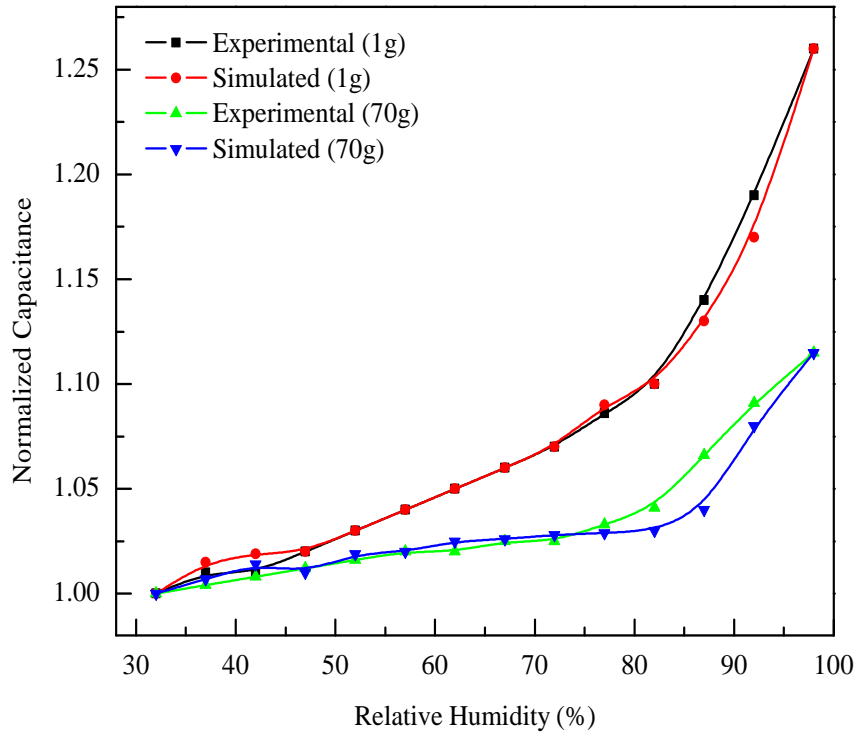
FIGURE 4.5: Comparison of experimental and simulated capacitance of the CuPc films deposited at 1 g and 70 g w.r.t. relative humidity.

presented in [189–191]:

$$\frac{C_H}{C_n} = \left[1 + \frac{2N_n\alpha_n(1 + k\Delta RH)}{3\varepsilon_0}\right] \bigg/ \left[1 - \frac{N_n\alpha_n(1 + k\Delta RH)}{3\varepsilon_0}\right]\varepsilon_0 \qquad (4.4)$$

where C_H represents the capacitance under humid condition and C_n represents capacitance at normal conditions. ΔRH represents a change in relative humidity ($\Delta RH = H - H_0$, initial relative humidity $H_0 = 32\%$ in case of CuPc film and k is a humidity capacitive factor. For dye film, the relative permittivity is assumed to be 4 [192]. The value of k determined by the above expression at $\Delta RH = 66\%$ and $N_n\alpha_n$ was determined from Eq. (4.4). At maximum humidity, experimental value of C_H/C_n was equated to theoretical value and it was found that $k = 0.0858$.

Figure 4.5 shows the comparison of experimental and simulated capacitance versus relative humidity for CuPc samples fabricated at 1 g and 70 g. It can be seen from the figure that the simulated data comply with reasonable accuracy to the experimental characteristics.
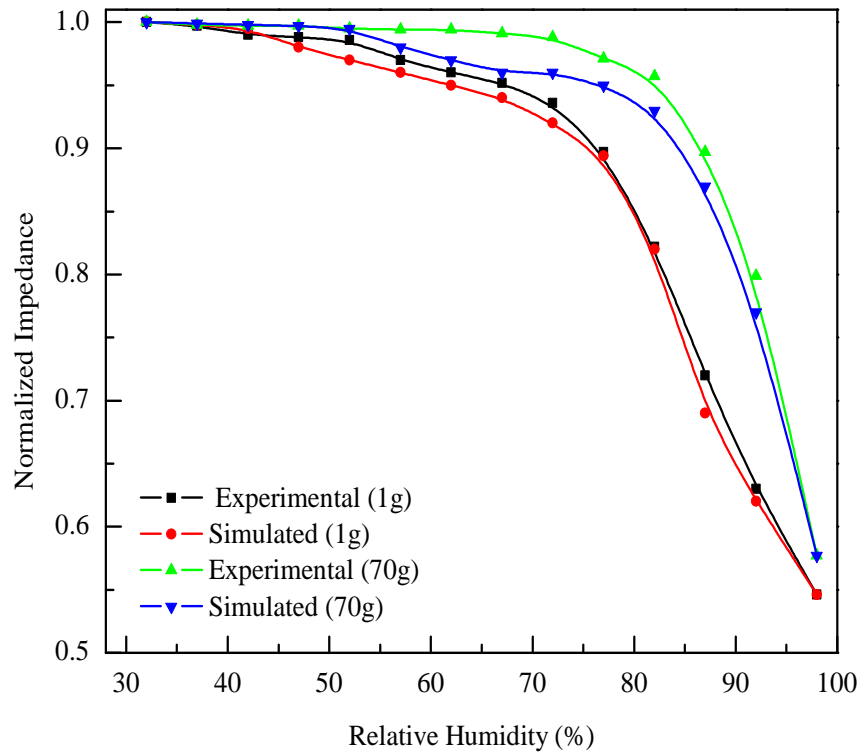
FIGURE 4.6: Comparison of relative experimental and simulated impedance of the CuPc films deposited at 1 g and 70 g with respect to relative humidity.

For simulation of relative impedance vs. humidity characteristics, a simplified expression is proposed as given below:

$$\frac{Z}{Z_0} = \gamma \exp\left[-\frac{H}{H_0}\right]^2 \tag{4.5}$$

where γ is a fitting variable. The simulated impedance-humidity relationship in comparison with experimental results is shown in Fig. 4.6.

The simulated capacitance and impedance results both for 1 g and 70 g samples offer reasonable conformity to the experimental data as evident from Figs. 4.5 and 4.6. The discrepancy in the observed and simulated data of could be associated with the fact that films grown at different gravity conditions may have different structures and compositions with varying percentage of solvent molecules.

Sensitivity (S) of CuPc base humidity sensors can be assessed as [186]:

$$S_Z = \frac{\Delta Z}{\Delta RH} \tag{4.6}$$

TABLE 4.1: Impedance S_Z and capacitance S_C sensitivities of the CuPc samples deposited at 1 g and 70 g.

Sample No.	Material	Deposition	S_Z	S_C
		g	(M $\Omega\%^{-1}$)	(pF $\%^{-1}$)
1.	CuPc	1	0.441	0.010
2.	CuPc	70	0.421	0.005

$$S_C = \frac{\Delta C}{\Delta RH} \tag{4.7}$$

where ΔZ, ΔC and ΔRH are the changes in impedance, capacitance and relative humidity, respectively.

Table 4.1 shows the maximum average values of S_Z and S_C for CuPc samples deposited at 1 g and 70 g. It is evident from Table 4.1 that CuPc films deposited at high gravity are less sensitive to the varied humidity conditions as compared to the films deposited at 1 g.

Presently, researchers are working not only in the area of high gravity processing of semiconductor materials but also in micro-gravity based fabrication. In [143], the properties of tellurium, Te-Se and $Te_{80}Si_{20}$ crystals grown under micro-gravity level and up to 10 g were discussed. In general, the gravity conditions influence upon: (a) defects distribution; (b) conductivity and (c) Hall effect mobility of the grown film.

4.4 Summary

CuPc thin films were deposited at different gravity conditions (1 g and 70 g) from a solution in benzene by using drop-casting and centrifugation. Variation in impedance and capacitance as a function of ambient humidity levels was assessed. It was noted that impedance of CuPc thin films decreases, whereas their capacitance increases with increasing values of ambient humidity. Samples fabricated at 1 g exhibited a maximum change of 45.4 and 26.5% in their impedance and capacitance values, respectively, whereas samples grown at 70 g demonstrated a

maximum change of 42.2 and 15.7% in their impedance and capacitance values, respectively. The observed response was also simulated, and a plausible explanation was presented. It was demonstrated that the humidity-dependent electrical performance could be associated both with increased polarization and increased doping concentration caused by absorbed water molecules. It was further shown that CuPc films can potentially be used as a humidity-sensing material whose sensitivity would be dependent on the chosen fabrication parameters.

Chapter 5

NiPc Based Humidity Sensors

5.1 Introduction

Humidity sensors play an important role in today hi-tech era, especially in the field of metrology and environmental assessment [193–198]. On the basis of their measuring standards, humidity sensors are categorized as resistive, capacitive, gravimetric, or hydrometric [158]. To fabricate a humidity sensor, diverse methodologies and materials have been reported in the literature [199]. A plainer construction of capacitive humidity sensors, using phthalocyanine films was reported in [6]. Humidity effects on electrical conductivity of carbon nanotubes (CNTs) were studied by many researchers, and it has been reported that the water molecules act as a donor and modify the electrical properties of single-walled carbon nanotubes (SWNTs) [200]. Whereas, investigation pertaining to the electrical transportation of double-walled carbon nanotubes (DWNTs) showed that water molecules act as an acceptor in DWNTs [201]. Humidity sensors, based on Ce-doped nanoporous ZnO, Fe_2O_3 and polyaniline were also investigated and reported in [110, 202, 203]. As a result of these investigations, it can be said that different materials with different compositions have a useful potential for humidity sensing applications.

Nickel phthalocyanine (NiPc) is an organic semiconductor that was considered a promising phthalocyanine for optoelectronic devices and gas sensing applications [204–213]. NiPc has a charge carrier mobility of 0.1 $cm^2(Vs)^{-1}$, which is 1000 times greater than copper phthalocyanine (CuPc) [211]. Its energy bandgap is 2.24 eV and 3.2 eV for indirect and direct allowed transitions, respectively [214]. Zubair [151] and Shah [215] fabricated and investigated NiPc based Schottky barrier diodes, and their studies confirmed the potential of NiPc as an organic semiconductor material to be used in electronic devices and sensors technology.

It is an established fact that the performance of organic semiconductor devices is heavily dependent on the chosen technology. Thin films of organic semiconductors, which usually act as a conducting channel, can be deposited by: a) vacuum evaporation; b) drop-casting or c) spin-coating. At the same time, in the recent past, organic semiconductor thin films deposition by centrifugation at high gravity was also reported. In [145], heterojunctions of silicon and thin layer of poly-Nepoxypropylcarbazole with tetracyanoquinodimethane (TCNQ) impurities were fabricated. The poly-N-epoxypropylcarbazole films on silicon wafers were deposited at normal temperature, but at various gravity conditions: 1 g; 123 g; 277 g and also at 1107 g. A smooth layer and strong adhesiveness was obtained by this process of deposition. Current-voltage characteristics of the deposited hetrostructures as a function of temperature ranging from 20-60 °C were assessed. It was observed that almost every sample exhibited p-p isotype heterojunctions. Temperature dependent junctions parameters such as reverse saturation current, rectification ratio, junction resistance and threshold voltage were measured.

In 2009, Tahir et al. [216] manufactured many organometallic vanadium complexes such as VO_2(3-fl), $VO(PBO)_2$ and VO(DBM), and deposited the thin films by centrifugation process at 183 g, 733 g and 1650 g. As a result, sandwich type samples were fabricated based on Al/VO_2(3-fl)/Ga, Cu/VO_2(3-fl)/Ga, Al/-Vanadyl(acac)/Ga, Cu/Vanadyl(acac)/Ga, Al/$VO(PBO)_2$/Ga, Cu/$VO(PBO)_2$/Ga, Al/VO(DBM)/Ga, Cu/VO(DBM)/Ga, Al/Vanadyl(acac)/TiO_2/Ga, and Cu/VO_2(3-fl)/TiO_2/Ga. Current-voltage characteristics of the finished devices showed non-linear rectification behavior. Samples fabricated using VO_2(3-fl) and Vanadyl(acac)

showed switching effect. These samples also exhibited two distinct conductance states referred to as low and high conductance states. Such behavior is typically known as memory cell characteristics of the type called as write-once-read-many-times (WORM). It is worth mentioning that memory cell characteristics were observed only in those devices which were fabricated using Cu electrodes.

This chapter deals with fabrication and characterization of NiPc based humidity sensors and their optimization as a function of fabrication parameters. Finished devices were characterized using a humidity chamber fitted with LCR meter to assess the change in the device impedance and capacitance by varying ambient humidity. The composition of the rest of the chapter is that Section-2 deals with experimental techniques used to fabricate NiPc thin films sensors at 1 g and also at 70 g. Section-3 describes experimental results and their plausible explanation followed by the summary drawn from this study.

5.2 Experimental

Figure 5.1 illustrates molecular structure of NiPc organic semiconductor. For thin films deposition, commercially available NiPc ($C_{32}H_{16}N_8Ni$) of Sigma-Aldrich was used. The thin layers of NiPc were deposited from 5wt.% of its solution in chloroform at normal (1 g) and high (70 g) gravity. The films were deposited at 1 g by drop-casting and at 70 g by centrifugation in a table-top centrifuge HETTICH EBA-20 S. Acceleration (a) was calculated by using Eq. (5.1).

$$a = r\omega^2 \tag{5.1}$$

where r is a radius and ω is the angular velocity.

Figure 5.2 shows schematic diagram of the substrate used for the deposition of NiPc thin films. It is made of ceramic alumina sheet having 14 mm length and 7 mm width. It contains surface-type interdigitated silver electrodes having 0.21
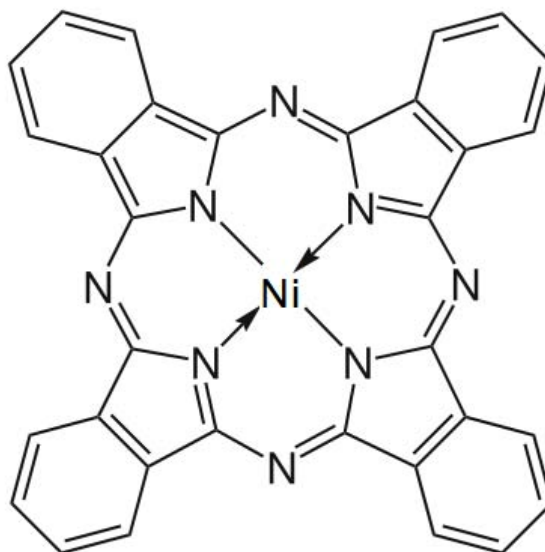
FIGURE 5.1: Molecular structure of NiPc organic semiconductor.
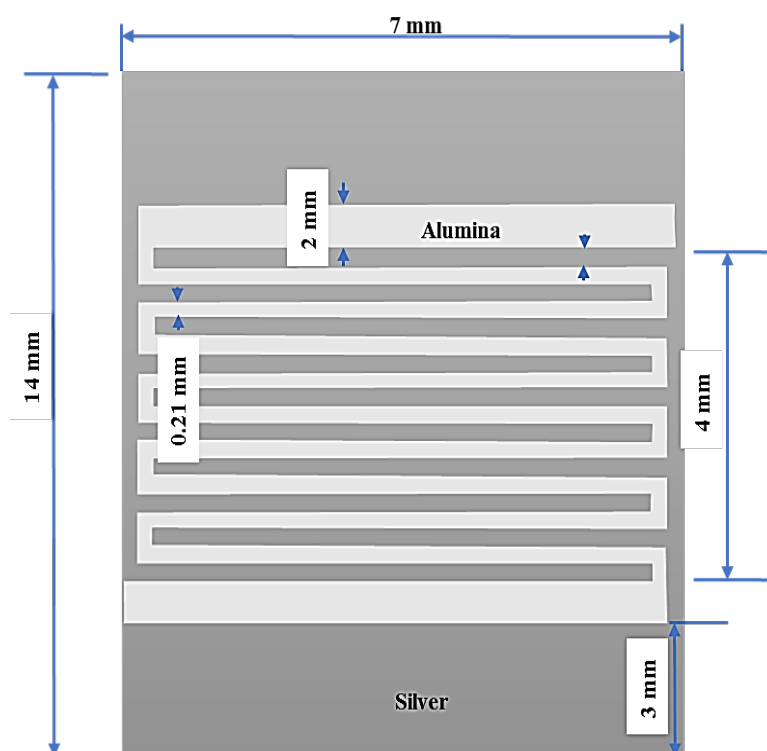
FIGURE 5.2: Ceramic alumina substrate with surface type silver electrodes.

mm interelectrode distance, fabricated by screen printing and followed by chemical etching [202].

During centrifugation process, each experiment was performed using two symmetrically installed glass tubes filled with equal volume of solution (0.5 ml). The tube
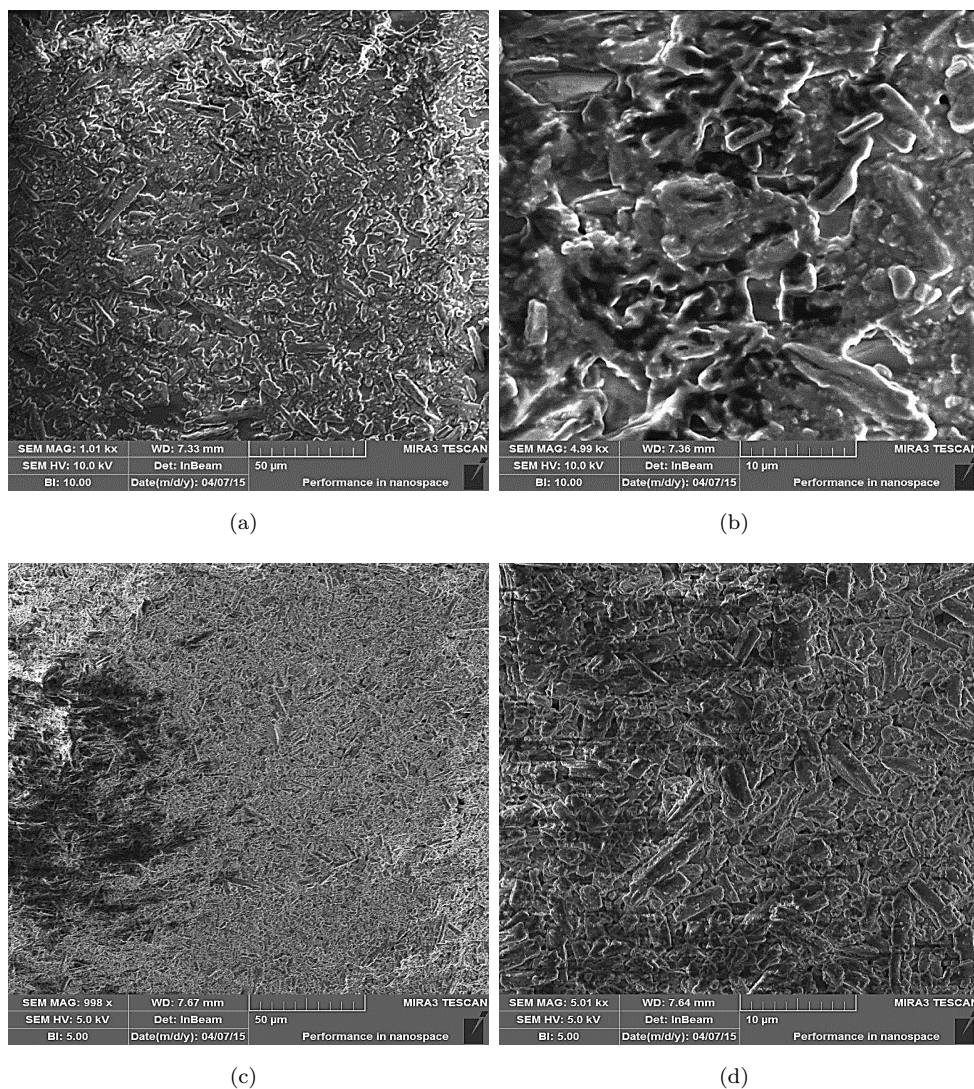
FIGURE 5.3: SEM images of the NiPc films deposited at 1 g (a) 50 μm and (b) 10 μm and 70 g (c) 50 μm and (d) 10 μm.

has internal diameter of 12 mm and length of 95 mm. The centrifuge's rotation speed was set at 5000 rpm. The deposited NiPc films thickness were in the range of 7-10 μm. It was observed that the layers achieved at 1 g were usually thicker compared to those grown at 70 g, which means the acceleration and thickness have an inverse relation. The same behavior was observed and reported in [145, 148].

As a rule in the centrifugal procedure, evaporation of the solution was done at room temperature and atmospheric pressure. At centrifugation, the thin films deposition times were equal to 10-15 minutes. Figure 5.3 shows SEM images of the NiPc films deposited at 1 g and 70 g from solution prepared in chloroform.

The obtained SEM image of the NiPc films showed that the films deposited at 1 g seems to be more uniform and smooth but with larger grain size. On the other hand, SEM images of the films deposited at 70 g showed relatively rough surface morphology, but with smaller grain size. The impact of roughness of the films and unit grain size on the humidity sensing properties is discussed in Section 3. Electrical properties of the sensors have been investigated as a function of ambient humidity. For measurements of impedance and capacitance of the samples, LCR meter MT 4090 was used at frequency and voltage level of 1 kHz and 1V.

5.3   Results and Discussion

Figure 5.4 (a) shows impedance-humidity and capacitance-humidity relationships for NiPc samples deposited at 1 g by drop-casting. It can be seen that impedance decreases 1.5 times and capacitances increases 1.1 times with the increase in humidity 25% to 95%. Figure 5.4 (b) shows impedance-humidity and capacitance-humidity profiles for NiPc samples deposited at 70 g by a centrifugation process, respectively. In the figure, the impedance of the sample is shows 1.8 times decrease in its magnitude while changing the humidity in same range; whereas, for the same change in humidity the capacitance exhibited an increase of 1.5 times with respect to its initial values.

The impedance-humidity and capacitance-humidity relationships shown in Fig. 5.4 can be modeled by placing a resistance (R) and a capacitance (C) in parallel [186, 217, 218], and can be calculated by using Eq. (5.2).

$$Z = \frac{R}{1 + j\omega RC} \tag{5.2}$$

Their simulation was based on Clausius-Mosotti relationship [187].

$$\frac{\varepsilon - 1}{\varepsilon + 2} = \frac{N_n \alpha_n}{3\varepsilon_0} \tag{5.3}$$
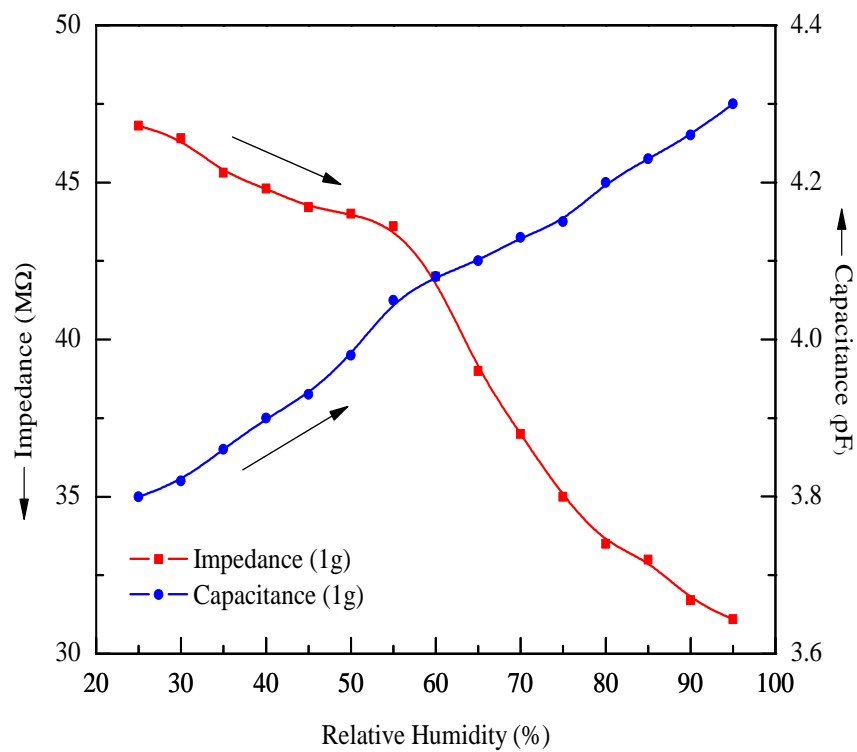
(a)
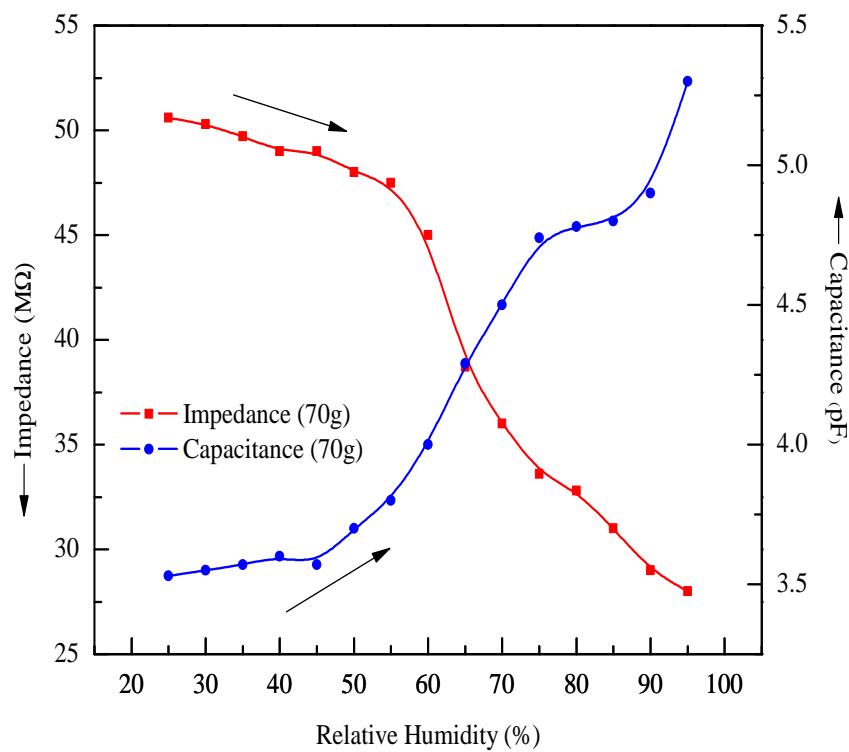
(b)

FIGURE 5.4: Impedance- and capacitance- relative humidity relationships for the NiPc samples deposited at (a) 1 *g* and (b) 70 *g*.

where ε is relative permittivity, N_n is the concentration of water molecules at normal conditions, α_n is the polarizability of dye film due to absorption of water molecules at usual conditions and ε_0 is the permittivity of free space. Considering the proportionality of capacitance with permittivity, we can use the expression presented in [189–191]:

$$\frac{C_H}{C_n} = \left[1 + \frac{2N_n\alpha_n(1 + k\Delta RH)}{3\varepsilon_0}\right] \Bigg/ \left[1 - \frac{N_n\alpha_n(1 + k\Delta RH)}{3\varepsilon_0}\right]\varepsilon_0 \qquad (5.4)$$

The evaluated value $N_n\alpha_n$ can then be used in Eq. (5.3) and assuming $C_H/C_n = 1.13$ at $RH = 95\%$, the value of k is found to be $0.013\%^{-1}$. Thus, Eq. (5.4) can be used in first approximation to simulate the capacitance-humidity response of NiPc sample. Similarly, the effect of humidity to impedance and capacitance of the NiPc samples can be estimated by the sensitivity S_Z through Eq. (5.5) and S_C by using Eq. (5.6).

$$S_Z = \frac{\Delta Z}{\Delta RH} \qquad (5.5)$$

$$S_C = \frac{\Delta C}{\Delta RH} \qquad (5.6)$$

where ΔZ, ΔC and ΔRH are the changes in impedance, capacitance and relative humidity, respectively. It can be shown that in average $S_Z = -0.32$ MΩ $\%^{-1}$, $S_C = 0.025$ pF $\%^{-1}$ for samples deposited at 70 g, and $S_Z = -0.22$ MΩ $\%^{-1}$, $S_C = 0.007$ pF $\%^{-1}$ for samples deposited at 1 g, at frequency of 1 kHz. The effect of humidity to impedance and capacitance of NiPc samples can be potentially used for fabrication of humidity sensors and they can be implemented in humidity meters for environmental monitoring and assessment.

To evaluate the dynamics of the water vapor absorption and desorption processes of NiPc samples, the average response and recovery time were evaluated by impedance-time measurements at the change of the humidity from 25% to 95% and from 95% to 25% and they are found to be 1.0 minute and 2.5 minutes, respectively. The response and recovery times were measured accordingly at the

change of impedance from 90% to 10% of maximum impedance and from 10% to 90%.

5.4   Summary

In this study, thin films of Nickel Phthalocyanine (NiPc) were deposited by centrifugation at high gravity (70 g), and also at normal gravity (1 g) conditions to fabricate humidity sensors. Ceramic alumina sheet, coated with silver electrodes, having interelectrode distance of 0.21 mm were used to assess the electrical properties of the sensors. Room temperature capacitance and impedance variations were measured as a function of relative humidity ranging from 25%-95% at 1 kHz frequency. It was observed that sensors fabricated at 70 g were more sensitive compared to sensors fabricated at 1 g. Sensors fabricated at 70 g exhibited 1.8 times decrease in their impedance and 1.5 times increase in their capacitance at peak ambient humidity. SEM images showed more roughness for the films deposited at 70 g compared to films deposited at 1 g. It was assumed that surface irregularities might have increased active surface area of 70 g sensors hence changed the electrical response. Impedance-humidity and capacitance-humidity relationships were modeled and a good agreement was observed between experimental and modeled data. Experimental data showed that NiPc films could be useful for instrumentation industry to fabricate organic humidity sensors.

Chapter 6

VOPcPhO-Alq$_3$ Based Humidity Sensors

6.1 Introduction

Over the last couple of decades, researchers in the field of sensors have been attracted to the field of organic based sensing devices due to their low production cost, simple and easy fabricating technologies, and their multi-functionality over a single substrate. Organic materials are very sensitive towards moisture and are good applicants to fabricate sensors for humidity measurements [172, 173, 219, 220]. In order to employ a humidity sensor in a wide range of applications, it must possess superior sensitivity, slight hysteresis, short response time, adequate durability, and a low manufacturing cost [221, 222]. However, in the current scenario, researchers are struggling to introduce correct material combinations, which possess outstanding properties of superior sensitivity and stability, while preserving a low manufacturing cost, a moderately simple processing method, and eco-friendly techniques [220, 223–225]. Even though, researchers have managed to introduce various simple fabricating processes, which can be coupled with physical and chemical flexibility from polymer organic-based materials, mass production of

these types of sensing devices seems promising only once their other limitations have been overcome.

Humidity is a universal phenomenon because of the general presence of moisture contents in air. Control or measurement of humidity is becoming more important, not only for human well-being but also for various industrial applications such as meteorology, process control techniques, agriculture, and medical equipment. Based on requirements or applications, various kinds of humidity sensors are used and they can be classified based on their sensing mechanisms. Humidity sensors based on inorganic materials [226, 227] are costly, and require high power for operation, whereas organic material-based humidity sensors have advantages of low cost, light weight, flexibility, and simple technology.

Even though, organic materials are highly responsive to humidity, many of them are easily dispersed in water, which makes them impractical in highly humid conditions [6, 228]. Among organic materials, the phthalocyanines group has hydrophobic properties and is insoluble in water and hence, is considered as a good candidate for humidity meters [229]. Phthalocyanines are macro-cyclic and hetero-cyclic compounds, which exhibit a ring structure containing nitrogen atoms in addition to carbon as a part of the ring. Most phthalocyanines are considered as p-type semiconductors [230] and they possess sufficiently good charge carrier mobility [231] and significant conductivity for utilization in potential applications with organic electronic devices. Among the phthalocyanines, VOPcPhO is available as a green colored dye that is insoluble in water. It exhibits very good chemical and environmental stability and has been extensively studied for various types of sensors [220, 232–235], whereas Alq₃ is a pi-conjugated small molecular material [236]. In pi-conjugated materials, single and double or single and triple bonds alternate throughout the backbone of a molecule. The second and third bonds of a double or triple bond are pi-bonds [237]. The gap between LUMO and HOMO is typically in the 1.5-3 eV range, i.e., the materials are organic semiconductors [237]. Even though Alq₃ is mostly utilized as an exciton blocking layer and a light emitting layer in photovoltaic applications, it can be utilized to obtain a high-quality thin film with high electron mobility by a simple spin-coating method [226].

In this chapter, the compositional engineering of the pi-conjugated small molecular VOPcPhO : Alq$_3$ complex was performed to develop a sensitive humidity sensor with a linear response. The bulk heterojunction of the two materials was expected to have the characteristics of the both components and is assumed to be more linear in response towards humidity than VOPcPhO and more sensitive than Alq$_3$ alone. The aim of this research is to boost the humidity sensing potential of VOPcPhO by making its complex with Alq$_3$ to develop a cheap and reliable sensing element for assessing humidity in the surrounding environment.

6.2   Experimental

Tris-(8-hydroxyquinoline)aluminum (Alq$_3$) and vanadyl 2,9,16,23-tetraphenoxy-29H,31H-phthalocyanine (VOPcPhO) were purchased from Sigma-Aldrich (USA). Figures 6.1 (a) and (b) shows their molecular structures, respectively. Surface type humidity sensing devices were fabricated from glass slides which were cleaned with acetone for 10 min followed by cleaning with ethanol for another 10 min in an ultrasonic cleaner. Afterwards, the slides were washed with distilled water and dried with a N$_2$ blower. Then the substrates were processed in an oxygen plasma etcher for 5 min under a pressure of 1 mbar followed by an additional 5 min plasma cleaning in 10^{-3} mbar pressure inside a vacuum thermal evaporator. Later, 100 nm thick aluminum electrodes were deposited with equal inter-electrode gaps of 40 μm, over which the active layers were deposited using a spin coater (Laurell WS-650-23NPP) at 2500 rpm and an acceleration of 500 ms^{-2}. Al/active layer/Al sensors consist of stand-alone films of VOPcPhO and Alq$_3$ plus their composite in various proportions (i.e. 2:1, 1:1 and 1:2). Samples were assessed in the setup of a humidity controlled chamber as shown in Fig. 6.1 (c). Thicknesses of thin films were in the range (composite-raw material) of ∼200 nm measured by a KLA-TENCOR P6 Surface Profiler. The devices were annealed at different temperatures, i.e. 75, 100, and 125 °C for 20 min and then cooled down gradually by WiseStir heating. For capacitance-relative humidity and resistance-relative

(a)

(b)

(c)
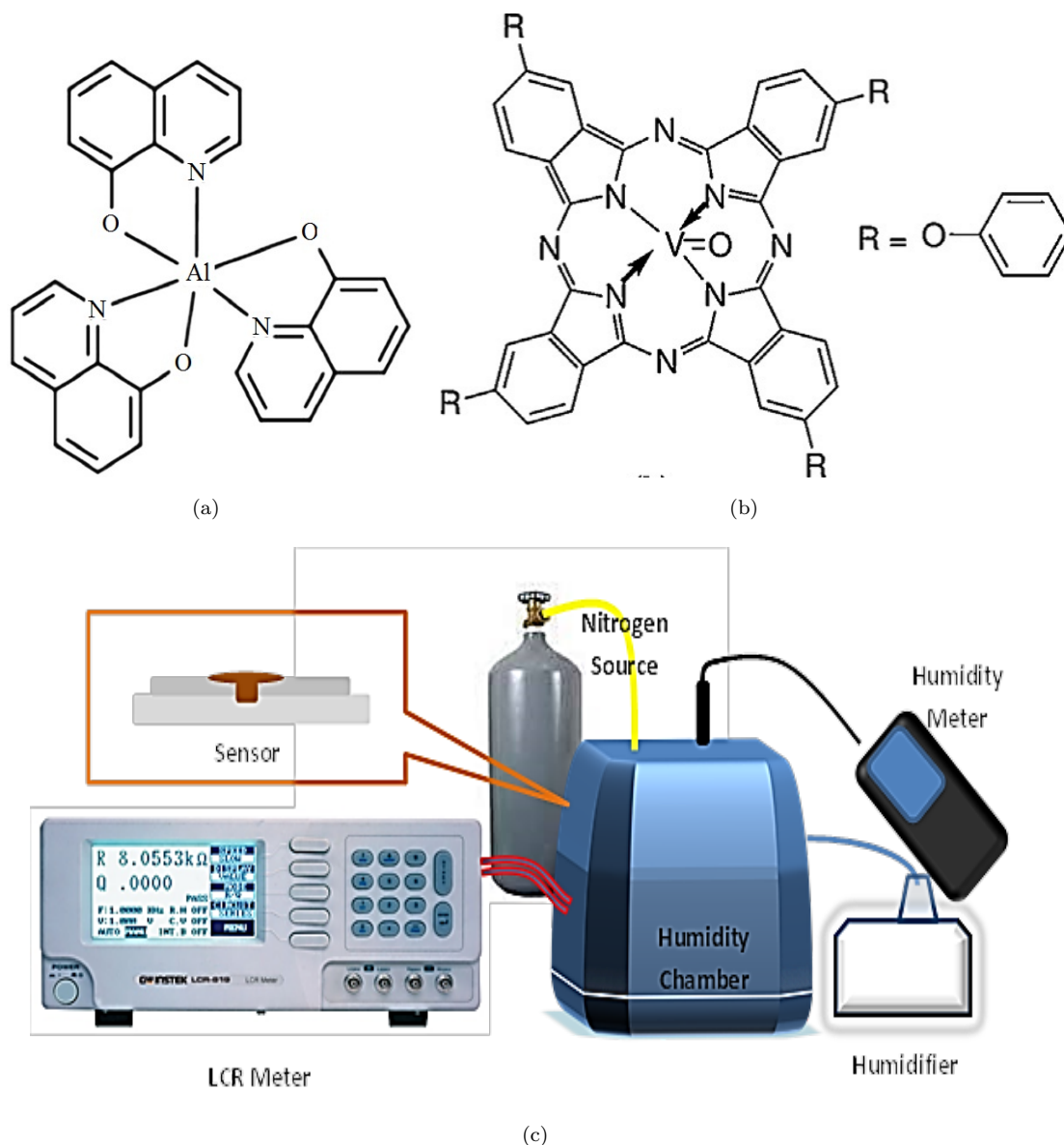
FIGURE 6.1: The molecular structure of (a) tris-(8-hydroxyquinoline)aluminum (Alq$_3$) and (b) vanadyl 2,9,16,23-tetraphenoxy-29H,31H-phthalocyanine (VOPcPhO), and (c) setup of the humidity chamber and schematic diagram of surface type sensors.

humidity measurements a INSTEK LCR-819 meter was used. A Veeco Dimension 3000 AFM was utilized to measure surface morphology of the organic thin films. Sensors were characterized for their humidity response, w.r.t capacitance, and resistance.

6.3 Results and Discussion

A well-organized study was carried out to optimize various parameters, including the composition and annealing temperature of VOPcPhO, Alq$_3$, and VOPcPhO : Alq$_3$ composite humidity sensors. Capacitance measurement was recorded at 100 Hz, 1 kHz and 10 kHz and the frequency-capacitance response of both VOPcPhO and Alq$_3$ are presented in Fig. 6.2. Best optimal composition of VOPcPhO : Alq$_3$ was V$_1$: A$_2$ selected on the basis of results presented in Fig. 6.3.

Capacitance responses of the fabricated sensors toward changes in relative humidity levels are shown in Fig. 6.4. The humidity dependent sensitivity of the sensors was investigated with respect to variation in RH % from 15 to 95 % at different annealing temperatures, i.e., 25, 75, 100, and 125 °C to obtain the best optimized device. We observed that the best sensitivity in the case of Alq$_3$ was obtained at 125 °C and at this temperature the sensitivity was 0.3125 pF RH $\%^{-1}$ as shown in Fig. 6.4(a). The device is more responsive in the range of 35-95% RH. On the other hand, Fig. 6.4(b) shows results of the VOPcPhO devices, which were also annealed at different temperatures for the same time, and these samples exhibit sensitivity in the range of 55-95% RH. The VOPcPhO showed higher sensitivity at 25 °C (1.06 pF RH $\%^{-1}$) as compared to other annealing temperatures. While the best concentration of VOPcPhO : Alq$_3$ was found as 1 : 2 (V$_1$: A$_2$). The V$_1$: A$_2$ based devices were also annealed at different temperatures and their most sensitive response was found to be 0.32 pF $\%^{-1}$ at 75 °C. The most responsive behavior of the device is seen from 40 to 95% RH as shown in Fig. 6.4(c). It is important to note that the Alq$_3$ exhibits a more linear response than the VOPcPhO, whereas the VOPcPhO exhibits more sensitivity at higher humidity levels as compared to the Alq$_3$. Hence, to retain greater sensitivity at higher *RH* levels, the ratio V$_1$: A$_2$ was selected. Both these properties are very important for a good sensor. The bulk heterojunction of both materials is expected to consist of both characteristics and is assumed to be more linear than VOPcPhO and more sensitive than Alq$_3$ alone.
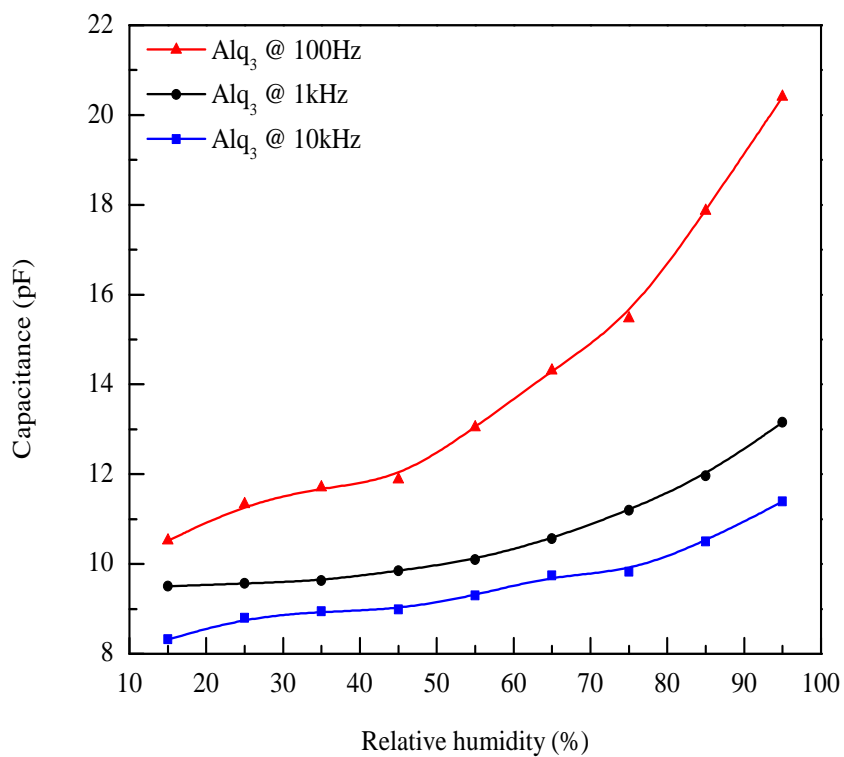
(a)
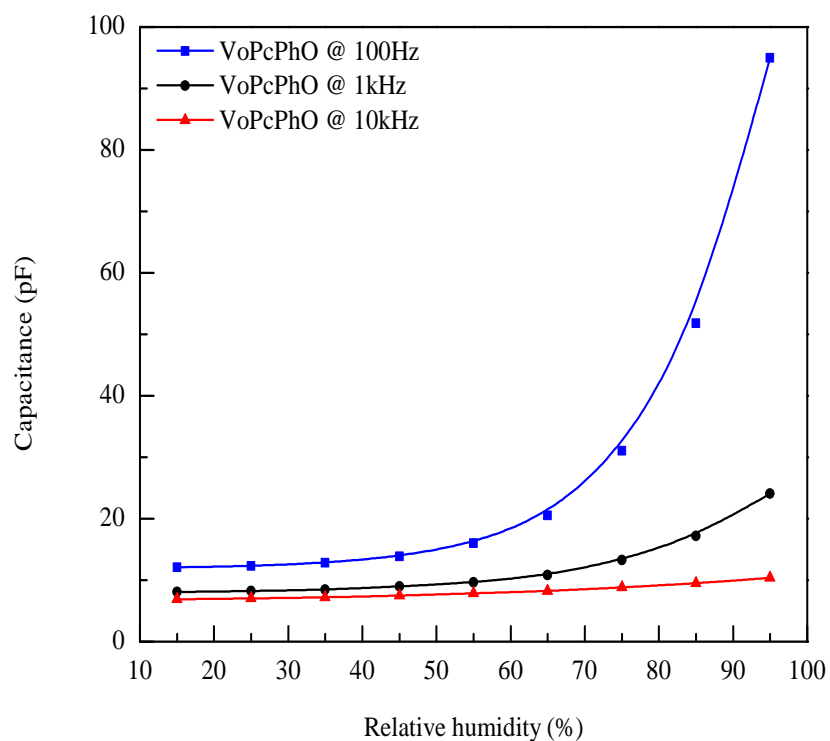
(b)

FIGURE 6.2: Dynamic variation of (a) Alq₃ and (b) VOPcPhO Capacitance to Relative Humidity at different frequencies.
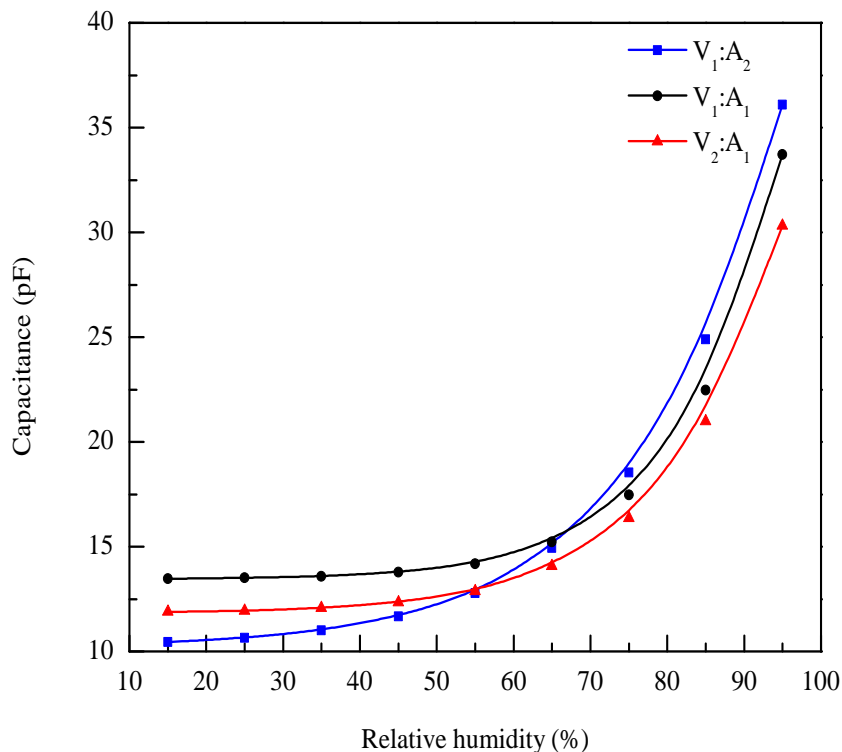
FIGURE 6.3: Dynamic variation of different composites (VoPcPhO:Alq$_3$) Capacitance to Relative Humidity at 100Hz and 25 °C.

Many factors, including porosity of the sensing films, dielectric constant, the materials dynamic sensing area, and polarizability, significantly participate in capacitance and resistance variation in response to ambient relative humidity levels. Relative permittivity of organic-based materials with small molecular sizes lies between 4-8 in [238]; on the other hand, water permittivity is almost 80.4. The dielectric constant of water remarkably increases capacitance of a sensor because of a large difference between the relative permittivity of water and active thin film of respective materials and their composites. Figure 6.4 (d) shows the relationship between resistances and relative humidity levels for the composites ($V_1 : A_2$) at 75 °C, Alq$_3$ at 125 °C, and VOPcPhO at 25 °C based humidity sensors. It was observed that the resistance responses of VOPcPhO and Alq$_3$ were more obvious in the range of 15-60% RH; after that they seem to tend to be saturated values. However, in the case of $V_1 : A_2$, the resistive device was sensitive over the whole measured range.

Surface morphology of thin films of Alq$_3$, VOPcPhO, and their composites was
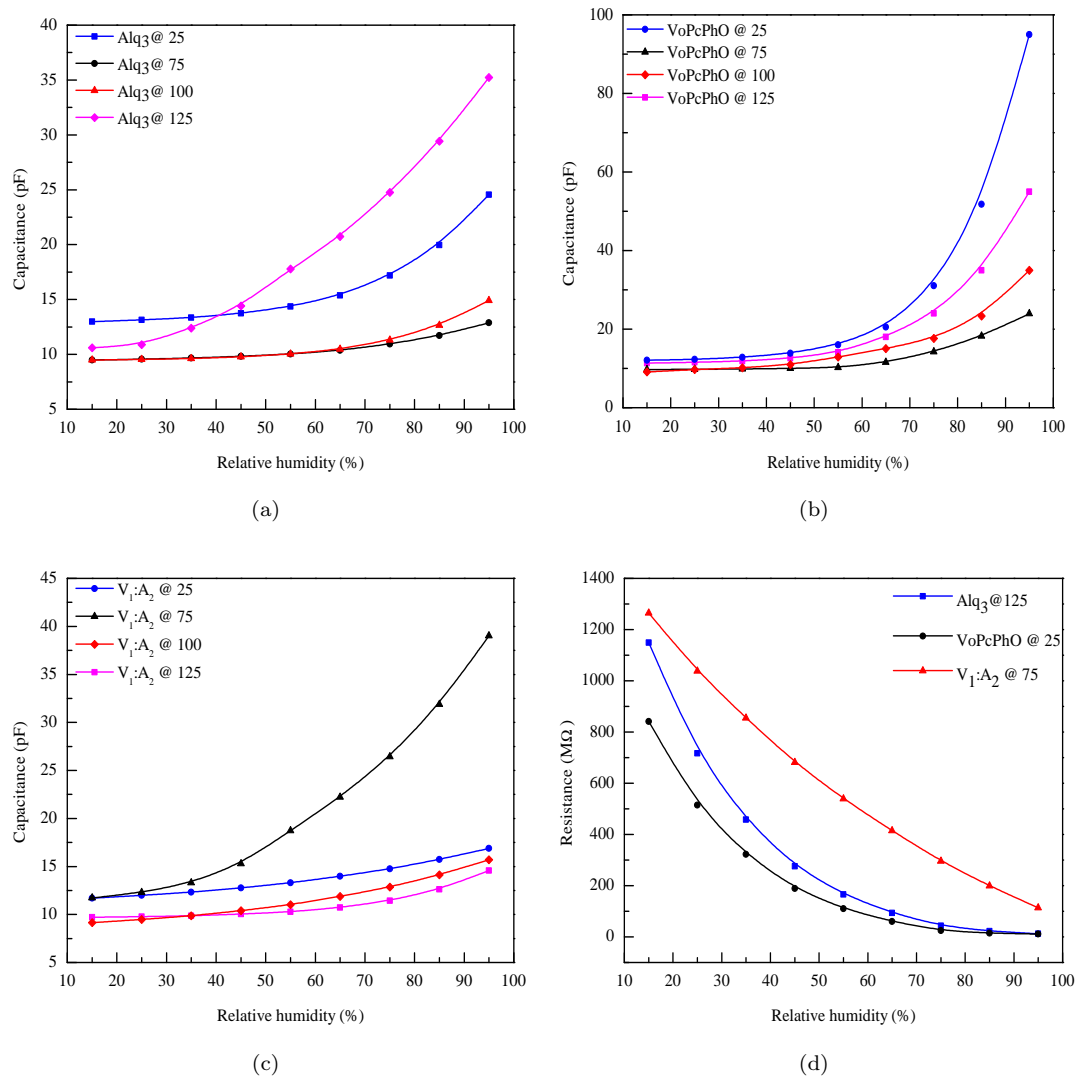
FIGURE 6.4: Capacitance vs. humidity sensing behavior of (a) Alq$_3$, (b) VOPcPhO, (c) composite (VOPcPhO : Alq$_3$) at various ambient temperatures, and (d) resistance response of the best selected sensors i.e. composite (V$_1$: A$_2$) at 75 °C, Alq$_3$ at 125 °C, and VOPcPhO at 25 °C.

studied using atomic force microscopy (AFM) and field emission scanning electron microscope (FESEM). Figure 6.5 shows the AFM and FESEM micrographs of VOPcPhO annealed at 25 °C (Figs. 6.5 a and b), Alq$_3$ annealed at 125 ° (Figs. 6.5 c and d), and composite VOPcPhO : Alq$_3$ Fig. 6.6 FTIR spectra of (a) Alq$_3$, (b) VOPcPhO, and (c) composite thin film of Alq$_3$ and VOPcPhO annealed at 75 °C (Figs. 6.5 e and f), respectively. Micrographs of the composite films (Figs. 6.5 e and f) display a rough surface with uniform distribution of the textured appearance. The image of Fig. 6.5(e) indicates that the Alq$_3$: VOPcPhO composite

thin film, when annealed at 75 °C , results in much rougher surface with a sharp peak like structures.

The rms roughness measured for VOPcPhO and Alq$_3$ thin films were 0.832 nm and 0.597 nm, respectively. The composite film V$_1$: A$_2$ has rms roughness of 0.937 nm which exhibits a slightly rougher surface than the stand-alone films. The annealed composite thin film provides more absorption sites for moisture content to be adsorbed. Sensitivity of the humidity sensors depends upon the amount of water absorbed corresponding to the increased surface area. It can be inferred that the greater roughness with uniform distribution leads to larger surface area exposure and more moisture adsorption as well [158]. Sensitivity (S) of the humidity sensors can be assessed by using the equations (4.6) and (4.7) [239].The chemical bonding structures of Alq$_3$, VOPcPhO, and their blend thin films were investigated by FTIR and the results are shown in Fig. 6.6. In line (a), C=C aromatic stretching vibrations are observed in the range of 1601-1497 cm^{-1}. The absorption bands at 1385 cm^{-1} to 1114 cm^{-1} represent the resonance of aromatic amine (C-N-C) [240]. The band at 918 cm^{-1} is due to an Al-N stretching vibration. Moreover, out-of-plane quinoline CH wagging vibration can be seen at 744 cm^{-1}. The weaker band at 555 cm^{-1} originates from the stretching vibration of Al-O [241]. Line b in Fig. 6.6 represents the characteristic spectrum of VOPcPhO. The peak at 1057 cm^{-1} shows the presence of a single V-O stretching motion which was already reported by Miller and Cousins [242]. This peak has been assigned to shorter V-O bonds. However, the peak at 895 cm^{-1} also shows the presence of V-O bonds but this band is due to the characteristic of longer V-O bonds [243]. Moreover, the band at 746 cm^{-1} corresponds to out-of plane C-H bending modes and this peak is a characteristic of almost all phthalocyanines [244]. The FTIR of the blend of Alq$_3$ and VOPcPhO is presented in Fig. 6.6(line c).

Response times, τ_{res} and recovery times, τ_{rec} for Alq$_3$, VOPcPhO, and their composites (V$_1$: A$_2$) are given in Fig. 6.7(a-c); they are 6 s, 13 s, and 4 s and 4 s, 8 s, and 3 s, respectively. The response and recovery time of the composite is better than others. The response time and recovery time of the sensors were measured as follows: initially the sensors were placed in a sealed chamber with 20% RH and
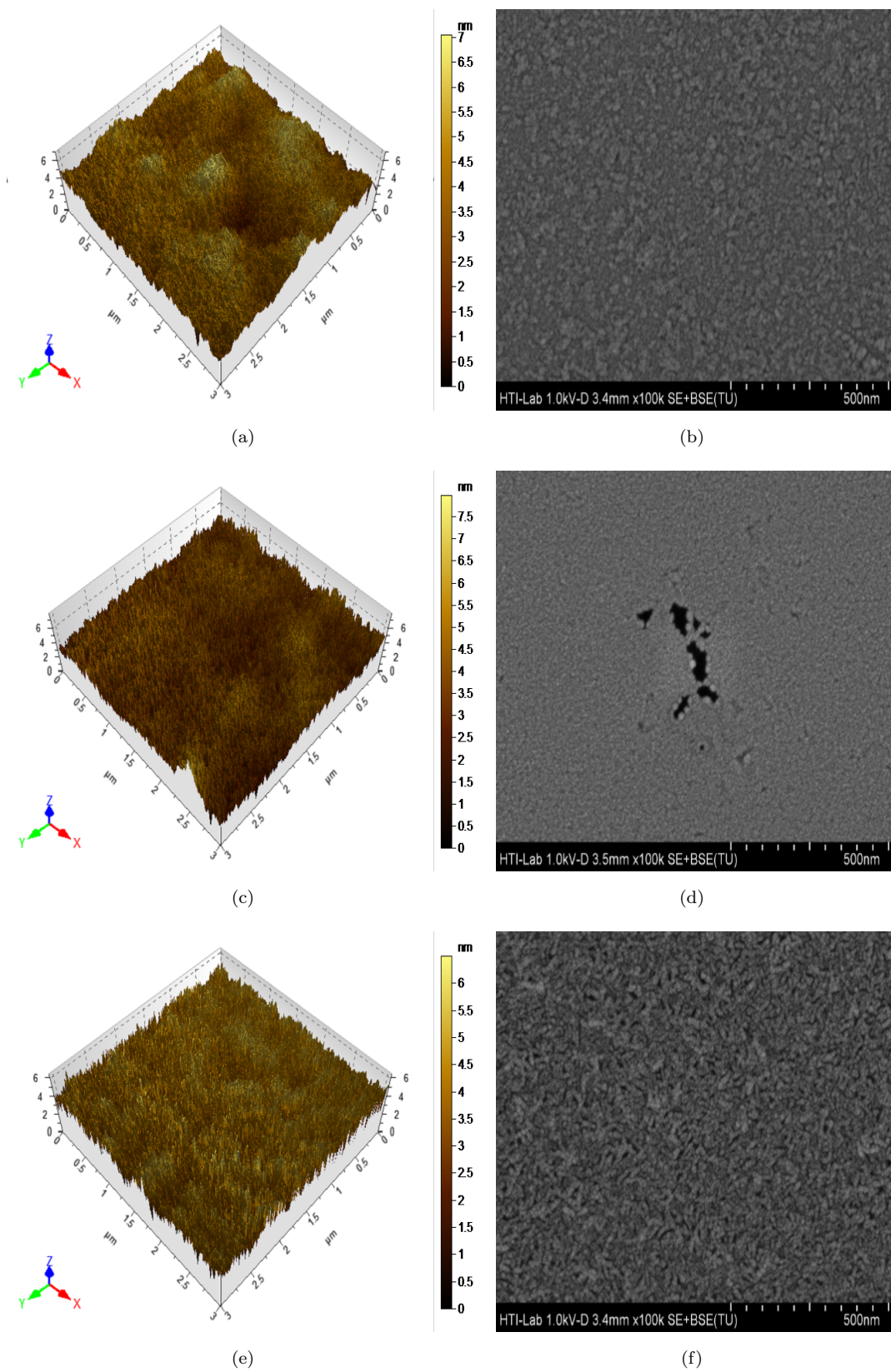
FIGURE 6.5: AFM images of (a) VOPcPhO at 25, (c) Alq$_3$ at 125, (e)V$_1$: A$_2$ at 75, and FESEM (b) VOPcPhO at 25, (d) Alq$_3$ at 125, and (f) V$_1$: A$_2$ at 75.
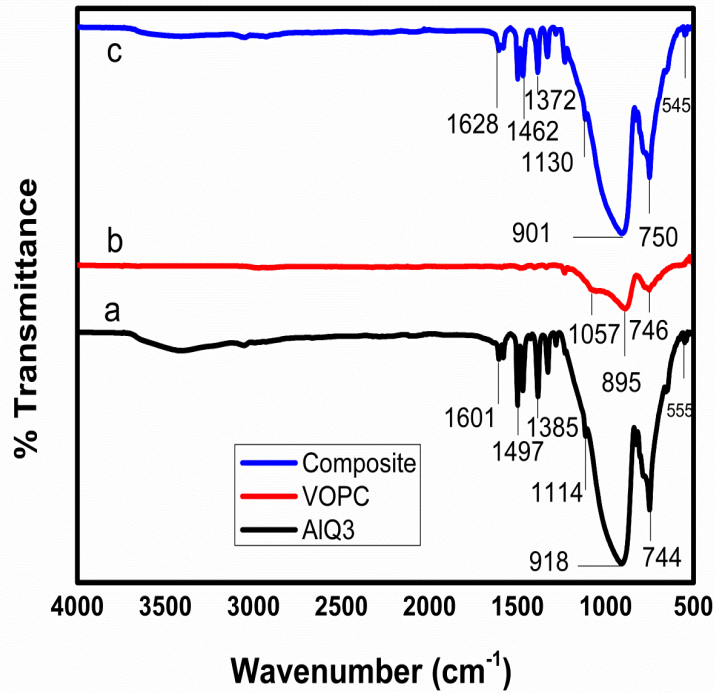
FIGURE 6.6: FTIR spectra of (a) Alq$_3$, (b) VOPcPhO, and (c) composite thin film of Alq$_3$ and VOPcPhO.

then they were exposed to an environment with 70% RH level, thereby enabling them to adsorb water vapor and hence increasing their capacitance. The recovery time of a sensor was achieved by first exposing it to a humidity level of 70% RH and then immediately back to 20% RH. Figures 6.7 (d-f) shows the hysteresis of Alq$_3$, VOPcPhO, and their composites at the ratio V$_1$: A$_2$ at 100 Hz frequency. The up and down arrows show the increase and decrease in % RH, respectively.

A summary of the devices is described in Table: 6.1.

TABLE 6.1: Summary of the properties of thin film sensors.

Thin Film	Annealing Temp	S_C	S_R	τ_{res}	τ_{rec}	Surface Roughness
	°C	pF %$^{-1}$	MΩ%$^{-1}$	s	s	nm
VOPcPhO	25	1.06	9.68	13	8	0.83
Alq$_3$	125	0.3125	12.81	6	4	0.57
V$_1$:A$_2$	75	0.325	14.5	4	3	0.937

(a)

(b)

(c)

(d)

(e)

(f)
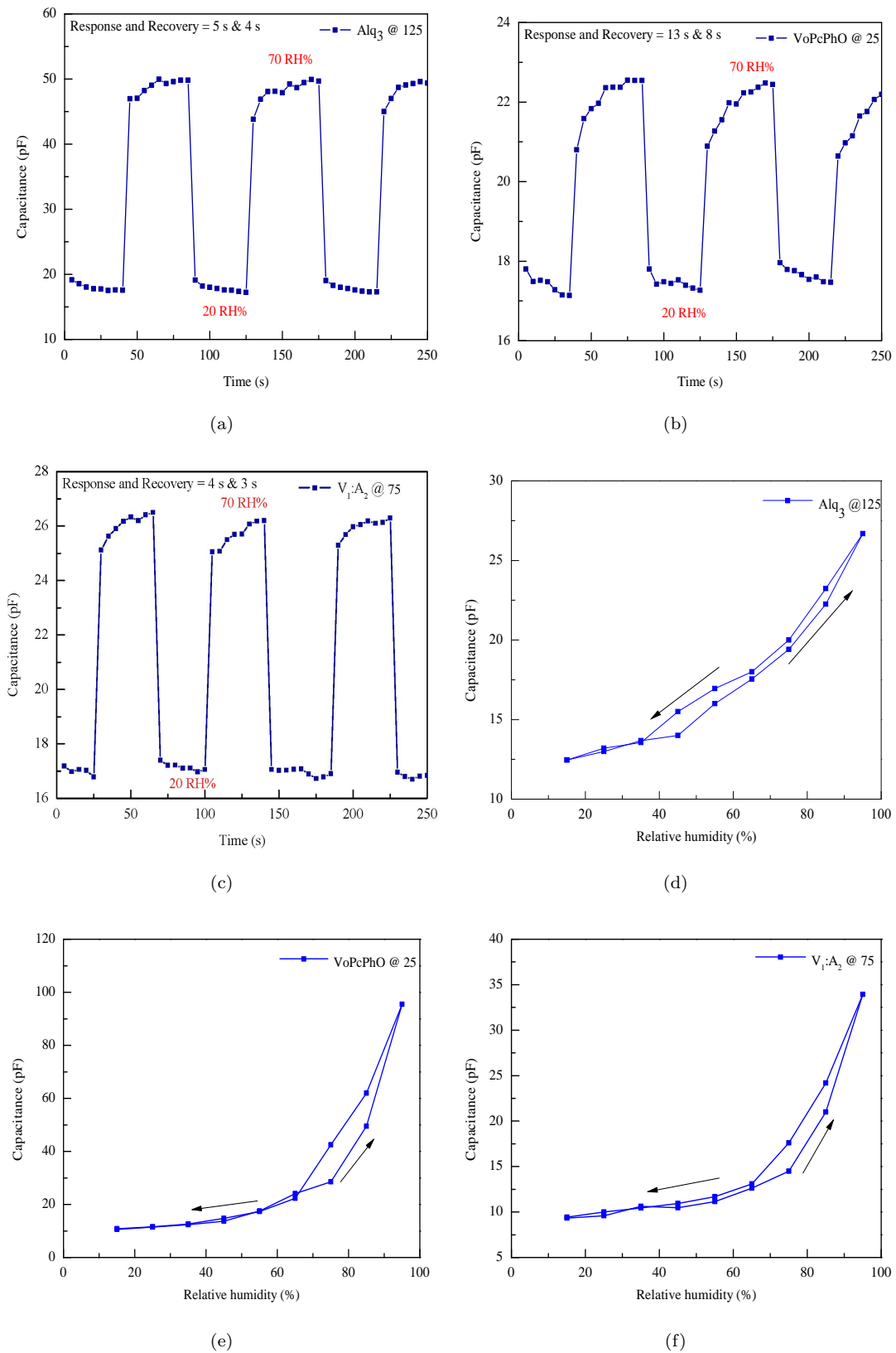
FIGURE 6.7: Transient response of capacitance to time of (a) VOPcPhO at room temperature, (b) Alq₃ at 125 °C, and (c) VOPcPhO : Alq₃ (1 : 2) at 75 °C. Hysteresis behavior of capacitance-*RH* of (d) Alq₃, (e) VOPcPhO and (f) composite (VOPcPhO : Alq₃) at room temperature.

The impedance- and capacitance-RH responses of fabricated sensors discussed in Chapter 4, 5 and 6 are not linear in nature therefore, while fabricating a sensor using the proposed technologies, due care should be taken in order to keep the responses of the sensors linear. Piecewise linear approximation can be applied during calibration process such that each region is approximated as a linear region with its own calibration factor.

In relative terms, sensors discussed in Chapter 4 and 5 are fabricated using same methodology and by using metal-Pc based organic semiconductors. In the first case, metal was substituted with Cu, whereas in the second case, it is substituted with Ni. Observing the performance of Ni/Cu-Pc based sensors, one can conclude that NiPc organic semiconductor based sensors are relatively better compared to CuPc if fabricated at high gravity. But, in general, both are equally good to be used in organic semiconductor industry specially, in sensor fabrication. On the other hand, the material and sensor technology discussed in this chapter both are different from Chapter 4 and 5. Since, the technology employed in the fabrication of VOPcPhO-Alq₃ based humidity sensor is a high-tech technology therefore, the devices achieved are of better quality and also offer relatively better performance compared to those discussed in Chapter 4 and 5.

6.4   Summary

This study exhibits a solution-processed organic semiconductor humidity sensor based on vanadyl 2,9,16, 23-tetraphenoxy-29H, 31H-phthalocyanine (VOPcPhO), tris-(8-hydroxy-quinoline)aluminum (Alq₃), and their composites. Compositional engineering of the VOPcPhO : Alq₃ complex was performed to develop a sensitive humidity sensor with a linear response. Thin films of VOPcPhO, Alq₃, and composites were spin-coated over pre-deposited aluminum (Al) electrodes, whereas the other electrodes were deposited through a thermal evaporation technique. Both capacitive and resistive responses were measured as a function of different relative humidity levels. Morphological and structural properties of the organic thin films

were characterized by atomic force microscopy (AFM), field emission scanning electron microscopy (FESEM), and Fourier transform infrared spectroscopy (FTIR). Compared to the VOPcPhO and Alq$_3$ stand-alone sensors, the VOPcPhO : Alq$_3$ composite-based sensor demonstrated superior performance with significantly improved sensing parameters, highlighting unique advantages of the low-molecular composite-based thin film organic humidity sensors.

Chapter 7

NiPc-CoPc Based Optical Sensors

7.1 Introduction

Phthalocyanines (PCs) are a class of organic semiconductors, which have received substantial consideration due to their potential applications in a variety of fields. Their distinctive characteristics include semi-conductivity, photo-conductivity, chemical stability and optical absorption in the visible regime [245]. Thin films of PCs can be deposited either by vacuum evaporation, drop-casting or spin-coating [246]. Among the PCs, nickel phthalocyanine (NiPc) is considered as a promising phthalocyanine for optoelectronic devices and gas sensing applications [204, 205, 247]. NiPc has a charge carrier mobility of 0.1 $cm^2(Vs)^{-1}$, which is 1000 times higher than copper phthalocyanine (CuPc) [213]. The energy band gap of the NiPc is equal to 3.2 eV and 2.24 eV for direct and indirect allowed transitions, respectively [214]. Maximum optical absorption bands (in the visible region) of the NiPc films have been observed at 300 nm and 650 nm. Schottky diodes of the NiPc have been investigated by Ahmad et. al. [236] and Shah et al. [215].

Composite prepared with proper selection of the HOMO-LUMO of the two dyes could enable better exciton dissociation and improve the photon to current conversion. Most of the research work performed on the dyes composite films is either mixed with nano materials or polymer in the matrix of individual component of the

dye. Bulk heterojunction structures of CuPc and H_2Pc under varying illumination conditions have been studied by Farooq et. al. [248]. A comparative analysis of *I-V* characteristics in dark and under illumination showed that the devices were sensitive towards visible light. Semiconductor device's properties depend on fabrication technology. The properties of the electronic devices based on dyes grown by organic molecular beam deposition (OMBD) technique have been investigated by C.N. Colesniuc [176]. He reported that the conductivity of the grown films increases exponentially with temperature, whereas it decreases exponentially with increasing the thickness of the films. Organic field effect transistors have also been fabricated using dyes with standard vacuum evaporated method [177]. However, no work has been reported in the case of bulk heterojunction of the two or more dyes deposited under different conditions. It is expected that different deposition conditions will change the sensitivity of the dyes based bulk heterojunction optical sensors.

Previously, the effect of varying light intensity on the electrical parameters of NiPc and CoPc has been investigated experimentally [190, 249–251], as well as theoretically [252]. NiPc and CoPc have different work functions, 4.0 eV and 4.4 eV, respectively. The combination of the integrated capacitive and impedance based optical study on NiPc and CoPc has been demonstrated in this work. This integrated platform is expected to enhance the conductivity possesses the desired features of an optical sensor, i.e., better linearity, better capacitive sensitivity and fewer impedance, which can be further optimized by film deposition techniques.

In this chapter, the thin NiPc and CoPc heterojunction films have been prepared at different gravity and the effect of light on the capacitance and impedance of the samples have been investigated.

7.2   Experimental

Commercially available NiPc ($C_{32}H_{16}N_8Ni$) and CoPc ($C_{32}H_{16}N_8Co$) was purchased from Sigma-Aldrich and used without further purification. Figure 7.1(a)

shows the schematic diagrams of the both deposition processes. Whereas, Fig. 7.1(b) shows the ceramic alumina substrate with surface type silver electrodes. It is interdigitated silver electrodes coated on ceramic alumina sheet (of size 14mm: 7mm with an interelectrode distance of 0.21 mm) fabricated by screen printing and chemical etching technology [202]. Figures 7.1(c) and (d) shows the molecular structure of organic semiconductors NiPc and CoPc. Both have the same structure, only the central metal Ni is replaced by the Co. The thin films of NiPc and CoPc composite were deposited from their 5wt. % solution in chloroform by dropcasting and centrifuge HETTICH EBA-20 S. As per our previous optimization, it was decided to fabricate the sensors at 5000rpm. Film thickness decreases by increasing the rpm and vice versa. During the centrifugal process, acceleration, a was calculated by by the expression (7.1).

$$a = r\omega^2 \tag{7.1}$$

where r is the radius and ω is the angular velocity of the centrifugal machine. For every experiment, there were two symmetrically glass tubes installed and they were filled by an equal volume of solutions (0.5 ml). The solution was allowed to evaporate at room temperature and atmospheric pressure, which is ruled at the centrifugal process. The centrifugation thin film deposition time was ~40 min without heating. The average thickness of the NiPc and CoPc heterojunction thin films were equal to ~60-70 nm.

Figure 7.2 shows the atomic force microscope (AFM) images and roughness of the NiPc and CoPc composite films deposited by drop casting and centrifugal force. It is observed that the films deposited under centrifugal force have more developed surface structure so these will be more sensitive as compared to drop casted samples. The electrical parameters such as, impedance and capacitance of the samples have been measured as a function of intensity of light by LCR meter Mo-Tech 4090 that was used at frequency and voltage levels of 1 kHz and 1V, respectively. As a light source, the filament lamp of 100 W was used.
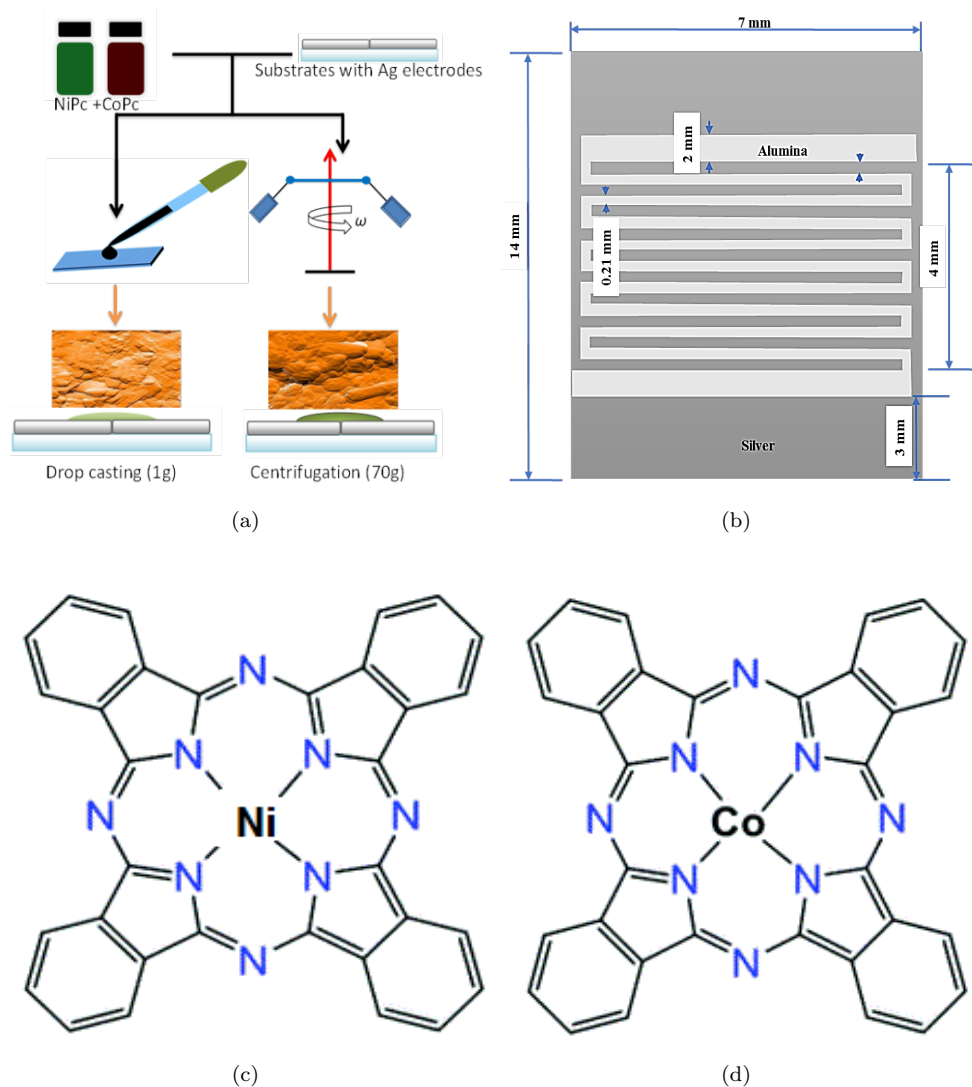
FIGURE 7.1: (a) Schematic diagram of the drop casting and centrifugal deposition, (b) Ceramic alumina substrate with surface type silver electrodes. Molecular structure of organic semiconductor (c) NiPc and (d) CoPc.

7.3 Results and Discussion

From the point of optical properties, the absorption level of NiPc and CoPc is approximately the same as shown in Fig. 7.3(a) [252, 253]. HOMO and LUMO energy diagrams of the NiPc and CoPc bulk heterojunction is shown in Fig. 7.3(b). In the design of Fig. 7.3(b), it was taken into consideration that the HOMO-LUMO gaps are equal to 1.47 eV and 1.87 eV for NiPc and CoPc, respectively [254]. Their respective work functions are 4.0 eV and 4.4 eV, while the work function of the silver electrodes is equal to 4.3 eV. These samples contain bulk heterojunctions in
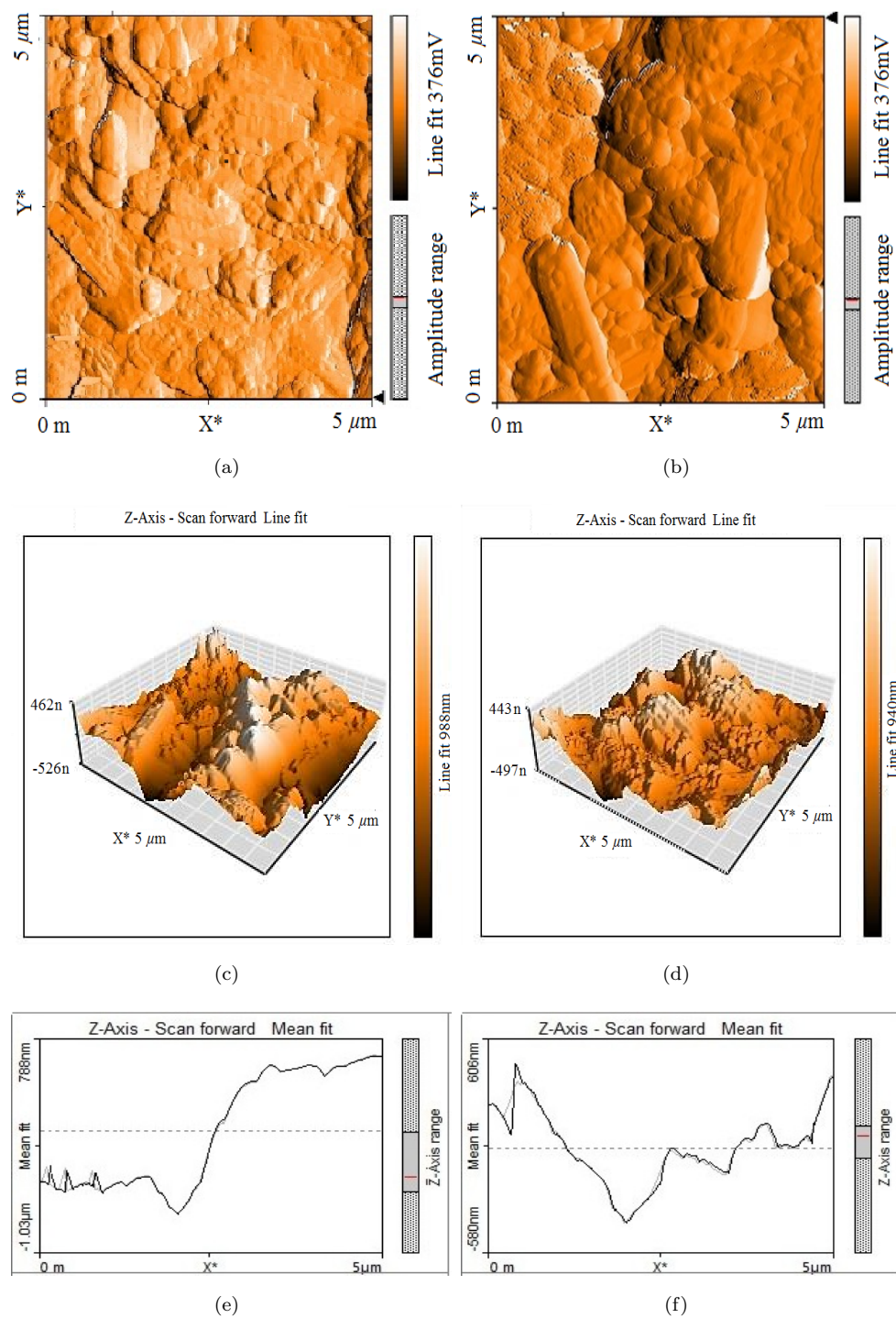
FIGURE 7.2: Atomic force microscope (AFM) images 2D, 3D and roughness of the NiPc and CoPc composite films deposited by drop casting (a), (b) and (c) and centrifugal force (d), (e) and (f), respectively.

micro level. As the work function of NiPc is lower than that of CoPc, therefore the transfer of charges takes place from NiPc to CoPc. It means molecule of NiPc plays the role of donor, whereas the molecule of CoPc act as an electron acceptor. The transfer of charges brings to formation like to dipoles in the bulk of the sample, which is chaotically oriented in the space between the Ag electrodes, resulting zero electric field because there is no contribution of electrode potential (as both electrodes have the same material). These samples are showing good response as impedance and capacitance elements.

Figure 7.4(a) shows impedance-illumination relationships for the NiPc and CoPc heterojunction samples fabricated by drop casting and under centrifugal force. It has been seen that impedance decreases in both cases with the increase in the intensity of light up to 23 mWcm $^{-2}$. It was calculated that impedance decreases 1.4 and 2.1 times for the samples fabricated by drop casting and under centrifugal force, respectively. Figure 7.4(b) shows capacitance-intensity of light relationships for the NiPc and CoPc heterojunction samples. It is found that the capacitance increases with the increase in intensity of light as 1.3 and 2.1 times, respectively, for the samples made by drop casting and under centrifugal force. The relationships shown in Fig. 7.4 have the following peculiarities: the samples fabricated under centrifugal force show more changes of the impedance and capacitance under effect of light. The thickness of the samples was almost same. It can be considered that the samples grown in different deposition conditions have different structures as shown in Fig. 7.2(a-d). The samples deposited by centrifugal force have more roughness as a result of which the sensitivity is increased.

By comparing the impedances and capacitances (given in Fig. 7.5) of the samples fabricated by drop casting and under centrifugal force, it can be assumed that the centrifugal processing could bring to proper rearrangement of the NiPc and CoPc molecules, which results to make the transfer of the charges from donor to acceptor easier.

From electronic point of view, decrement in the impedance (Z) with an increment in the light intensity can be described by resistance (R) decrease and the
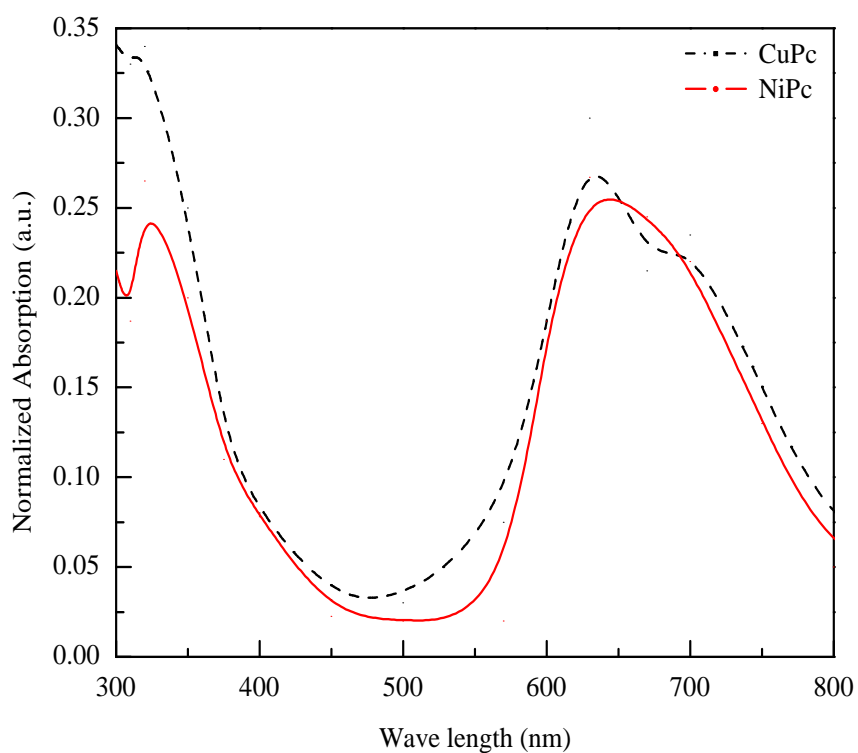
(a)
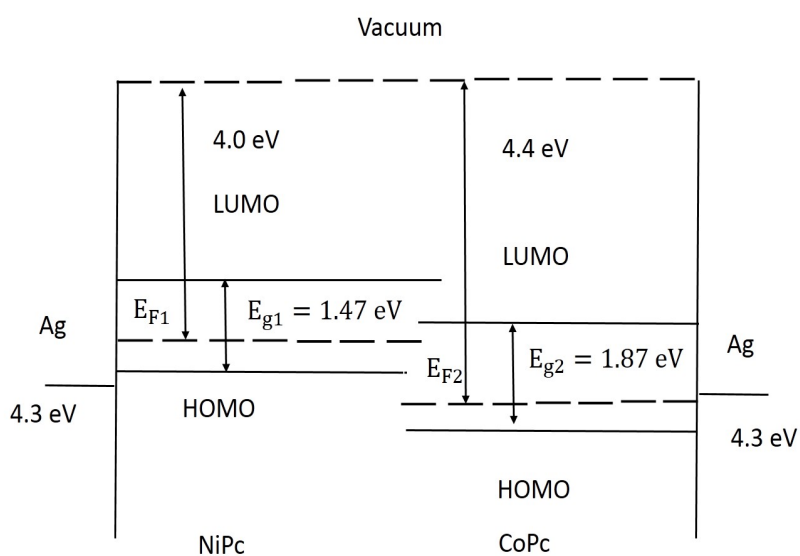
(b)

FIGURE 7.3: (a) Absorption spectra of NiPc and CoPc films and, (b) HOMO and LUMO diagrams for the NiPc and CoPc bulk heterojunction.
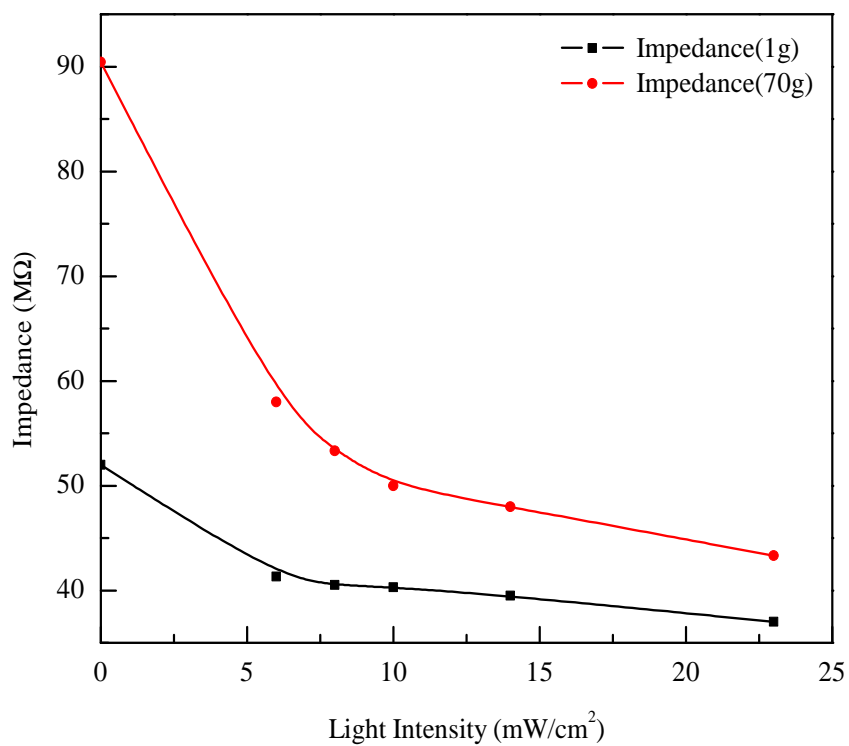
(a)
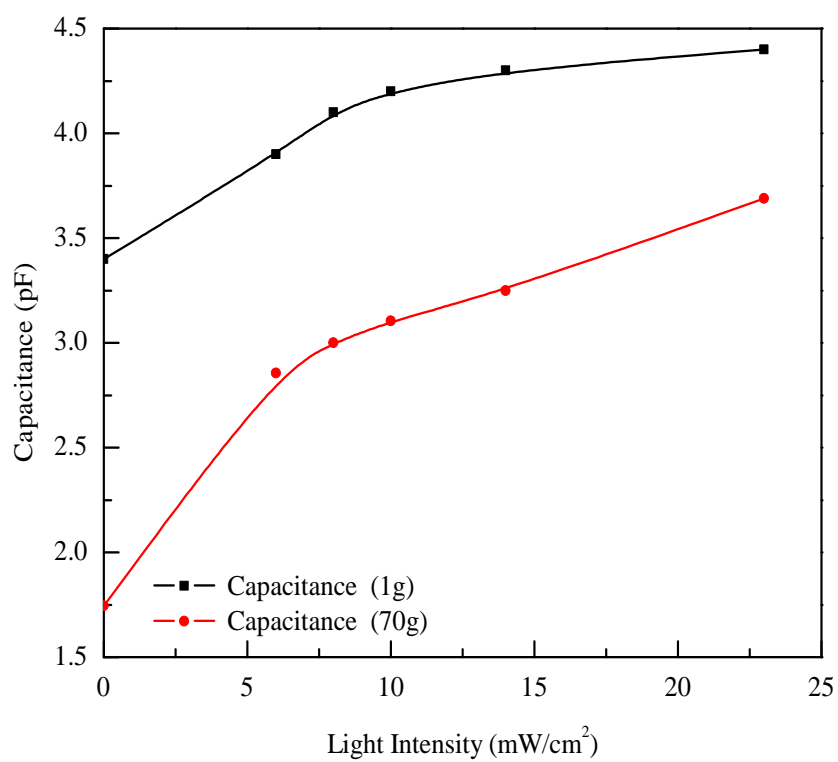
(b)

FIGURE 7.4: (a) Impedance intensity of light relationships and, (b) Capacitance intensity of light relationships for the NiPc-CoPc samples.

capacitance (C) increase and can be represented by Eq. (7.2) [186, 255].

$$Z = \frac{R}{1 + j\omega RC} \tag{7.2}$$

where ω is the circular frequency.

The decrease of the impedance and increase of the capacitance is due to the increased concentration of charge carriers and change in permittivity, which can be explained by the effect of light [181, 256]. The capacitance also relies upon material's polarizabilities such as electronic (α_e), dipolar (α_{dip}) and ionic (α_i) [257]. Another form of polarizability, that is known, is due to transfer (α_{tr}) of charge carriers (electrons and holes), which depends on concentration of charge carriers [258, 259]. It should be differentiated that α_e is due to the relative displacement of orbital electrons, whereas the α_{tr} is due to charges participating in conduction process. The Clausius-Mosotti relation [257], if we take into consideration only polarizability due to transfer of charge carriers, can be represented as in Eq. (7.3).

$$\frac{\varepsilon - 1}{\varepsilon + 2} = \frac{N\alpha_{tr}}{3\varepsilon_0} \tag{7.3}$$

where ε is the relative permittivity, N is the total concentration of charge carriers, and ε_0 is the permittivity of free space.

The impedance-light intensity relationship for the NiPc and CoPc heterojunction can be described by the Eq. (7.4).

$$y = e^{-x} \tag{7.4}$$

Assuming that $x = ab$, where b is the light intensity and a is the fitting parameter that is calculated as 0.0319 for sample deposited by drop casting and 0.0149 for the sample deposited under centrifugal force.

Figure 7.5(a) shows that simulated relationships have quasi-exponential behavior. The normalized capacitance-intensity of light relationships for the NiPc and CoPc heterojunction sample can be simulated by the equation, (assuming that $x = ab$,
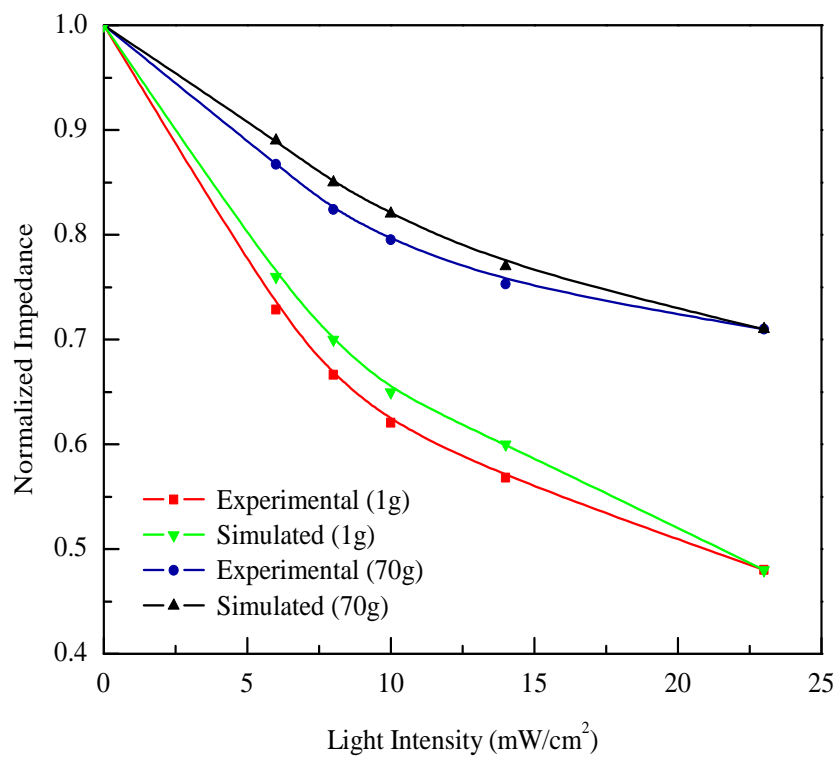
(a)
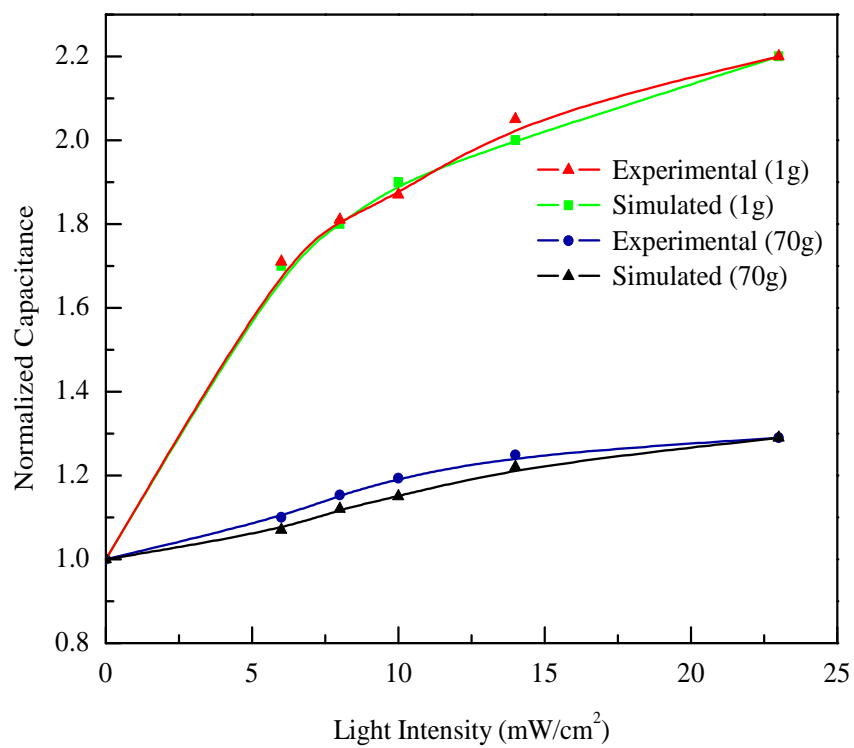
(b)

FIGURE 7.5: (a) Normalized impedance vs intensity of light relationship. (b) Normalized capacitance vs. intensity of light relationship.

where b is light intensity and a is fitting parameter). For the sample deposited by drop casting and under centrifugal force, it was calculated that a=0.041 and 0.646, respectively. The effect of light on the capacitance and impedance of the NiPc and CoPc heterojunction samples can be predicted through the impedance (S_Z) and capacitance (S_C) sensitivities and can be presented by Eqs. (7.5) and (7.6) [186].

$$S_Z = \frac{\Delta Z}{\Delta G} \tag{7.5}$$

$$S_C = \frac{\Delta C}{\Delta G} \tag{7.6}$$

where ΔZ, ΔC and ΔG are change in impedance, capacitance and light intensity (in mW cm^{-2}). The S_Z were -1.83 MΩcm^2 m^{-1}W^{-1} and -5.365 MΩcm^2 m^{-1}W^{-1} for the samples fabricated by drop casting and under centrifugal force, respectively. Similarly, S_C were equal to 0.083 pF cm^2(mW)$^{-1}$ and 0.185 pF cm^2(mW)$^{-1}$ for the samples fabricated by drop casting and under centrifugal force. The effect of light intensity on capacitance and impedance of NiPc-CoPc samples can be possibly utilized for production of the light sensors.

7.4   Summary

In this chapter, solution processed composite films of nickel phthalocyanine (NiPc) and cobalt phthalocyanine (CoPc) have been deposited by drop casting and under centrifugal force. The films were deposited on surface-type interdigitated silver electrodes on ceramic alumina substrates. The effect of illumination on the impedance and capacitance of the NiPc-CoPc composite samples have been investigated. The samples deposited under centrifugal force showed better conductivity with respect to samples deposited by drop casting technique. In terms of impedance and capacitance sensitivities, the samples fabricated under centrifugal

force are more sensitive than the drop casting samples. Impedance sensitivity (S_Z) was equal to -1.83 MΩ cm^2 (mW)$^{-1}$ and -5.365 MΩ cm^2 (mW)$^{-1}$ for the samples fabricated using drop casting and under centrifugal force, respectively. Similarly, the capacitance sensitivity (S_C) was equal to 0.083 pF cm^2 (mW)$^{-1}$ and 0.185 pF cm^2 (mW)$^{-1}$. The films deposited using different procedures could potentially be a viable for different operational modes (i.e., conductive or capacitive) of the optical sensors. Both experimental and simulated results have been discussed.

Chapter 8

ZnPc-PC$_{71}$BM Based Organic Photo Diodes

8.1 Introduction

Solution processable organic semiconductors permit envisioning the development of ambient conditions sensitive devices by facile, eco-benign and low thermal budget fabrication techniques [234, 260–262]. π-conjugated organic semiconductors are particularly attractive for humidity, temperature and light sensing utility by virtue of their unique features such as low-cost, significantly strong absorption coefficients and tune-able spectral sensitivity [263, 264].

Current research on organic devices generally focuses on bulk hetero junction (BHJ) theme in which π-conjugated p-type donor (hole conducting) and n-type acceptor (electron conducting) organic semiconductors are intimately blended. In the resulting photo active film, π-conjugated D material serves as the primary incident light absorber and creates photogenerated columbically bound electron-hole pair (excitons). Therefore, the choice of D material with wide optical absorption profile is a basic requirement toward the design of ideal photoactive donor and acceptor dyad. Furthermore, the favorable energy offset at donor and acceptor heterointerface is also essential to yield efficient exciton separation leading to high

photocurrent. The key sensing parameters of the BHJ in electronic devices such as bandwidth and sensitivity are, therefore, primarily determined by the choice of the donor and acceptor moieties. Dyes such as, metal phthalocyanines (MPc) are versatile *p*-type organic semiconductors, which possess unique electronic absorption characteristics, high thermal stability and environmental stability [161–163].

Structurally, MPc are related to azaporphyrins and consist of four benzoindole nuclei connected by nitrogen bridges in a 16-membered ring of alternating carbon and nitrogen atoms around a central metal atom (i.e. $C_{32}H_{16}N_8M$), which form a stable chelates with metal cations [265]. The extensive delocalized π-electron distribution in the chemical structure of phthalocyanine molecules is the key to their good photosensitivity [266]. However, in general, the MPc are insoluble and sometimes soluble to limited extent in most common organic solvents due to their strong intermolecular π-interactions and the lack of flexible chains [267]. Therefore, in most of the studies (particularly those related to photovoltaic applications), MPc are deposited by energy intensive physical vapour deposition (PVD) technique [268–270].

Among the metal phthalocyanine, zinc phthalocyanine (ZnPc) is sufficiently soluble in toluene [271, 272]. It may also act as an efficient light harvesting photosensitizer by virtue of its superior photo-induced charge transfer property, when intermixed with a suitable acceptor material (possessing complementary absorption spectra and excellent electron transport characteristics) [271].

Conjugated fullerene (C_{60} or C_{70}) derivatives with high electron affinity are generally utilized as acceptor materials in optoelectronic devices. The visible light absorption by C_{60} derivatives however, remain low due to the symmetry forbidden ($h_u \rightarrow t1_u$) transition [273, 274]. Contrariwise, C_{70} derivative (such as PC$_{71}$BM) exhibit lower degree of symmetry and, therefore, low energy transition are permissible in them [275]. Resultantly, PC$_{71}$BM exhibits extended absorption spectrum in contrast to PC$_{61}$BM [261].

In this work, PC$_{71}$BM has been opted as an acceptor material (to be mixed with ZnPc donor) by virtue of its broad absorption profile, high electron mobility and its

energetically deep lying lowest unoccupied molecular orbital (LUMO) as compared to that of ZnPc donor. The significant energy difference between LUMO of ZnPc and PC$_{71}$BM is expected to facilitate efficient charge transfer instead of energy transfer from photoexcited donor molecule to PC$_{71}$BM.

We find it interesting to utilize ZnPc:PC$_{71}$BM as photoactive dyad in OPD's fabrication, for several reasons. Foremost, ZnPc and PC$_{71}$BM may be conveniently dissolved in a common solvent (toluene), which renders them amenable to facile and economical solution processable fabrication techniques. Secondly, by virtue of synergetic or complementary absorption profile of ZnPc and PC$_{71}$BM thin films, the donor and acceptor photoactive blend is expected to exhibit improved light harvesting in full visible spectrum. Furthermore, the energy level cascade at the donor and acceptor interface is also believed to be sufficient to yield efficient charge carriers generation in the ZnPc:PC$_{71}$BM photoactive dyad.

This chapter describes the investigation of organic semiconductors photo sensitive devices. In past few decades, number of research groups have developed organic semiconductor based opto-electronic devices, i.e. photo detectors including photodiodes, phototransistors and optical sensors. Useful reviews of organic photodetectors are presented in [1, 2], helping to motive and divert the interest towards optical devices. In this context, organic photo diodes (OPDs) are the focus of research strives by virtue of their promising application in the domains of image sensors, automation, remote sensing and optical communication [276, 277].

8.2   Experimental

Zinc phthalocyanine (ZnPc) was purchased from Sigma Aldrich with 97% purity. [6,6] -phenyl-C$_{71}$-butyric-acid methyl ester (PC$_{71}$BM) was procured from Luminescence Technology Corp. (Taiwan, China). Poly(3,4-ethylenedioxythiophene): poly(styrene sulfonate) (PEDOT:PSS) aqueous solution (PH ~1000, conductivity
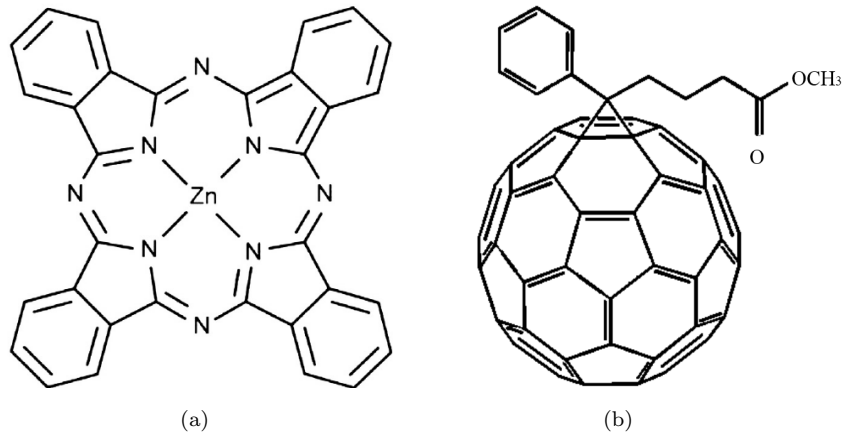
FIGURE 8.1: The molecular structures of the investigated materials (a) Zinc phthalocyanine (ZnPc) and (b) [6,6]-phenyl-C$_{71}$-butyric–acid methyl ester (PC$_{71}$BM).

900-1000 Scm^{-1}) was purchased from H.C. Starck Clevios GmbH (Goslar, Germany). These commercially available materials were used without any further purification. Molecular structures of ZnPc and PC$_{71}$BM are presented in Fig. 8.1.

For photodiode fabrication, transparent Indium tin oxide (ITO) substrates were thoroughly cleaned with detergent and later ultrasonicated in de-ionized (DI) water, acetone, isopropyl alcohol and DI water sequentially. The ITO substrates (25×25 mm^2, sheet resistance ∼20 Ωsq^{-1}) were later oven dried at 100° C for 1 hour. Aqueous PEDOT:PSS solution was initially filtered (via 0.45 μm nylon filters) and later spun-cast onto the ITO substrates to produce PEDOT:PSS anodic buffer layer (∼45 nm). The buffer layer was subsequently dried at 110°C for 30 minutes on a hot plate. PEDOT:PSS buffer layer is usually adopted as a hole extraction and electron blocking layer in photodiodes. 15 mg ml^{-1} concentrated solutions for both ZnPc and PC$_{71}$BM were prepared in toluene separately and stirred overnight at room temperature using a magnetic stirrer. The solutions were later filtered by commercially available 0.20 μm filter to avoid any solid contents. The organic donor and acceptor dyad was then prepared by mixing ZnPc and PC$_{71}$BM solutions in five different stoichiometries by volume (1:0.6, 1:0.8, 1:1, 1:1.2, 1:1.4). The organic donor and acceptor binary dyad with optimum stoichiometric ratio was subsequently spun-cast on the ITO/PEDOT:PSS substrates at a speed of 2000 rpm to achieve ∼140 nm thickness of photoactive thin film. The

ZnPc:PC$_{71}$BM photoactive thin film was subjected to thermal annealing at 110 ^{0}C for 30 min. A lithium fluoride (LiF, 5 $\mathring{A}$) and aluminium layer (100 nm) was deposited on the donor and acceptor dyad films by thermal evaporation ($2 \times 10^{-6}C$ mbar) through a shadow mask with circular openings of 2 mm^2. LiF is usually deposited before the top metal cathode (Al) to hinder metal diffusion inside the photoactive matrix. It also functions as a hole blocking layer. Post-fabrication thermal annealing was also performed by placing the fabricated photodiode on a hot plate at 110°C for 30 minutes. In general, post fabrication annealing facilitates the reorientation and enhanced ordering of the organic semiconductors, which is considered beneficial for efficient charge transport [43]. All the fabrication process was conducted in open air inside the clean room.

The photodiode configuration and corresponding energy level diagram is shown in Fig. 8.2 (a) and (b), respectively. As is well known that while selecting the photoactive donor acceptor pair, the LUMO energy levels of acceptor should be positioned below that of donor, so as to enable effective unrestricted and directed charge separation at the donor and acceptor interface. In fact, the energy offset of the LUMO energy levels of the donor and acceptor materials should be large enough to dissociate the photoexcitons (typical binding energy 200-500 meV) [278]. ZnPc has a bandgap of ~1.39 eV which is smaller than that of PC$_{71}$BM (2 eV). The HOMO energy level of ZnPc is located at ~5.17 eV, about 0.83 eV higher than that of PC$_{71}$BM. This aforementioned values indicates that after exciton dissociation at donor and acceptor interface, electron transfer from ZnPc to PC$_{71}$BM and hole transport in reverse direction is energetically possible. The energy-level diagram of the OPD therefore shows a good choice of organic ZnPc (D) and PC$_{71}$BM (A) materials, exhibiting sufficient offset for the efficient charge separation [279]. Further the Fermi energy levels of metallic electrodes also match well with the respective HOMO and LUMO energy levels of the donor and acceptor materials.

In the present study, UV-vis absorption spectra was studied by using a UV-vis-NIR spectrophotometer (Shimadzu UV-3101PC). The photoluminescence (PL) characteristics were measured by RENISHAW inVia Raman microscope (laser wavelength ~325 nm). All spectroscopic properties were measured as thin films
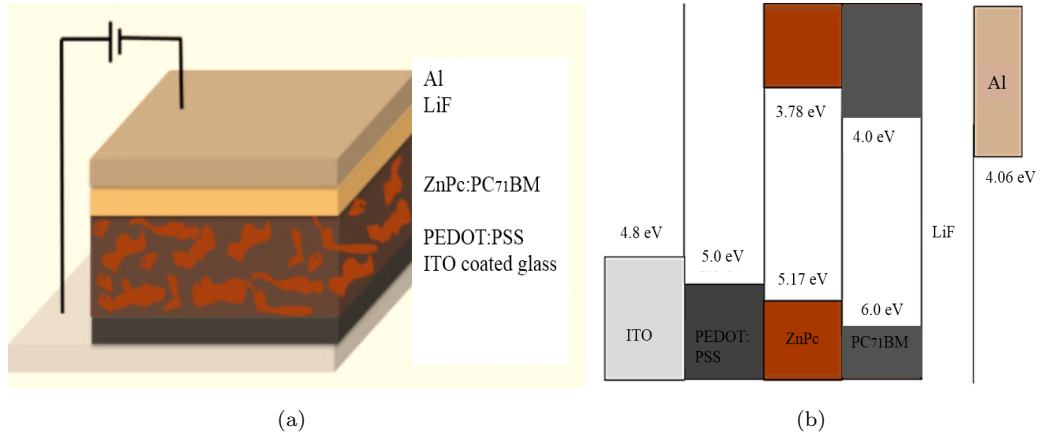
FIGURE 8.2: a) Schematic diagram of the ITO/PEDOT:PSS/ZnPc:PC$_{71}$BM/LiF/Al photodiode (b) energy band diagram of the photodiode relative to the vacuum level.

of photoactive materials. Thermal annealing of the photodiode was performed by directly placing the devices on a digitally controlled hot plate. The photodiode current density-voltage (J-V) measurements were estimated in dark and under simulated solar light using computer interfaced Keithley 236 source measure unit (SMU) in combination with Oriel 67005 solar simulator. Laboratory assembled solar simulator using Xe and Hg(Xe) bulb, sourced by NEWPORT 69907 Oriel Digital Arc Lamp Power Supply, was used to simulate concentrating light with varied illumination levels.

8.3 Results and Discussion

Figure 8.3 shows steady state absorption spectra of pristine thin films of ZnPc and PC$_{71}$BM in visible light range. It is evident from the results that the absorption spectrum of pristine ZnPc thin film exhibits two main bands, usually denoted as Q and B bands [280]. The strong Q band, which exists in the 600-760 nm visible region of spectrum is split into a doublet at 687 and 626 nm. However, the Soret (B) band of ZnPc absorption spectrum covers near UV radiation range of 300-420 nm. The Q band generally arise from $\pi - \pi^*$ transition (a$_{1u}$ to e$_g$) [281] whereas, the B band arise from $\pi - \pi^*$ transition (b$_{2u}$ to e$_g$) in the phthalocyanine
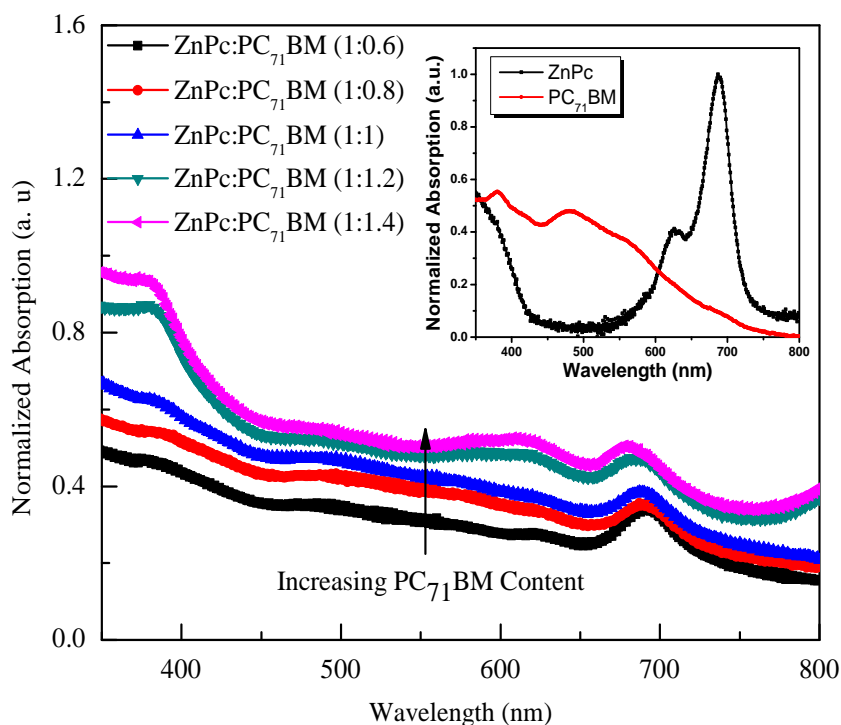
FIGURE 8.3: Steady state absorption spectra of binary (donner and acceptor) blends in five different volumetric ratios. (Inset) absorption spectra of pristine thin films of ZnPc and PC$_{71}$BM.

macrocycle [280]. The favorable spectroscopic feature (broad visible light absorption) is typical in metal phthalocyanine group and it arises due to the aromatic and highly conjugated $18-\pi$ electrons system. It may, however, be observed that the UV-vis spectrum of ZnPc thin film exhibits an absorption lack in 420-600 nm [282]. PC$_{71}$BM thin film exhibits strong absorption ability at shorter wavelengths (350-600 nm). In the present study, PC$_{71}$BM has been blended with ZnPc in order to realize broader (350-800 nm) and consistent absorption spectrum of the photoactive film. Figure 8.3 depicts the normalized spectroscopic response of ZnPc and PC$_{71}$BM interpenetrating binary blends in five different stoichiometries by volume (1:0.6, 1:0.8, 1:1, 1:1.2 and 1:1.4). It is evident from the figure that the absorption spectra of donor and acceptor blend is identical to the superposition of absorption spectra of individual D and A components. It can be further inferred from Fig. 8.3 that by increasing the loading ratio of PC$_{71}$BM in ZnPc:PC$_{71}$BM dyad, increased absorption is observed in 420-600 nm region.

As is known that upon photoexcitation the excitons, generated in interpenetrating bicontinuous (donor and acceptor) photoactive matrix, diffuse to the donor acceptor interface and undergo dissociation process. The photoexcitons may either undergo charge transfer (whereupon charges diffuse to their respective electrodes, producing photocurrent) or energy transfer followed by radiative recombination [283]. The photoluminescence (PL) quenching in solid state photoluminescence spectra is generally considered as a crucial indicative of the efficient non-radiative channel for charge transfer between the donor and acceptor phases. Therefore, in this chapter, solid state photoluminescence spectra of the organic composite have been conducted to investigate the optimum loading ratio of ZnPc:PC$_{71}$BM (by volume) expected for efficient charge transfer. Figure 8.4 presents PL measurements of the pristine ZnPc and PC$_{71}$BM thin films, independently. Whereas, Fig. 8.4 shows that the PL spectra of ZnPc:PC$_{71}$BM bi-continuous organic blend in five different volumetric ratios (1:0.6, 1:0.8, 1:1, 1:1.2, 1:1.4), measured at room temperature in the wavelength range of 400-1000 nm. A prominent photoluminescence quenching (by a factor of $\sim$20) in the solid state is observed for optimal 1:0.8 volumetric ratio of donor and acceptor blend relative to PL emission of pristine ZnPc thin film. The significant PL quenching suggests that the phase separation in 1:0.8 stoichiometric composition of donor and acceptor blend (electronically active materials ZnPc and PC$_{71}$BM) occurs closer to the exciton diffusion length.

The reverse biased current density-voltage (J-V) characteristics at varied incident light intensities are typically investigated to study the photo-response of the photodetector. The order-of-magnitude change in photoconductivity provides with the basis for precise light detection. The change in photoconductivity depends upon multiple factors such as, the extent of light absorption by photoactive film, dissociation of photo-induced excitons into charge carriers and the effective transport of mobile charge carriers to the electrodes. The proposed ZnPc:PC$_{71}$BM dyad exhibits significantly high optical absorption in nearly whole visible spectrum. Furthermore, the desirable donor and acceptor interfacial potential barrier may induce effective excitons disintegration into the mobile charge carriers (holes in ZnPc phase and electrons in PC$_{71}$BM phase). It is also well-known that the
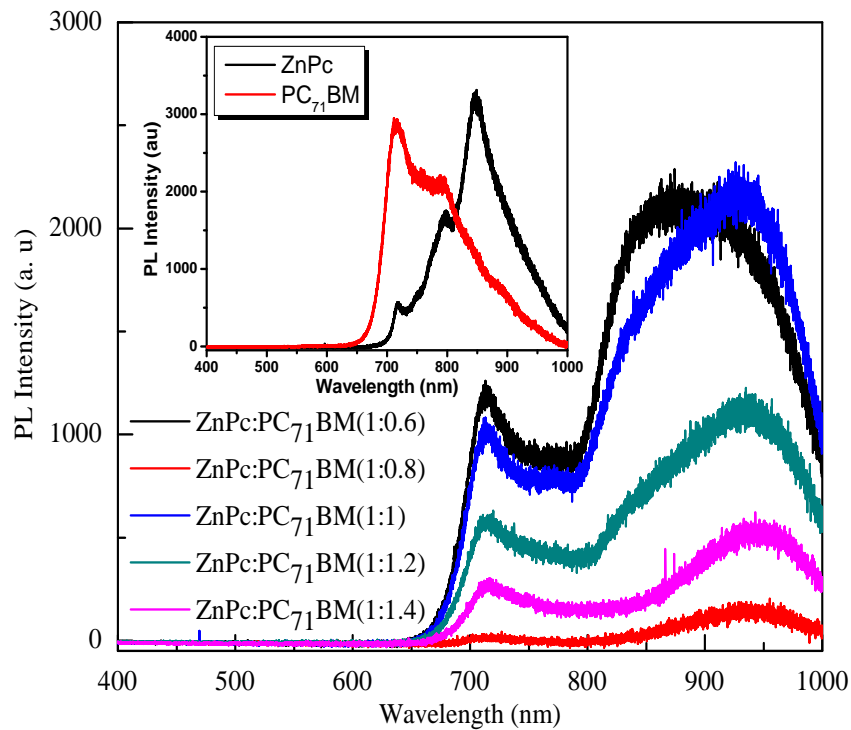
FIGURE 8.4: Solid state photoluminescence spectra of ZnPc and PC$_{71}$BM blends in various volumetric ratios. (Inset) PL spectra of pristine thin films of ZnPc and PC$_{71}$BM.

free charge carriers are drifted to the corresponding electrodes through well connected networks of D and A moieties in the binary blend, thereby contributing to photocurrent. By virtue of the higher hole carrier mobility of ZnPc and superior electron transport ability of PC$_{71}$BM, high photocurrent may be realized.

Figure 8.5 depicts the photocurrent density of the fabricated photodiode at various illumination intensities between 0 and 150 mWcm^2. It can be observed that the photoconductivity of the donor and acceptor blend exhibits a noticeable upsurge induced by the increase in illumination intensity. At higher intensity of light, more excitons are assumed to be generated and eventually disintegrated (sourced by internal donor and acceptor energy offset) in the photoactive film. Hence, a pronounced photocurrent has been observed in the OPD with an increase in incident photon density. Moreover, it can also be observed that under influence of higher order of reverse bias, higher magnitude of photocurrent is observed. This phenomenon may be attributed to the efficient transport of mobile charge
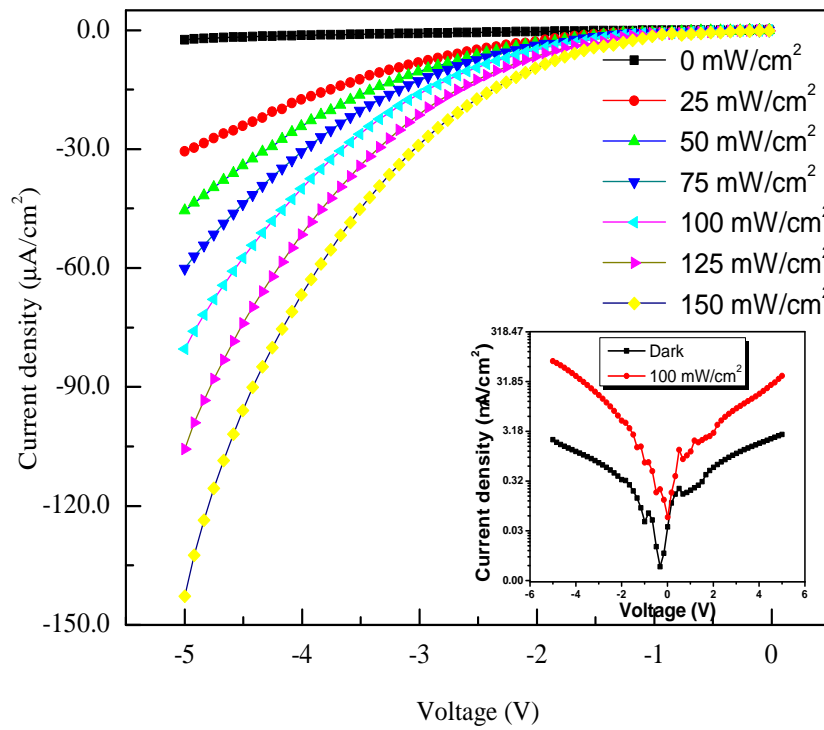
FIGURE 8.5: The *J-V* characteristics of the fabricated photodiode measured at various illumination intensities (0 and 150 mWcm^2). The *J-V* characteristics of the fabricated photodiode under forward and reverse bias in light and dark conditions.

carriers towards respective electrodes under the influence of higher external electric field (sourced by external applied bias). The responsivity of the sensor has been measured as 162.4 μAW^{-1}. The light to dark current density ratio (J_{ph}/J_d) of the fabricated OPD at 3V operational bias has been calculated to be $\sim$20.12.

The transient photocurrent density response of the fabricated OPD has characterized at -4V operational bias under step-like switch ON and OFF illumination (100 mWcm^{-2}), chopping interval of 20s). Four-cycle plot depicted in Fig. 8.6 reveals that the fabricated OPD exhibits considerably fast change of states and significantly stable plateau value. However from Fig. 8.6 it may be observed that when light is switched on, an initial spike and overshoot photocurrent is observed. H. K. Dunn et al. [284] have previously suggested that such response is typical during photocurrent transient measurement and it may be due to imbalance in electron-hole kinetics and surface electron-hole recombination. Furthermore, L. Hu et al. [163] have also reasoned that the charge accumulation and trapping at
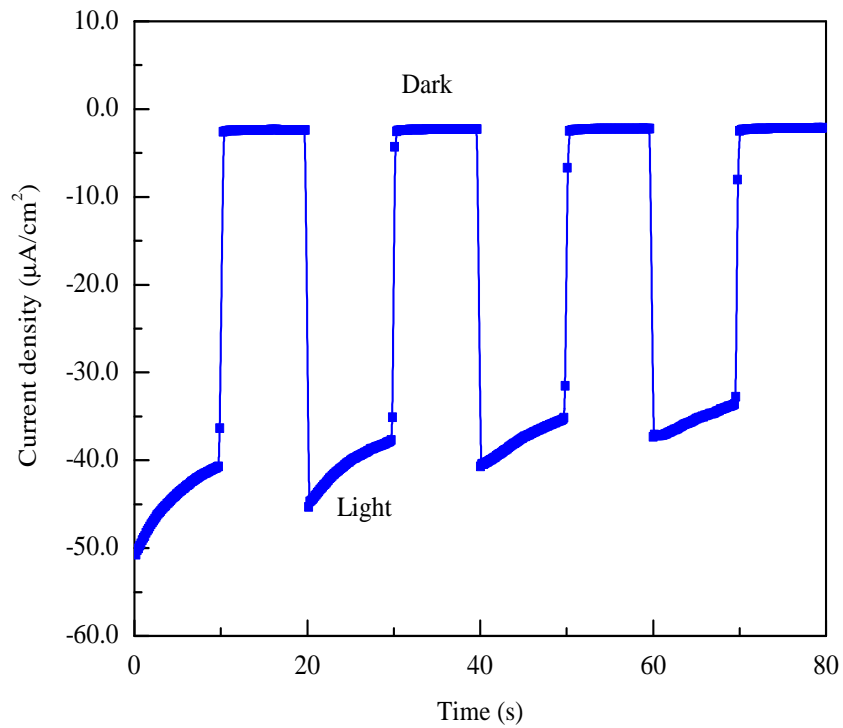
FIGURE 8.6: Photocurrent transient measurement of the fabricated OPD under pulsed light signal (intensity $\sim$100 mWcm^{-2}) at -4V operational bias.

semiconductor and blocking layers interface may also be assumed to be the origin of this phenomenon. The measured response and recovery time for the fabricated OPD are $\sim$200 and 300 ms, respectively. Similar robust response and reset times have been measured for all the OPD devices (9 devices measured). The stability of the OPD under ambient conditions has been studied and no significant change in the photo-response performance has been observed over a period of 1 week.

From Table 8.1., it can be clearly understood that ZnPc-PC$_{71}$BM based OPD has demonstrated relatively high current density at the same voltage compared with the reported references. Significantly high responsivity and superior light to dark current ratio may be assumed to be co-determined by the broad-band visible light absorption and desirable energy levels alignment of ZnPc and PC$_{71}$BM. The observed responsivity of fabricated sensor is higher than the P3HT:C60 photodiode, which exhibited responsivity $\sim$2.52 mAW^{-1} [285]. In fact, the OPD performance of fabricated organic device is superior than organic-inorganic OPD (n-SI/PANI:Boric acid:Nickel phthalocyanine) as well, which yielded significantly

TABLE 8.1: Comparison of photo-sensing parameters of the fabricated OPD with previously reported inorganic, organic inorganic hybrid and organic based devices.

OPDs	Bandwidth (nm)	Responsivity (μAW^{-1})	τ_{res} and τ_{rec}	Reference
Pt/Al$_2$O$_3$/ZnO	–	0.644	>100 ms	[287]
CH$_3$NH$_3$PbI$_3$/TiO$_2$	$350-800$	0.49	$\sim$20 ms	[288]
MEHPPV:VOPcPhO	$350-800$	58	$\sim$4s both	[289]
VOPcPhO:PCDTBT	$350-800$	23.5	$\sim$800 ms both	[290]
ZnPc:PC$_{71}$BM	$350-800$	162.4	$\sim$200 and 300 ms	Present Study

lower $\sim$0.8 mA photocurrent under 105 mWcm^{-2} [286].

8.4 Summary

This chapter demonstrates a solution-processed visible wavelength organic photodiode (OPD) using donor/acceptor dyad of zinc phthalocyanine (ZnPc) and [6,6]-phenyl-C$_{71}$-butyric-acid methyl ester (PC $_{71}$BM), respectively. The synergic absorption profiles of both ZnPc and PC$_{71}$BM moieties have been exploited to realize broader (350 and 800 nm) and consistent absorption spectrum of the photoactive film. The optimum loading ratio (by volume) of D and A dyad has been estimated to be 1:0.8, via quenching phenomenon in ZnPc photoluminescence spectrum. The performance of the OPD has been evaluated by detecting the photocurrent density with respect to varied illumination levels (0 to 150 mWcm^{-2}) of impinging light at different reverse bias conditions. Under identical reverse bias mode, the photocurrent density has shown significant upsurge as the incident intensity of light is increased, ultimately leading to the significantly higher responsivity (162.4 μAW^{-1}) of the fabricated diode. The light to dark current density ratio (J_{ph}/J_d) of the device at 3V reverse bias has been calculated to be $\sim$ 20.12. The transient photocurrent density response of the fabricated OPD has also been characterized at -4V operational bias under switch ON/OFF illumination. The measured response and recovery time for the fabricated OPD are $\sim$200 and 300 ms, respectively.

Chapter 9

Orange Dye Based Multifunctional OFETs

9.1 Introduction

In the recent past, organic field effect transistors (OFETs) have gained much attention due to their lighter weight and lower cost [291]. Orange dye (OD) is a potential organic semiconductor material, which can be employed as a channel material in OFETs fabrication. Devices thus achieved can be used as sensing devices, as the majority of dyes play an important role in sensor fabrication. At low radiation intensities, ODs usually offer high optical sensitivity along with a high absorption co-efficient for a relatively wider spectrum range. OD is one of the most encouraging organic semiconductor dyes and, in recent times, it has received greater attention than ever before in the organic electronic industry because of its wide-ranging applications in humidity, photovoltaic and gas sensing [205–207, 209, 210, 212–214]. It is pertinent to mention here that organic transistors reported for sensing applications have a FET structure [6, 41, 181, 292, 293]. Electrical characteristics of dye-based FETs, i.e., CuPc-NiPc and CuPc-GaAs heterojunctions, are explored and discussed in [6, 291]. Furthermore, organic semiconductor FETs are sensitive not only to light and humidity but also to ambient

temperature. Temperature-dependent electrical properties of CuPc and metal-free phthalocyanine bulk heterojunctions were investigated and reported in [248]. In 2015, Chani et al. fabricated carbon nanotubes (CNT) sensors and evaluated their temperature-dependent characteristics [294]. In 2016, Fatima et al. demonstrated the potential use of NiPc FETs as heat sensitive devices [295].

It is an established fact that processing technology affects the structure and properties of materials, particularly in the case of organic semiconductors [158, 295]. A number of organometallic vanadium complexes such as VO_2(3-fl), $VO(PBO)_2$ and VO(DBM) were synthesized, and their thin films, along with those of commercially produced Vanadyl(acac), were deposited from solutions in organic solvent at different gravity conditions, $183g$, $733g$ and $1650g$, by centrifugation [216]. Sandwich-type samples having layered structures, Al/VO_2(3-fl)/Ga, Cu/VO_2(3-fl)/Ga, Al/-Vanadyl(acac)/Ga, Cu/Vanadyl (acac)/Ga, $Al/VO(PBO)_2$/Ga, $Cu/VO(PBO)_2$/Ga, Al/VO(DBM)/Ga, Cu/VO(DBM)/Ga, Al/Vanadyl(acac) $/TiO_2$/Ga and Cu/VO_2(3-fl)$/TiO_2$/Ga were fabricated. The $I - V$ characteristics of the fabricated devices were then evaluated and it was reported that all the samples exhibited non-linear rectification behavior. Switching characteristics associated with low conductance state to high conductance states were reported for the devices fabricated using VO_2(3-fl) and Vanadyl(acac) films. Furthermore, when Cu electrodes were used, the same devices exhibited memory cell-like characteristics of the type write-once-read-many-times. Farag and Yahia [165] reported the fabrication of humidity sensors using the drop-casting method. It has been reported in the literature that OD-PANI composite films can be deposited from the blend of OD and PANI in distilled water. The sensors then achieved were characterized for their capacitance and impedance versus relative humidity (RH) sensitivities. It has been reported that the impedance of the sensor decreases exponentially, but capacitance increases, with increase in RH due to the humidification process in the film [165].

Properties of OFETs are particularly sensitive to the heating process: the concentration of the charges and their mobility change by changing ambient temperature. These properties are generally engaged in fabricating temperature sensors using
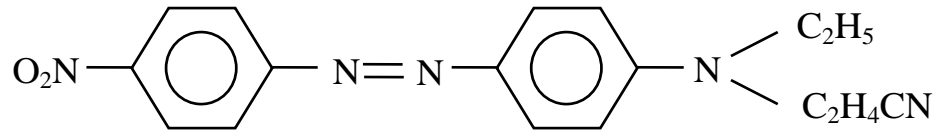
FIGURE 9.1: Molecular structure of organic semiconductor orange dye.

carbon-based semiconductor materials. It is important to mention here that at the metal-semiconductor interface, there is an interfacial layer with interface states [296], which may perform the role of traps for free carriers, thus affecting the response of the device. Furthermore, there is time-dependent device degradation, a universally observed phenomenon in organic semiconductor devices, which apart from other causes is associated with contact resistance degradation. This type of degradation, as a result, generates an extra concern in measuring the resistance of the device with reasonable accuracy. Therefore, impedance is measured as an alternative of the resistance of the samples, because in this case the effects of the traps in the metal-semiconductor contact will possibly be minimized.

In this chapter, OD and OD:sugar-based FETs were fabricated and their temperature and humidity-dependent electrical properties were investigated. The organization of the rest of this chapter is such that the Experimental section describes the experimental details regarding device fabrication and measurements and the Results and Discussion section deals with plausible explanations of the observed results and finally the summary drawn from this research.

9.2 Experimental

For the production of OFETs, high-purity commercially available 3-[ethyl[4-[(4-nitrophenyl)azo]phenyl]amino]propanenitrile, usually known as orange-dye 25 (OD) ($C_{17}H_{17}N_5O_2$), from Sigma Aldrich (CAS RN: 31482-56-1) was used without any further purification. The molecular weight and the density of OD are 323 g and 0.9 $g$cm^{-3}, respectively. The molecular structure of OD is shown in Fig. 9.1.
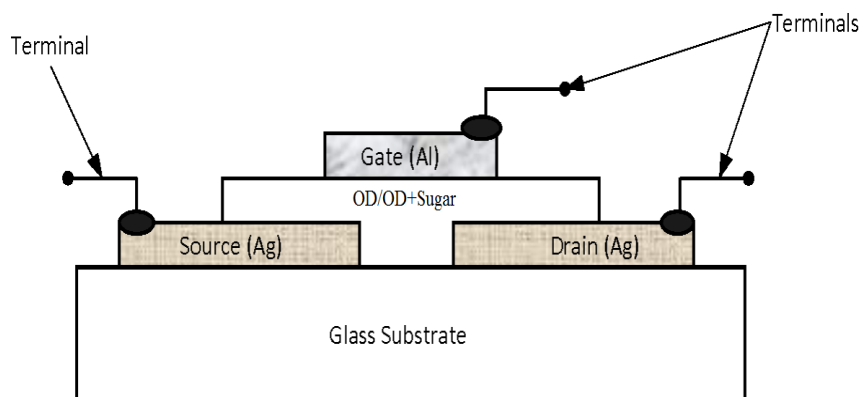
FIGURE 9.2: Cross-sectional view of an organic field effect transistor (OFET).

A cross-sectional view of the fabricated OFET is shown in Fig. 9.2. Surface-type 100-nm-thick Ag electrodes (drain and source) having 2 mm length and 10 mm width at a distance of 30 μm were fabricated by screen printing and chemical etching on a glass substrate. Thin films defining the channel of OFETs were attained from 10 wt.% of OD aqueous solution, while OD composite films were deposited from a mixture of 10 wt.% of OD and 5 wt.% of sugar aqueous solution by using drop-casting technique. The solution in both cases was fairly aqueous and its viscosity was such that it stayed on the substrate even under -1 g condition. The thickness of the films was within the range of 10-15 μm. To define the gate electrode, a 25-nm-thick Al layer was then evaporated using thermal vacuum evaporation. As is well known, Al film usually forms a rectifying (Schottky) junction with organic semiconductors [146]. Thus, the device so achieved is a three-terminal OFET, as shown in Fig. 9.2.

Atomic force microscopy (AFM) of the samples was carried out using Nanosurf AFM apparatus called Flex AFM. Figure 9.3 shows AFM images of the samples grown at different gravity conditions. It is obvious from Fig. 9.3 micrographs that the surface morphologies of grown films are dependent upon the solution as well as gravity conditions. Through AFM, it was found that the average roughness of OD devices fabricated at +1 g was 544.98 nm and at -1 g it was 565.36 nm, whereas OD:sugar at +1 g exhibited an average roughness of 216.27 nm and at -1 g it was 351.02 nm. These data show that composite films are less rough compared to
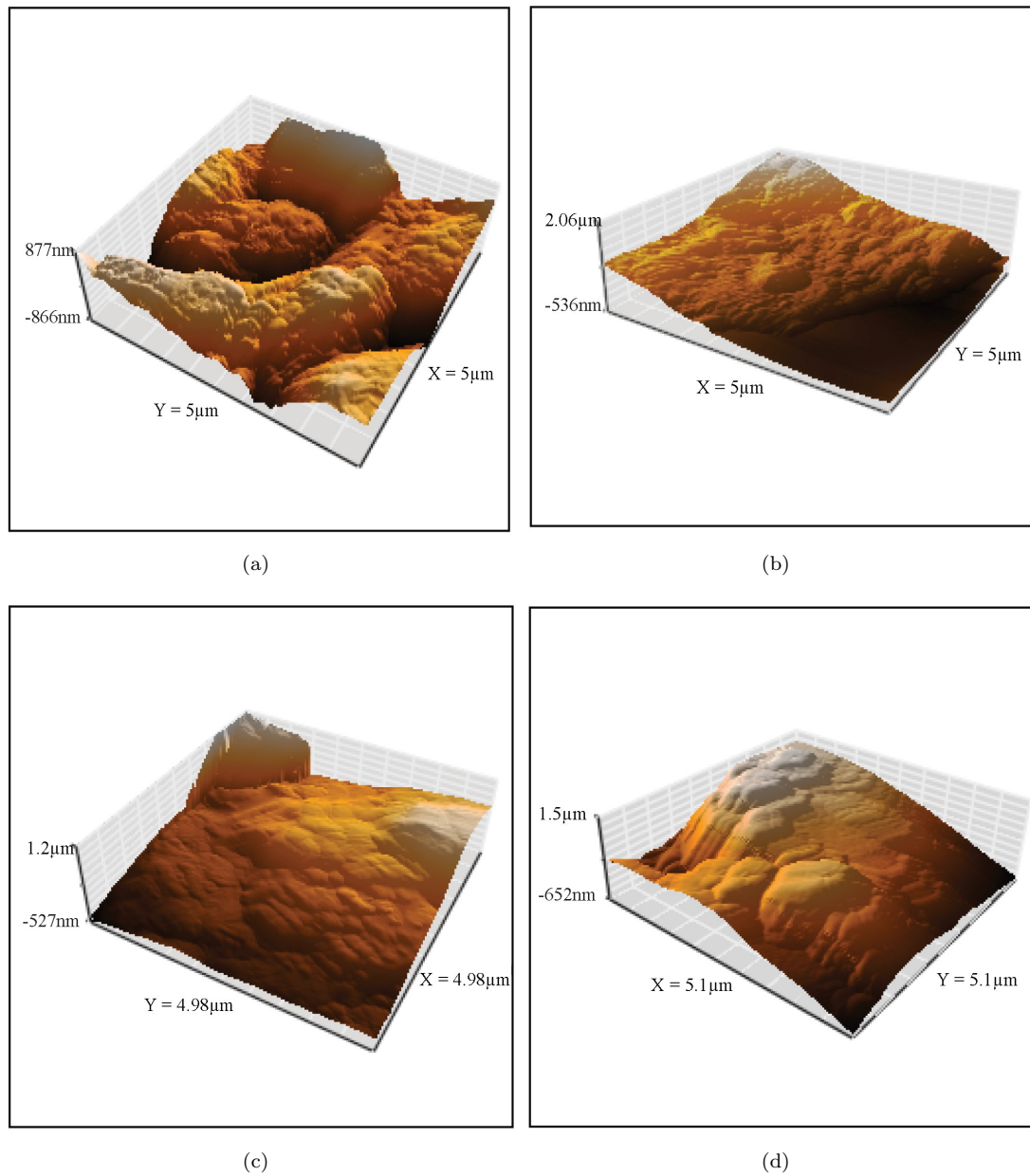
FIGURE 9.3: AFM images of OD films deposited at (a) +1 *g*, (b) -1 *g* and OD:sugar films deposited at (c) +1 *g* and (d) -1 *g*.

porous OD samples, while in both cases, it is clear that films grown at -1 *g* show relatively more roughness than films grown at +1 *g*.

Keeping in mind the surface roughness as depicted by the AFM data, it is obvious that a 25-nm-thick layer of Al, defining the Schottky barrier gate, will remain porous and will allow H_2O molecules to diffuse into OD and its composite.

Solution deposition of thin films of OD or its composite at +1 *g* was carried out

by fixing substrates in the horizontal position such that the solution was dropped on the top of the substrate with pre-fabricated Ag electrodes. The solution was then allowed to dry at room temperature under the usual conditions. On the other hand, for -1 g deposition, OD or its composite was applied to the substrate by a pipette such that the Ag electrodes were facing downward, i.e., towards the ground.

At +1 g deposition, the force which affected the drop and influenced the growth of the film was the sum of the gravitational and surface tension forces, while at -1 g, the force which controlled the film deposition was the difference between the gravitational and surface tension forces. As the growth conditions of the deposited layers were different, it was expected that the properties of the grown films would also be different.

It was noted by optical examination that the films grown at -1 g had relatively less uniformity compared to the films grown at +1 g. Since, at -1 g, the drop was sticking to the substrate under a resultant force caused by gravity and surface tension, therefore, as a natural outcome of this process, this gave a relatively thicker film at the middle of the drop.

Finished devices were characterized in a chamber fitted with humidity (TECPEL 322) and temperature (FLUKE 87) gadgets. Impedance and capacitance variations as a function of ambient humidity and temperature were assessed using MT 4090 LCR meters operated at frequency, $f = 100$ Hz.

9.3   Results and Discussion

The impedance-RH relationship of the fabricated FETs is shown in Fig. 9.4. It is found that, with an increment in humidity, the impedance of all the devices under consideration exhibits a reduction. This reduction may be associated with increased water molecules concentration in the samples, which can cause an increase in the displacement current of the devices [110]. Examination of Fig. 9.4 also
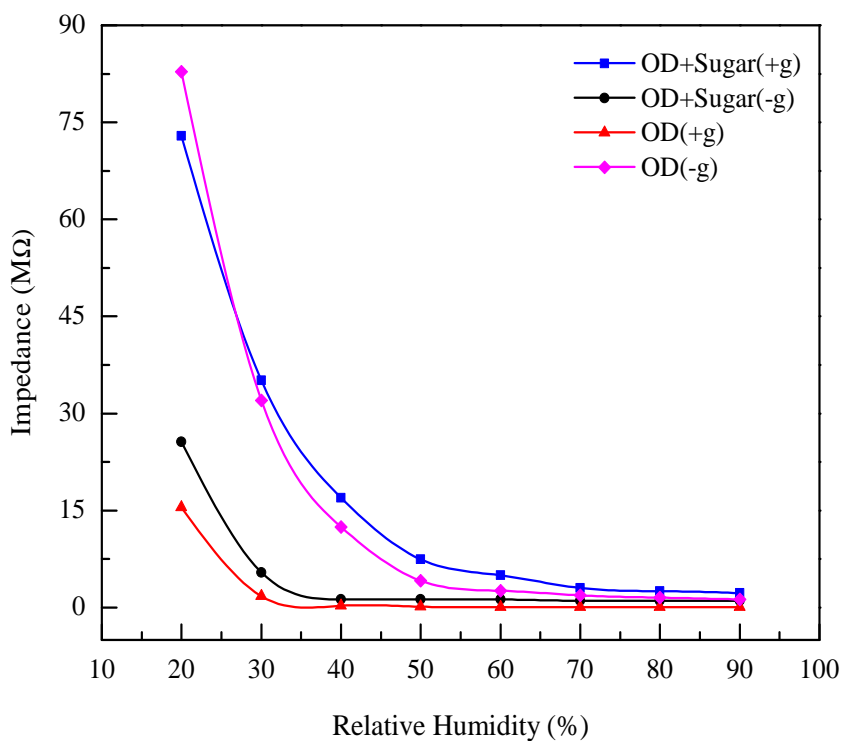
FIGURE 9.4: Impedance-relative humidity of OD and OD composite FETs fabricated at different gravity conditions.

reveals that OD devices fabricated at -1 g and OD composite devices fabricated at +1 g offer a relatively higher impedance at low ambient humidity. Moreover, both the devices exhibited a relatively greater change in their impedance values by increasing the ambient humidity. One can, therefore, conclude that the characteristics of organic semiconductor devices are heavily dependent on their fabrication conditions. For an optimum sensor performance, it is therefore imperative that the sensors should be fabricated by complying with those conditions that offer the highest sensitivity for the variables, which ought to be assessed.

Figure 9.5 shows capacitance-RH relationships of OD and OD composite samples at different gravity conditions. It can be seen that, due to increasing humidity, all the fabricated devices demonstrated an increasing trend in their capacitance such that a maximum variation in capacitance is observed in OD composite FETs fabricated at +1 g and -1 g. This can be explained by assuming that permittivity value of the grown films increased with the increasing concentration of water molecules [297]. Figure 9.5 also shows that capacitance values of composite-based devices
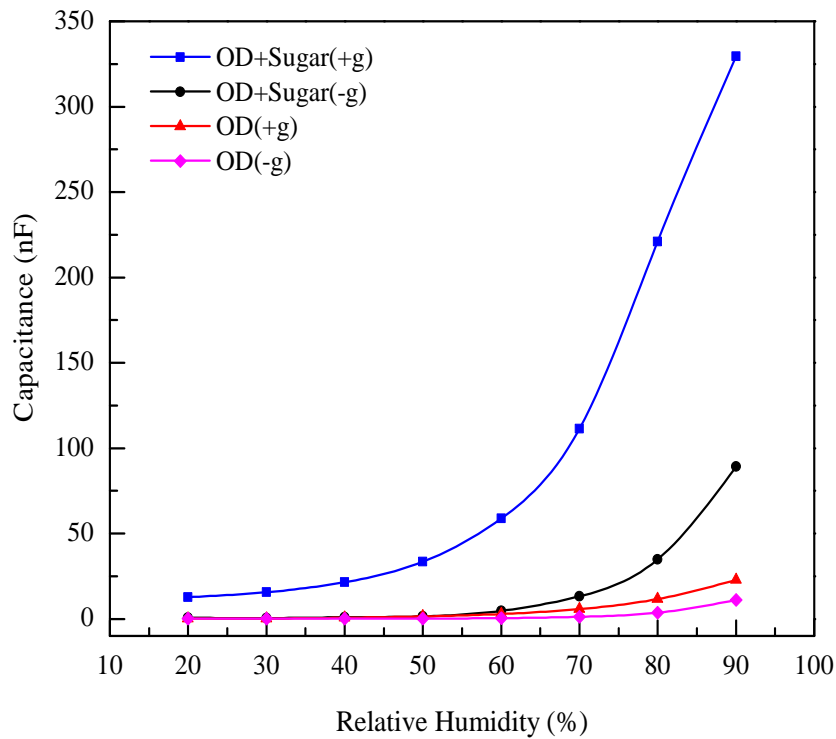
FIGURE 9.5: Capacitance-relative humidity characteristics of OD and OD composite FETs fabricated at different gravity conditions.

are higher than the devices fabricated using pure OD, irrespective of the gravity conditions. Thus, one can say that the device capacitance is more sensitive to channel material composition rather than to fabrication conditions, i.e., the value of g.

Figure 9.6 shows a set of impedance-temperature characteristics measured using OD and OD composite FETs fabricated at different gravity conditions. It is observed that, by raising the temperature, the impedance of all the devices under discussion shows an increase, especially for the devices fabricated at $+1$ g using pure OD. On the other hand, OD composite FETs fabricated at -1 g showed least temperature sensitivity as is evident from the figure.

Capacitance-temperature characteristics measured using OD and OD composite FETs are shown in Fig. 9.7. It is obvious from the figure that, by increasing the temperature, the capacitance decreases. Further, one can also see from the plot of Fig. 9.7 that OD composite devices fabricated at -1 g demonstrated the
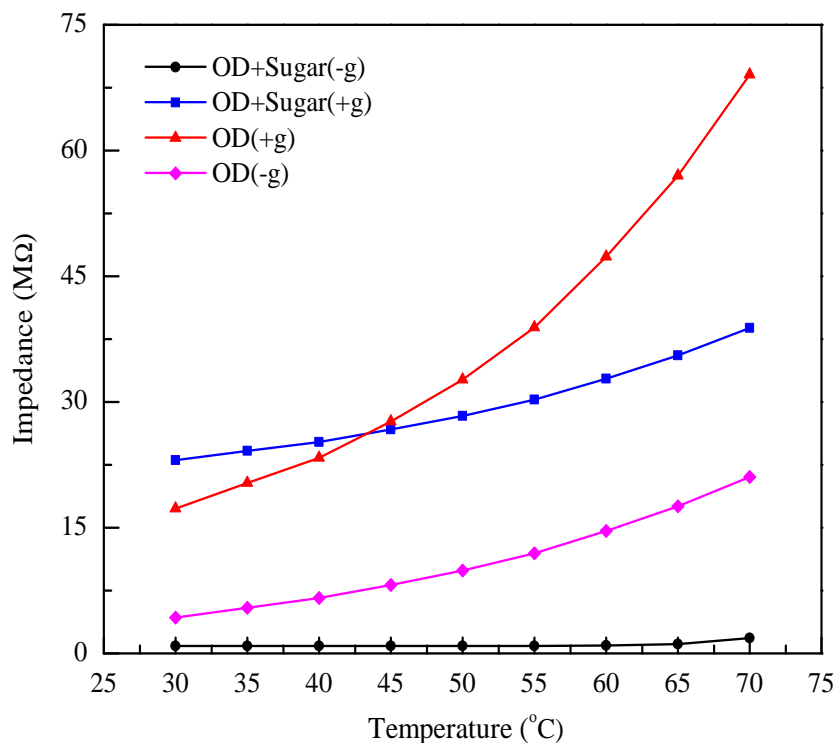
FIGURE 9.6: Impedance-temperature characteristics of OD and OD composite FETs fabricated at different gravity conditions.

highest sensitivity in their capacitance values as a function of ambient temperature relative to other FETs.

The results shown in Figs. 9.6 and 9.7 present an unusual response; however, a plausible explanation of the same can be suggested by carefully evaluating the observed characteristics. In Figs. 9.4 and 9.5, it can be seen that an increase in ambient humidity increases water molecule concentration inside the samples, resulting in a decrease in impedances and an increase in capacitance values. When these samples are subjected to an increased ambient temperature, this initiates diffusion of the water molecules out of the samples, thus generating an upward trend in the impedance-temperature relationship and a declining profile for capacitance-temperature as observed in Figs. 9.6 and 9.7, respectively.

Table 9.1 shows a summary of sensitivities as a function of humidity and temperature for the samples fabricated at different gravity conditions. The reported sensitivities are relative and have been evaluated using final and initial values of either capacitance (C_f - C_i = ΔC) or impedance (Z_f - Z_i = ΔZ) divided by the
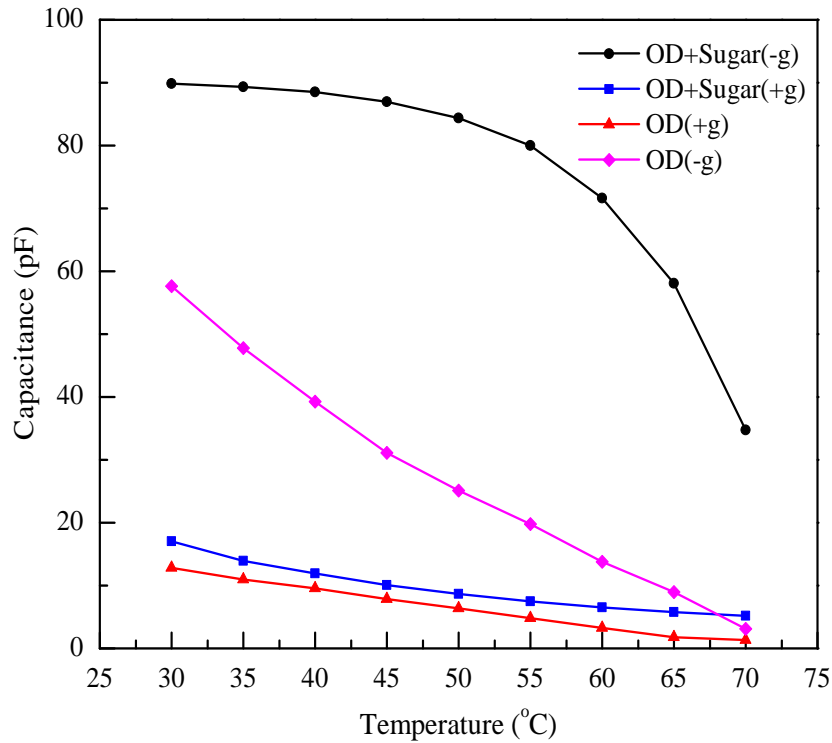
FIGURE 9.7: Capacitance-temperature characteristics of OD and OD composite
FETs fabricated at different gravity conditions.

relative change in humidity (RH_f - $RH_i = \Delta RH$) or temperature (T_f - $T_i = \Delta T$). In our case $T_i = 30$°C and $T_f = 70$ °C whereas, $RH_i = 20\%$ and $RH_f = 90\%$. For the given range, it was observed that each sample had the best response shown by the boldface in Table 9.1. The performance of a sensor is largely dependent on: (1) film thickness; (2) its uniformity and (3) surface morphology. OD and OD:sugar films grown at -1 g offered almost the same $S_{C_T} \approx 1.37$, as shown in Table 9.1. On the other hand, their other responses were not identical, indicating that their film thickness and other physical properties were not the same.

For all the devices listed in Table 9.1, two independent FETs were evaluated and readings were recorded by repeating the experiment four times. Experimental data exhibited a good repeatability of the device characteristics. Further, to assess degradation process with respect to time, the entire experimentation was repeated after 1 week and almost identical characteristics were observed. One can, therefore, assume that degradation, which is usually present in such devices, is relatively slower for OD and its OD:sugar composite.

TABLE 9.1: Sensitivity $(S_{C_T} = \frac{\Delta C}{\Delta T})$, $(S_{Z_T} = \frac{\Delta Z}{\Delta T})$, $(S_{C_{RH}} = \frac{\Delta C}{\Delta RH})$, $(S_{Z_{RH}} = \frac{\Delta Z}{\Delta RH})$ of the samples under effect of humidity (RH) and temperature (T)

Material	Gravity	S_{C_T}	S_{Z_T}	$S_{C_{RH}}$	$S_{Z_{RH}}$
		(pF $^0C^{-1}$)	(MΩ $^0C^{-1}$)	(nF $\%^{-1}$)	(MΩ $\%^{-1}$)
OD	+1 g	-0.2869	**+1.29**	+0.322	-0.22
OD	-1 g	-1.366	+0.418	+0.1576	**-1.164**
OD+sugar	+1 g	-0.295	+0.39	**+4.79**	-1.008
OD+sugar	-1 g	**-1.38**	+0.023	+1.26	-0.35

Since OD and its composite with sugar define the FET channel, the impedance (Z) can be modeled by a resistance (R) and a capacitance (C) in parallel. According to Nahar et al. [298], Au/OD/Al and Al/OD:sugar/Al, samples can be modeled using the equivalent circuit shown in Fig. 9.8. In this figure, C_{eff} represents the capacitance, which is defined by the sum of the dielectric of the air-filled pores of the film, coupled with the dielectric of the active layer, both of which are sensitive to RH and temperature. Moreover, R_{eff} represents the cumulative resistance, which is also a function of temperature and ambient humidity. From the electronic point of view, Z has the following relationship [186]:

$$Z = \frac{R}{1 + j\omega RC} \tag{9.1}$$

where $\omega = 2\pi f$.

Effects of humidity on the device channel, i.e., OD or OD:sugar can be either chemical or physical referred to as chemisorption or physisorption, respectively. In chemisorption, the formation of chemical bonds between OD or OD:sugar and water molecules can take place whereas, in physisorption, van der Waals electrostatic forces usually play a principal role in determining the electrical properties of the material. As is well known, the chemical absorption can sometimes be a slow process. Moreover, its effects on an organic semiconductor can potentially be irreversible in nature. On the other hand, physical absorption is a faster and normally a reversible process. Because of this, it was concluded that the fabricated
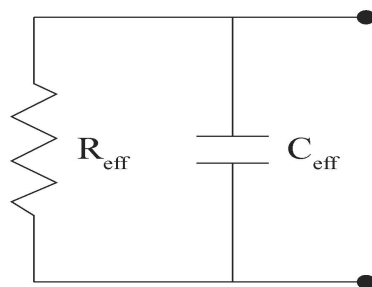
FIGURE 9.8: Schematic diagram of electrical equivalent circuit model of samples.

OFETs characteristics, such as humidity or temperature sensing, were predominantly controlled by the physisorption process occurring in OD and OD:sugar films. This plausible explanation was also supported by the fast response of the transistor, which, on average, was 5-6 s/% in the case of humidity and 7-9 s $°C^{-1}$ for temperature measurements.

Variation in FET electrical characteristics as a function of ambient humidity could be associated with two independent mechanisms. First and the foremost is the diffusion of H_2O molecules into noncrystalline OD or OD:sugar organic films, which is usually reversible. This will modify the electric field island inside the channel and also the associated Schottky barrier depletion. The second mechanism, which can potentially contribute to the electrical response of a FET, is the variation in its Schottky barrier potential caused by polar H_2O molecules. It is assumed that, as the number of H_2O molecules increases, the H_2O dipoles' electric field rises at the surface of the device, as shown in Fig. 9.9. It is also assumed that surface and diffused H_2O molecules collectively modify the Schottky barrier depletion of the device as shown in Fig. 9.9. However, the dominating factor will remain the modification from inside the channel caused by the diffused H_2O molecules. As a result, both the junction current, I_j (which flows from source to drain through the gate) as well as the channel current, I_{ch} (which flows from source to drain) increase [297, 299]. This allows the device to translate the effects of humidity and temperature into an electrical response.

It has been demonstrated that OD-based FETs can be employed as multi-functional
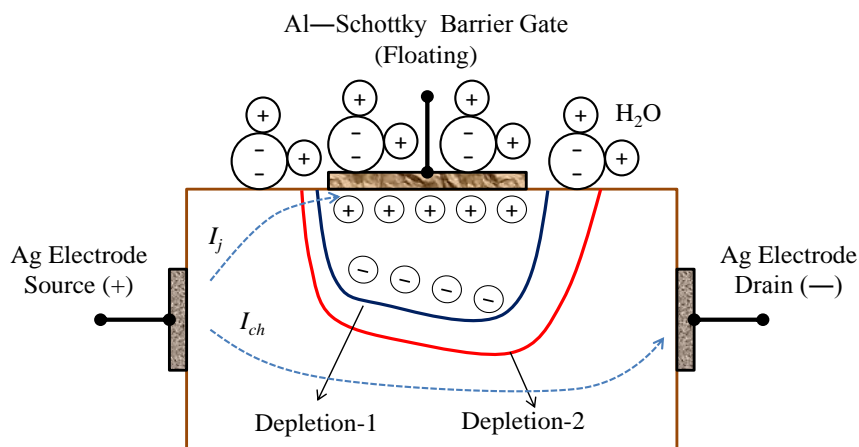
FIGURE 9.9: Effects of polar water molecules on junction depletion region and on source-drain current: depletion-1 represents region at low humidity whereas, depletion-2 at high humidity. I_{ch} and I_j are the channel and the junction current, respectively.

sensors, which can potentially be used for the measurement of humidity and temperature in environmental monitoring systems. The sensitivity of these sensors is dependent upon the fabrication technology as well as on the properties of the organic material used to define the FET channel.

9.4   Summary

This chapter reports the fabrication of organic field effect transistors (OFETs) using 3-[ethyl[4-[(4-nitrophenyl)azo]phenyl]amino]propanenitrile, usually known as Orange-Dye 25 (OD) and its composite with sugar. The study investigated heat- and humidity-dependent electrical characteristics of the fabricated devices. Fabrication was carried out from the aqueous solution of the materials using different gravity conditions, i.e., at positive (normal) gravity (+1 g) and at negative gravity (-1 g). A thin layer (10-15 μm) of OD or OD:sugar was deposited by drop casting on pre-fabricated drain and source silver (Ag) electrodes having 30 μm separation and 2 mm length followed by aluminum (Al) thermal evaporation to achieve Schottky barrier. Devices fabricated using OD at -1 g were more sensitive in capacitance-temperature and impedance-humidity relationships than those fabricated at +1 g. Moreover, OFETs fabricated at -1 g using OD:sugar offered

capacitance-temperature sensitivity much higher than devices fabricated at $+1$ g. It has been observed that, in drop casting method, properties of OFETs are dependent upon gravity as well as solution composition employed for channel definition.

Chapter 10

NiPc Based Multifunctional Transistors

As per commercial perspective, it is important to fabricate OFETs that should be cost effective, and sensitive enough to be employed in variety of applications. So, in this chapter, all these constraints are kept in mind and multifunctional transistors are fabricated, which can be utilized as both photo and temperature sensitive device. One by one each aspect are discussed.

10.1   Introduction

During the past decade, thin-film transistors (TFTs) and field-effect transistors (FETs) based on organic materials as conjugated polymers, oligomers and low molecular weight materials have been widely investigated. Owing to low material and fabrication cost, both organic semiconductor thin-film transistors and field-effect transistors (OTFTs and OFETs) have attracted a lot of interest for their potential applications in organic semiconductor industry [293, 300–303]. Wakayama et al. [304] classified OFETs into two catagories: a) light-emitting (LE) and b) light receiving (LR) OFETs. Wang and Yan investigated bulk hetero-structures fabricated using CuPc and F_{16}CuPc organic semiconductors [305]. On the other

hand, Patowary [193] presented a comprehensive review on OFETs and OTFTs for humidity sensing devices. He also reported the use of OFETs and OTFTs in different types of gas sensors, e.g. ammonia, nitrogen oxides, chlorine, hydrogen, etc. Moreover, it was found that pentacene, TCNQ, conjugated polymers like polythiophenes are sensitive to nitroaromatic compounds based on explosive vapors etc [193]. Abanoz and Dimitrakopoulos [300] reviewed the properties of OFETs fabricated during the years 1984 to 2014. As per their review, the highest reported mobility of an OFET was $43.0 \mathrm{~cm}^2(\mathrm{Vs})^{-1}$, observed in rubrene based macroscopic single crystal OFETs. In addition, some of the OFETs showed sensitivity not only to the applied voltage but also to the electric field of the molecules as well, which is explained by assuming that the gate of the device is effected by the charged molecules and uncharged dipole molecules or molecules that form donor-acceptor charge-transfer complexes or ion-radical salts [300]. Bartic et. al. [306] discussed an OFETs, which can detect charged and uncharged chemical species in aqueous media via field effect process. They also reported chemical sensitivity of OFETs for proteins and glucose.

Recently, researchers have shown interest in organic field effect transistors (OFETs) specially organic phototransistors (OPTs), because of their exciting characteristics especially, as sensing devices. Jakabovic et. al. [307] described photocurrent spectral properties of a double-layer 3,4,9,10 -perylenetetracarboxylic dianhydride and copper phthalocyanine (PTCDA and CuPc) OFET. The charge generation was predicted close to the organic-organic interface only. In [308], the effect of ultraviolet light irradiation on the characteristics of organic phototransistor containing sexithiophene (6-T) and pentacene is examined. The transistors showed two distinguishable responses: fast and slow. The slow response was observed during several weeks, which suggested its possible application in light-addressable memory devices.

In [309], the electrical performance of F_8T_2 [poly(9,9 - dioctylfluorene - co - bithiophene)] - based organic polymer thin-film transistors (OP-TFTs) under white-light illumination and their performance as photo detectors has been studied. These devices, under illumination, exhibited a significant increase in off-state

drain current, while a relatively smaller effect on the drain current was observed in strong-accumulation regime. Mukherjee et al. [310], in 2012, fabricated low-cost, high-performance OFETs by growing single crystalline ordered arrays of a $\pi-$conjugated organic molecule, N,N-dioctyl-3,4,9,10-perylene tetracarboxylic diimide (PTCDI-C_8), through solution processing. Devices fabricated using periodic arrays of elongated crystals exhibited a photoresponsivity (P) of *ca.* 1 AW^{-1} and a photo to dark current ratio of 2.5×10^3 at gate to source voltage, $V_{GS} = 12$ V. A maximum P of ca. 7 AW^{-1} at $V_{GS} = 50$ V with an optical power of ca. 7.5 mWcm^2 was also reported.

Majority of phthalocyanine materials offer high absorption coefficient in wide spectrum and also exhibit high photo-electromagnetic sensitivity even at low radiation intensities [11]. Moreover, the deposition of phthalocyanines thin films by vacuum sublimation is an easy process. Its purification is simple and economical because sublimation occurs at relatively low temperatures (400-600 °C). Copper phthalocyanine (CuPc) and inorganic ferroelectric $PbZr_{0.2}Ti_{0.8}O_3$ heterojunction gate and a ferromagnetic oxide semiconductor $La_{0.87}Ba_{0.13}MnO_3$ channel based photomemory cells have been developed.

The performance and fabrication of a number of OFETs based on dyes namely: copper phthalocyanine; zinc phthalocyanine; hydrogen phthalocyanine and tin phthalocyanine have been described by Bao [311]. He reported that properties of thin films and characteristics of transistors fabricated can be improved if films are deposited on heated substrates ranging from 30-200 °C. The observed field-effect mobility of such devices was greater than 10^{-3} cm^2(Vs)$^{-1}$. The properties of CuPc based OFETs were investigated by Karimov et. al. [6] wherein, they reported that CuPc based OFETs are sensitive to fabrication parameters.

As per commercial perspective, it is important that fabrication of OPTs should be cost effective and they should be sensitive enough to be employed in variety of applications. Under these constraints, NiPc is considered a promising phthalocyanine for OPTs fabrication. As a result, in recent years, NiPc has received much attention by the researchers who explored its potential applications in the fields of

photovoltaics and gas sensing [204–214]. NiPc has a charge carrier mobility of 0.1 $cm^2(Vs)^{-1}$, which is 1000 times higher than CuPc [214]. The energy bandgap of the NiPc is equal to 2.24 eV and 3.2 eV for indirect and direct allowed transitions, respectively [208].

Zubair [236] and Shah [215] fabricated and investigated NiPc based Schottky barrier diodes whereas, Chaabane et. al. [206] reported effects of annealing on NiPc based OPTs fabricated using 45 nm thick film. In this transistor, NiPc was deposited on Si_3N_4, which was grown on SiO_2 to fabricate Schottky barrier gate. This transistor showed good performance however, its fabrication process was quite complicated. It is a well-known fact that in FETs fabrication, metal-semiconductor junctions (Schottky junctions) are used to control the flow of current, which definitely gives a simple and cheaper option compared to oxide or insulator junctions [61]. The review of published research papers motivated us to fabricate NiPc based OPTs with varying NiPc film thickness and to investigate their properties under illumination. In these OPTs, Al-NiPc Schottky junctions are used that have the structure of MESFETs unlike to MOSFETs [61].

10.2   Experimental

NiPc was obtained from Sigma-Aldrich and used without further purification. Figure 10.1 shows its molecular structure of NiPc used as a *p*-type organic semiconductor. Thin films of NiPc were thermally sublimed on glass substrates having pre-deposited 100 nm thick silver film electrodes grown at 500 °C and $\sim 10^{-4} Pa$ in Edwards AUTO 306 vacuum coater equipped with diffusion pumping system and film thickness monitor. The substrates temperature in this process was held at ~ 40 °C. UV-VIS-NIR absorption spectrum of grown NiPc thin film having 300 nm thickness is shown in Fig. 10.2.

The absorption spectrum was obtained from Lambda 950, Perkin Elmer UV-VIS Spectrophotometer. El-Nahass et. al. [209, 312] investigated the absorption spectrum of NiPc films in UV-VIS region and observed two bands: the Soret and
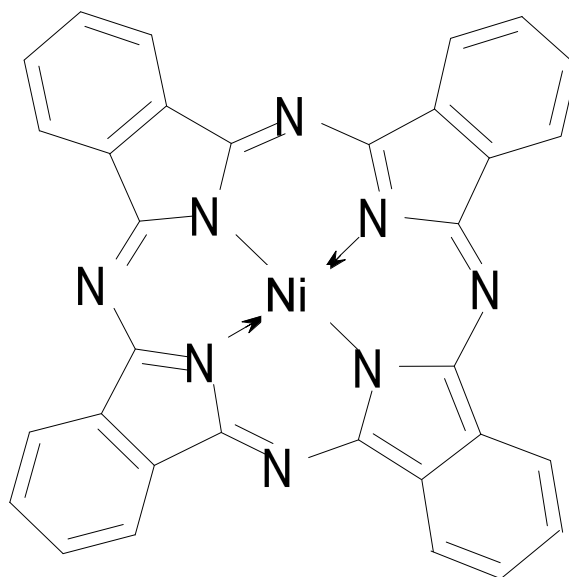
FIGURE 10.1: Molecular structure of NiPc used as a p−type organic semiconductor.
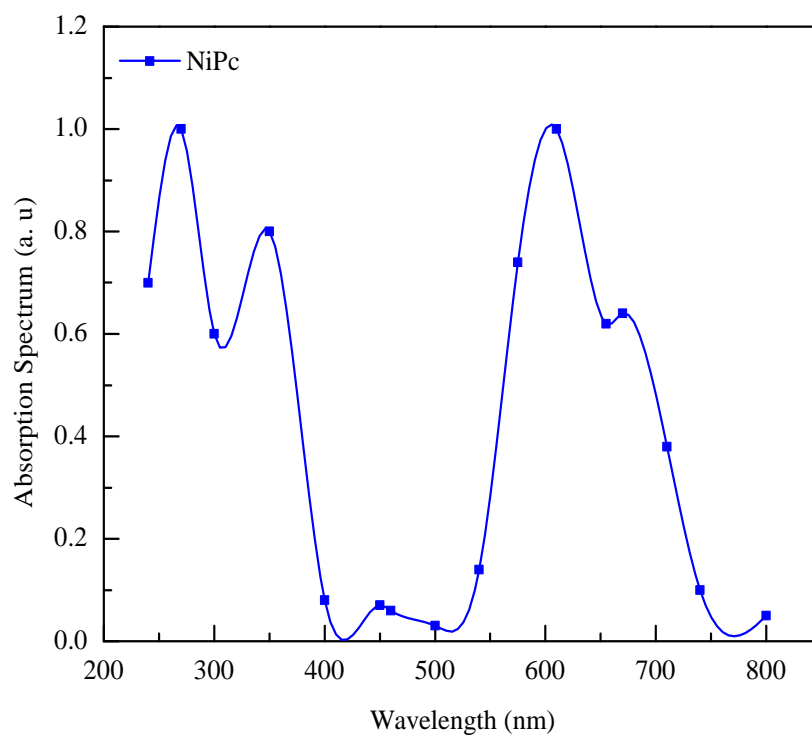
FIGURE 10.2: UV-VIS-NIR absorption spectrum of grown NiPc thin film (300 nm thickness).

(a) (b)
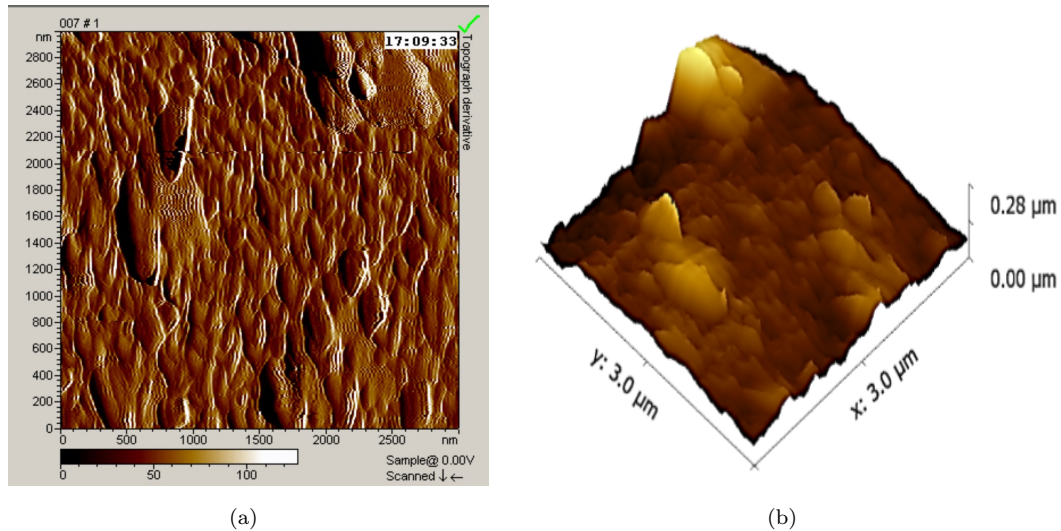
FIGURE 10.3: 2D and 3D AFM micrographs of NiPc film (300 nm thickness).

Q-band. They are associated with two indirect allowed transitions with energies 2.77±0.03 and 1.66±0.02 eV. Comparison of our results and those given in [209, 312] showed reasonable similarity.

Figure 10.3 presents 2D and 3D AFM micrographs of NiPc thin film obtained by Agilent Pico Plus under ambient condition with a scan size area of 2 μm. 2D micrograph is helpful to find the grain size whereas, 3D AFM image is used in understanding the orientation of the grains. As measured from film thickness monitor, the deposited film was 300 nm. However, from AFM 3D image, the evaluated thickness of the grown film was 280 nm.

To obtain Schottky barrier gate, a semi-transparent 22 nm thick Al film having 22 mm width and 10 mm length was deposited on NiPc film and a 10-15 % transparency in Al film was observed. Deposition rate of 8 nm/min, 2 nm/min and 5 nm/min for Ag, Al and NiPc films, respectively was observed. The finished devices were annealed at 150 °C for about 30 minutes in a vacuum chamber.

Figure 10.4 shows a cross-sectional view of fabricated OFET: source and drain terminals are connected with Ag films, and Al film is used as gate terminal. Cross-sectional area of the channel is 40 μm × 10 mm for each sample and thickness is 100 nm, 200 nm and 300 nm for sample 1, 2 and 3, respectively. A filament lamp was used as a source of light. The emission spectrum of the filament lamp covered
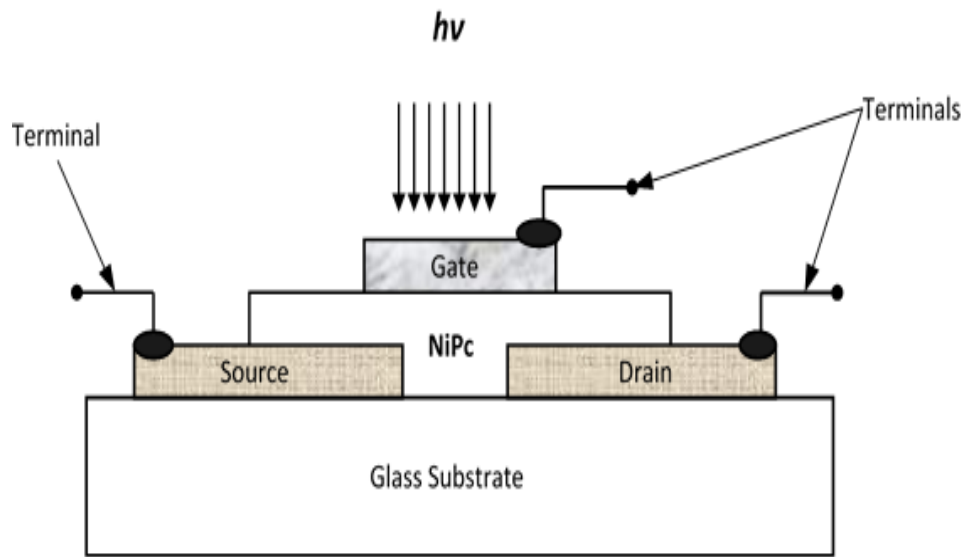
FIGURE 10.4: Cross-sectional view of the fabricated OFET: source and drain terminal connected with Ag films and Al film was used as a gate terminal.

a wide range of wavelengths starting from 200 nm to 2200 nm with maximum at 850 nm. The current-voltage $(I - V)$ measurements were carried out by digital meters 3256 HITES TER at room temperature.

10.3 Results and Discussion

10.3.1 Effect of Light on OFETs

Figure 10.5 (a) shows output characteristics: drain current (I_D) and drain-source voltages (V_{DS}), relationships for different V_{GS} of a NiPc FET having 300 nm thick channel film. Figure 10.5 (b) shows transfer characteristics of the same FET at $V_{DS} = $ -3 V. Techniques to simulate output and transfer characteristics of organic FETs have been developed in [41, 61], and the validity of the same have been assessed in [313, 314] for P$_3$HT:PCBM and CuPc based FETs. By employing the same approach in the saturation regime, the mobility (μ) of NiPc charges has been estimated as 3.05×10^{-2} cm^2(Vs)$^{-1}$. El-Nahass et al. [210] reported $\mu = 8.9 \times 10^{-3}$ cm^2(Vs)$^{-1}$ for NiPc based FET. The improved value of μ, in our case, may be
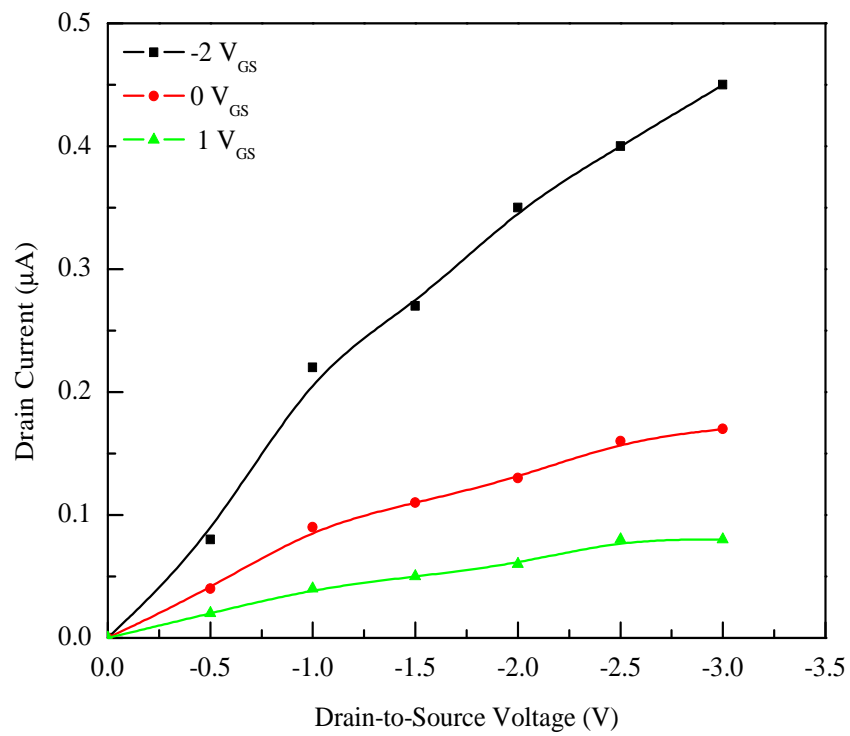
(a)
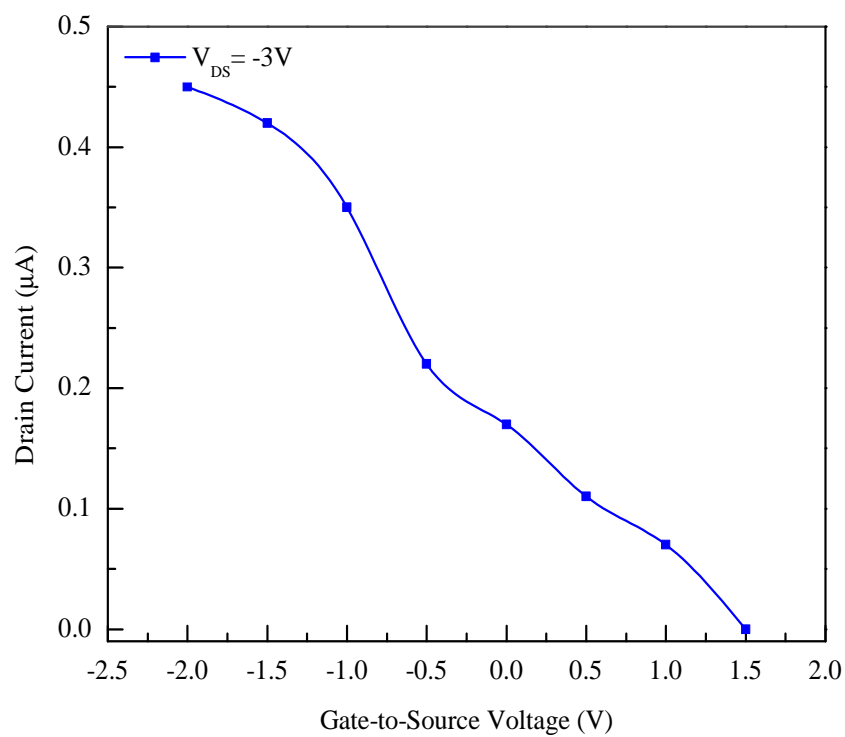
(b)

FIGURE 10.5: (a) Output characteristics: drain current (I_D) to drain source voltage (V_{DS}) relationships for NiPc based FET with 300 nm thickness of NiPc film at V_{GS}= -2 V, 0 V and 1 V, (b) Transfer characteristic of the FET at drain to source voltage of -3 V.

associated with changed fabrication conditions, which resulted in improved NiPc thin film and the device channel.

Figure 10.6 shows variation in I_D (V_{DS}) as a function of incident light intensity through semi-transparent gate electrodes of OFETs having channel thicknesses: (a) 100 nm; (b) 200 nm and (c) 300 nm. The value of V_{GS} for these measurements was kept at 0V. It was observed that the magnitude of I_D increases with increasing intensity of incident light for devices under consideration. At incident energy density of 34.4 mWcm^{-2} and at $V_{DS} = 3\ V$, an average increase in I_D is 7, 13 and 11 times (ratio of light ON and OFF currents) for 100 nm, 200 nm and 300 nm devices, respectively. These values are comparable with the responses of OFETs as described in [6].

Figure 10.7 shows variation in $I_D(V_{DS})$ characteristics as a function of irradiation for OFETs under consideration. During this experiment, V_{GS} was kept at 0V. Figure 10.7(a) shows that maximum observed value of I_D was at $V_{DS} = 3V$ when illumination intensity was 34.787 mWcm^{-2}, and this maximum value of I_D under the same biased and illumination conditions increases, as shown in Fig. 10.7 (b) and (c), by changing the thickness of the channel from 100 to 300 nm. This increase may be associated with: a) enhanced absorption of incident light inside the channel and b) change in cross-sectional area of the devices available for the flow of the current.

To design an equivalent circuit of the OPT under discussion, gate-source and gate-drain $I - V$ characteristics under dark conditions were evaluated, which exhibited rectifying behavior, confirming the Schottky nature of the junctions. In the second step, the same experiment was repeated under illumination and the generated voltages were measured. These experiments allowed us to design a simplified equivalent circuit of the OPT that is shown in Fig. 10.8.

In the design of equivalent circuit, we also used the circuits of OPTs [315], OPT [6] and organic-on-organic photoelectric cells [11]. While developing equivalent circuit it is assumed that: (i) the effects of light on independent current sources (I_1 and I_2) and also on dependent current source (I_3) are linear; (ii) the drain and
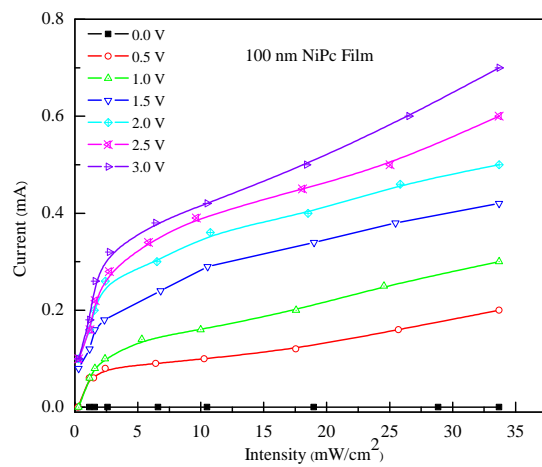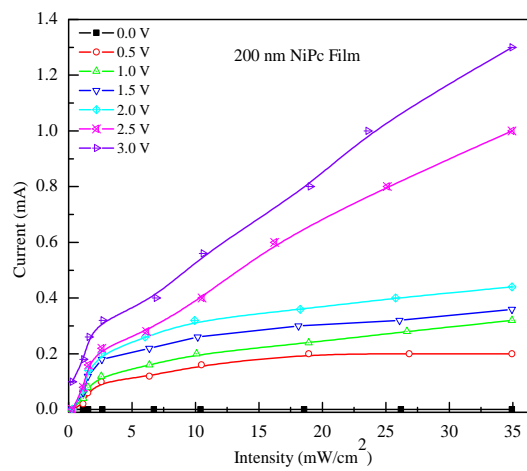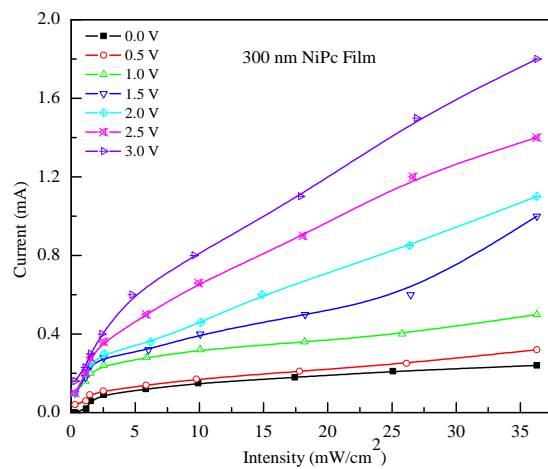
FIGURE 10.6: Drain current to light intensity relationships at different drain to source voltages with NiPc thickness of (a) 100 nm, (b) 200 nm and (c) 300 nm.
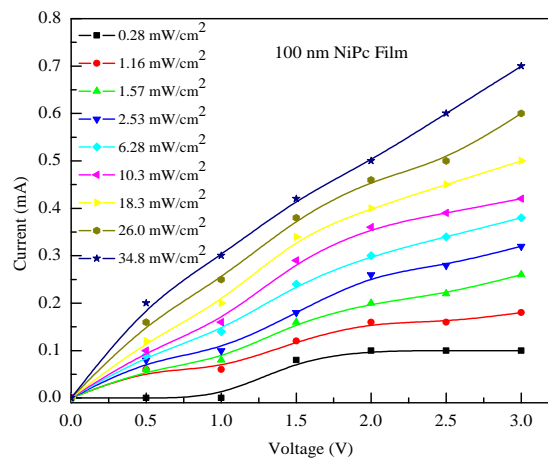
(a)
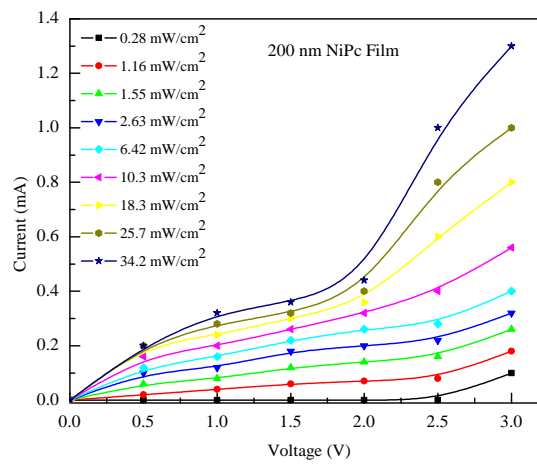
(b)
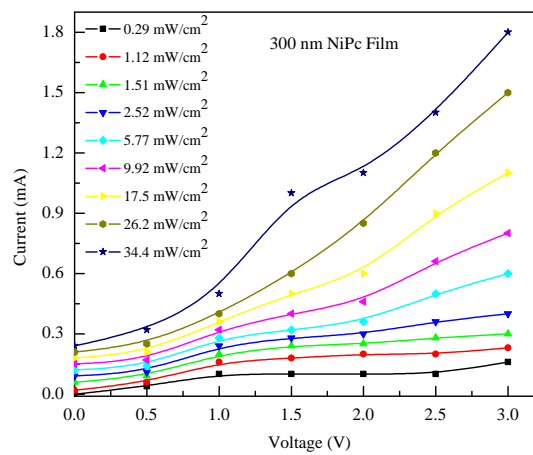
(c)

FIGURE 10.7: Drain current and drain to source voltage relationships at different illuminations with NiPc thickness of (a) 100 nm, (b) 200 nm and (c) 300 nm.
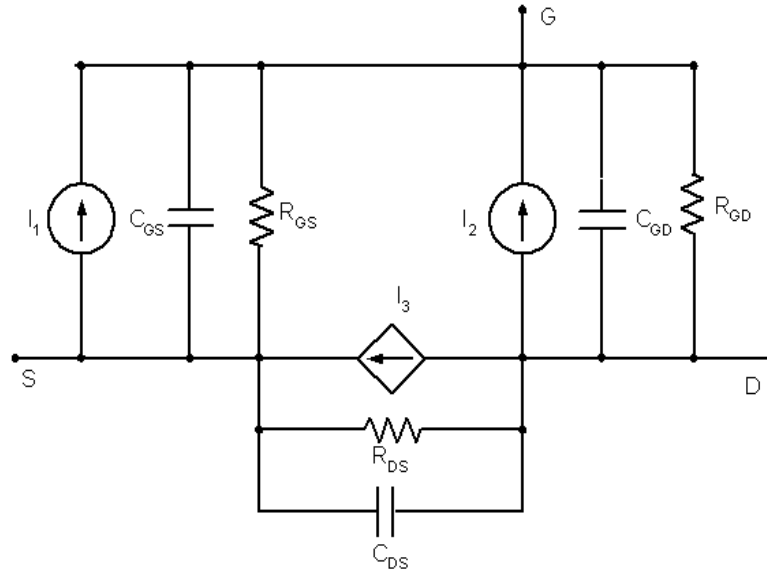
FIGURE 10.8: A simplified equivalent circuit diagram of OPT.

source series resistances are negligible; and (iii) V_{DS} is constant at $V_{GS} = 0$ V. In the circuit, shown in Fig. 10.8, the independent current sources I_1 and I_2 represent Al-NiPc junction based photoelectric cells whereas, the dependent current source I_3 represents the source-drain channel as a variable resistance. Gate to source resistor, R_{GS} and gate to source capacitor, C_{GS} are the diffusion resistance and junction capacitance, respectively. Likewise, the parameters R_{GD} and C_{GD} are the gate-to-drain resistance and capacitance, respectively. The resistance R_{DS} is the drain resistance and the capacitor C_{DS} is mainly a drain-to-source parasitic capacitance of the devices.

Two mechanisms, namely: photoconductive behavior and photovoltaic behavior are assume to be responsible for the observed photo response of the OPT as reported in [308]. Photoconductive behavior (increase in conductance under illumination) occurs probably due to the generation of excitons, which are of higher energy than the bandgap of the organic semiconductor (NiPc). Subsequently, these excitons split into electrons and holes under the influence of applied V_{DS} and thus contribute to the channel current, I_D of the device. On the other hand, the observed photovoltaic behavior (generation of voltage under illumination) could be associated with the rectifying metal-semiconductor junction with built-in potential barrier and electric field that in turn splits the excitons into electron-hole

pairs, which after the conduction define the device's current. Moreover, it is assumed that under irradiation, excess carriers are generated, which in turn reduce the metal-semiconductor potential barrier and its associated field. A reduction in barrier would mean more available channel cross-section for the flow of current and the process contributes to an increased conductivity of the channel. The performance of the photodetector is assessed by a parameter, R_{res} defined as [308]:

$$R_{res} = \frac{I_{ph}}{P} = \frac{I_{di} - I_{dd}}{EA_{eff}} \tag{10.1}$$

where R_{res} is the responsivity, I_{ph} is the drain current generated by light irradiation, P represents optical power incident on the channel of the device, I_{di} is the drain current under illumination, I_{dd} is the drain current under dark conditions, E is the irradiation of the incident light and A_{eff} is the effective device area (area of the channel). The ratio of photo (ON) and dark (OFF) currents, $r_{on/off}$ is represented as:

$$r_{on/off} = \frac{I_{di}}{I_{dd}} \tag{10.2}$$

For 200 nm thick NiPc device, the observed value of $R_{res} = 0.0087\ AW^{-1}$ and $r_{on/off} = 13$ at incident radiation intensity of 34.4 mWcm^{-2}. The obtained values are in good agreement with the data described in [308]. However, in the former case, the transistor fabrication is based on a simple technology (metal-organic semiconductor Schottky junction was fabricated) and thus economical due to its very nature compared to the latter case where organic semiconductor was deposited on SiO$_2$/Si substrate.

The performance of fabricated OPTs discussed hitherto is based on the concept discussed in [308] wherein, expressions for photocurrent caused by photovoltaic effects and photocurrent induced by photoconductive effects are presented. For further research, we are working on a mathematical model of OPTs based on its equivalent circuit proposed in Fig. 10.8 to develop a better understanding of its $I - V$ characteristics. This chapter focused on experimental characteristics of NiPc based Schottky barrier OPTs and their performance as a function of channel thickness [316, 317].
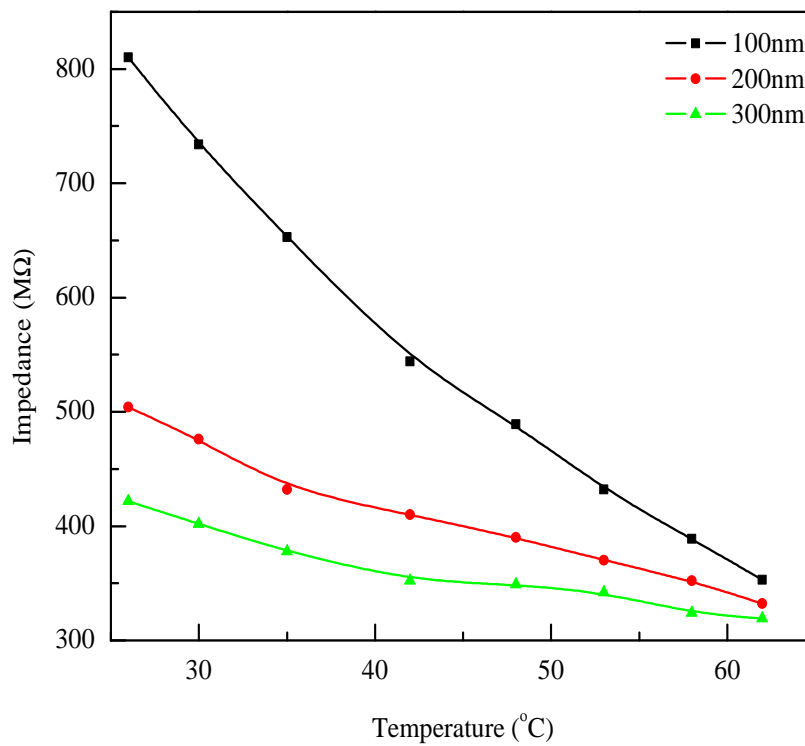
FIGURE 10.9: Impedance to temperature relationships for the FETs: thickness of NiPc films were 100 nm, 200 nm and 300 nm.

10.3.2 Effect of Heat on OFETs

For measuring the heat effect on same OFET, the devices were characterized in a chamber wherein, temperature and impedance were assessed by FLUKE 87 and MT 4090 LCR meter, respectively, at operating frequency of 100 Hz.

Figure 10.9, impedance-temperature relationships of NiPc organic semiconductor FETs are shown. In [318], it is established that FET with thinner NiPc have larger resistance. Here, similar results are obtained in Fig. 10.9 by measuring the impedance at 100 Hz. In Fig. 10.10, normalized impedance to temperature relationships are shown. It is observed that as temperature increases, impedance decreases for all transistors especially, for those transistors who have thinner NiPc films. It is obvious that as the thickness of the NiPc film is decreased, depletion region contribution, which is more sensitive to the heating effect, in the total cross-section of the films, is increased.
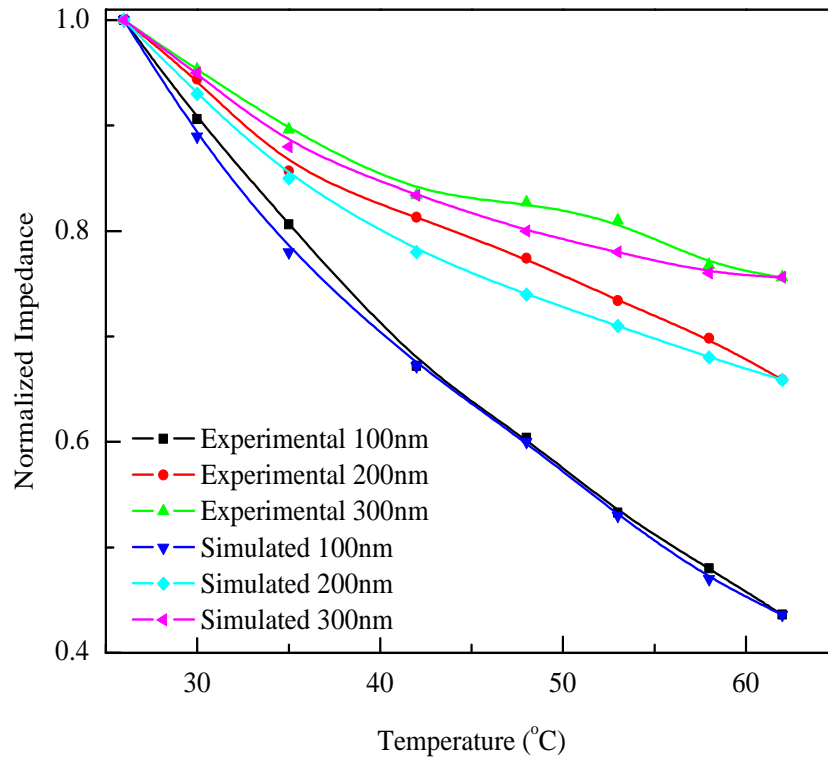
Thus, devices with thinner films exhibited pronounced heating effects. Relative impedance to temperature relationships for the NiPc film based FET were approximated by exponential function given as:

$$y = e^{-x} \tag{10.3}$$

where,

$$x = (T - 26)b \tag{10.4}$$

where 26 °C is initial temperature, T is temperature in °C, which is ≥ 26 °C and b is the fitting parameter. It was observed that simulation complies reasonably well with experimental data at $T = 62$ °C, as shown in Fig. 10.10. It was determined that $b = 0.0231$ °C^{-1}, 0.0121 °C^{-1} and 0.008 °C^{-1} for the simulated graphs related to the NiPc transistors (Fig. 10.10) for NiPc thickness of 100 nm, 200 nm and 300 nm, respectively.
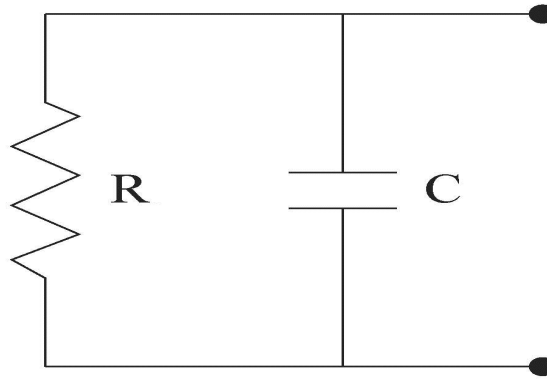
FIGURE 10.11: Equivalent circuit of the contact impedance of NiPc sample.

Assuming that FET in this case is a two-terminal temperature sensor then the following equation shows the sensitivity relationship of the sample [186]:

$$S = \frac{\Delta R}{R_0 \Delta T} \times 100\% \tag{10.5}$$

where, R_0, ΔR and ΔT represents the initial resistance, change in resistance and change in temperature, respectively.

For each sample, average temperature sensitivity was calculated and found to be -2.35% °C^{-1} (100 nm thick NiPc film), -1.39% °C^{-1} (200nm thick NiPc film) and -1.18% °C^{-1} (300 nm thick NiPc film) at 100 Hz. Temperature sensors, which are produced commercially (thermistors), usually offer DC sensitivity ranging from -3% °C^{-1} to -5% °C^{-1} [186].

In our case, the observed sensitivities are based on AC measurements, which are normally lower than DC sensitivities. However, AC sensitivities have the advantage, especially, for the devices based on organic semiconductor, because fluctuation in contact resistance and accordingly in the current causes less effect in AC measurements. This may be explained by the fact that the value of impedance associated with the capacitive component allows to by-pass the current (Fig. 10.11) by the equivalent circuit of a contact.

The circuit shown in Fig. 10.11 can be used not only as an equivalent circuit of contact impedance, but also as a simplified equivalent circuit of an OFET.

If an OFET is used as a two terminal temperature sensor, its response is quasi-exponential (Fig. 10.10) and for practical applications, its impedance-temperature relationship can easily be linearized by using a linearization circuit as shown in Fig. 10.11 [217]. For the equivalent circuit shown in Fig. 10.11, the impedance (Z) can be obtained as:

$$Z = \frac{R}{1 + j\omega RC} \tag{10.6}$$

where ω is the angular frequency, R and C is the resistance and capacitance, respectively. The decrease in impedance by the increase in temperature is associated with two main parameters: a) increase in the capacitance of the sample and b) decrease in its resistance value. Reduction in the sample resistance can be explained as: with increased temperature, there will be more bonds breaking causing increased carrier concentration (n_i) in NiPc film, which can be expressed as [21, 187, 246]:

$$n_i = N_0 \exp\left(\frac{-E_g}{2kT}\right) \tag{10.7}$$

where N_0 is the pre-exponential factor, E_g represents energy gap and k is the Boltzmann constant. On the other hand, there are a number of factors, which affect the capacitance of the samples. They are: a) relative dielectric constant of the thin film material; b) area of electrodes and c) gap between electrodes. Capacitance relies upon material's polarizability (α), sources of which are electronic (α_e), dipolar (α_{dip}) and ionic (α_i) [187]. Another form of polarizability, that is well known, is due to transfer (α_{tr}) of charge carriers (electrons and holes) as reported in [319]. It is worth mentioning that α_e is due to relative displacement of orbital electrons of atoms whereas, the α_{tr} is due to charges participating in conduction process, which can be trapped in the semiconductor-electrode interface. The Clausius-Mosotti relationship, if we take into consideration only polarizability due to transfer of charge carriers, can be represented by the following equation [187].

$$\frac{\varepsilon - 1}{\varepsilon + 2} = \frac{N\alpha_{tr}}{3\varepsilon_0} \tag{10.8}$$

where ε is the relative permittivity, $N \sim n_i$ is the total concentration of charge carriers [61] and ε_0 is the permittivity of free space.

Moreover, in organic semiconductors, mobility (μ) has also got temperature dependence and it increases with increasing temperature thus, contributing to the increase in conductivity as given below [21].

$$\mu(F,T) \approx \exp\left(\frac{-\Delta E}{kT}\right) \Big/ \exp\left(\beta\sqrt{\frac{F}{kT}}\right) \qquad (10.9)$$

where F, ΔE and β are electric field, activation energy and exponential factor, respectively.

Temperature dependent increase in mobility is usually associated with hopping mechanism [21, 187, 246]. On the other hand, mobility decreases in those materials wherein, conduction is primarily related to the energy bands [315]. If mobility of a sample is less than $1\ \mathrm{cm}^2(\mathrm{Vs})^{-1}$, it is considered that the hopping mechanism of charges transfer is a dominating one. For mobility greater than $1\ \mathrm{cm}^2(\mathrm{Vs})^{-1}$, the energy band related conduction would be a prevailing mechanism [21, 187, 246].

As shown above (Eq: (10.6) and Fig. 10.11), the parallel combination of capacitance and resistance can be used to model impedance. The resistance decreases as temperature increases, and capacitance increases, due to increase in permittivity. This definitely shows decrement in impedance because of the dominating fact of the resistor.

Figure 10.12 shows the simplified schematic diagram of an OFET, flow of currents and depletion region at low and high temperatures as well. In particular, the figure demonstrates the effect of heating on OFET channel area: depletion region at lower (1) and higher (2) temperatures, space charge (3 and 4), I_{ch} and I_j are the channel current and the junction current, respectively. The diagram illustrates that as temperature increases, width of the depletion region decreases thus, increasing the cross-section of the conductive channel of the OFET. It definitely decreases the resistor and accordingly impedance of the transistor, which was observed experimentally (Fig. 10.9 and 10.10). The summary of the temperature sensitivity is described by Table 10.1.
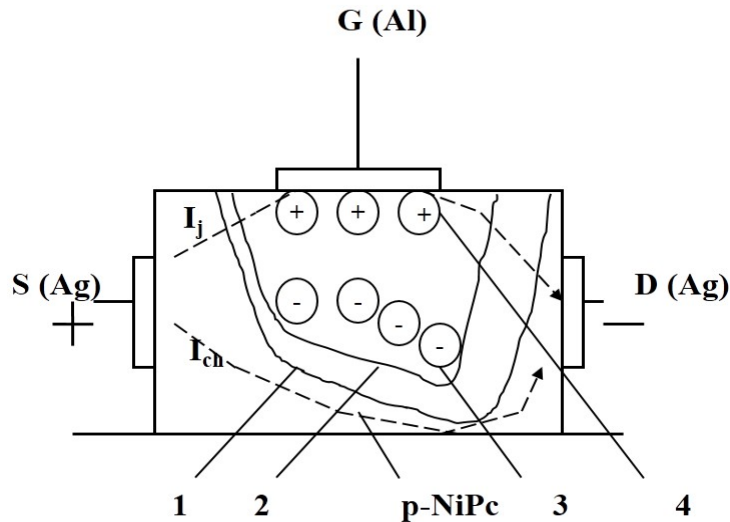
FIGURE 10.12: Effects of heating on junction depletion region and source-drain current of an OFET: depletion region at low (1) and high (2) temperatures, space charge (3 and 4), I_{ch} and I_j are the channel current and the junction current respectively.

TABLE 10.1: Temperature-impedance effect of Nickel Phthalocyanine based field effect transistor measured at 100 Hz.

Sample No.	Thickness (nm)	Initial Impedance ($k\Omega$)	Temperature Sensitivity (% ^{0}C^{-1})
1.	100	810	-2.35
2.	200	504	- 1.39
3.	300	422	- 1.18

10.4   Summary

Organic semiconducting field effect transistors have been fabricated by depositing nickel phthalocyanine (NiPc) and semi-transparent thin films of aluminum in sequence by vacuum evaporation on a glass substrate having silver source and drain electrodes. The thickness of NiPc film has been varied as 100 nm, 200 nm and 300 nm. The fabricated organic photo transistors (OPTs) having metal (aluminum) semiconductor (NiPc) Schottky junction are then characterized and the effects of light irradiation on its characteristics have been investigated. It is observed that the drain current of OPTs increases with increasing radiation intensity and the

OPTs having 200 nm thick NiPc film exhibited better performance compared to the transistors fabricated using 100 nm and 300 nm thick films.

Also the effects of heating on the impedance of NiPc based organic field effect transistors (OFETs) were investigated and it was observed that the transistors showed high temperature dependent responses. As NiPc is known to be a good light and humidity sensing material, it was demonstrated that the transistors fabricated using NiPc films can be used as multi-functional sensors to evaluate light, humidity and temperature variations. It was further established that NiPc based OFET can potentially be used in environmental monitoring equipment to assess light, humidity and temperature changes.

Chapter 11

Conclusion and Future Work

An appropriate selection of a device channel material lead to many exciting characteristics linked with efficiency and other attributes associated with humidity, light, temperature, absorption, charge transport and stability. Among the organic semiconducting materials, azo dye has attracted much interest during the past decades due to its wide applications in electronic and optoelectronic devices [109]. Organic dyes offer semiconductor properties, which can potentially be employed in organic electronics. Additionally, organic dyes based semiconductors are easily available, therefore, devices made with such materials will naturally lead to the reduction in the device cost. The electrical conductivity of an organic dye depends upon the mobility of its free carriers, temperature and charge carrier concentration. Usually, the mobility and charge carrier concentration in an organic semiconductor material is low compared to inorganic semiconductors. Hence, in this thesis, keeping all these aspects under consideration, devices were fabricated by using commercially available novel dyes along with their composites. It has been observed that output characteristics of an organic semiconductor device are heavily dependent on its geometry, technique employed to fabricate the device and the device physical parameters. Number of devices have been fabricated and their characterization were carried out at room and at elevated temperature, and also at varying humidity and ambient conditions. A summary of generalized conclusion drawn from this research is appended below.

(i) In this research, copper phthalocyanines (CuPc) thin films were deposited at different gravity conditions (1 *g* and 70 *g*) from a solution in benzene by using drop-casting and centrifugation. Variation in impedance and capacitance as a function of ambient humidity levels was assessed. Samples fabricated at 1 *g* exhibited a maximum change of 45.4% and 26.5% in their impedance and capacitance values, respectively; whereas, samples grown at 70 *g* demonstrated a maximum change of 42.2% and 15.7% in their impedance and capacitance values, respectively. It was shown that the humidity-dependent electrical performance could be associated both with increased polarization and increased doping concentration caused by absorbed water molecules. It was demonstrated that CuPc films can potentially be used as a humidity-sensing material whose sensitivity would be dependent on the chosen fabrication parameters.

(ii) In the second part, thin films of nickel phthalocyanines (NiPc) were deposited from NiPc solution in chloroform by centrifugation at high gravity condition (70 *g*), and also by drop-casting at normal gravity condition (1 *g*) on surface-type ceramic substrate with silver electrodes. Impedance and capacitance of the sensors have been investigated as a function of ambient humidity. It was observed that NiPc sensors fabricated at 70 *g* show larger response to the humidity than devices fabricated at 1 *g*. This could be associated with the roughness of the film deposited at 70 *g* compared to 1 *g*. Thus, as that of CuPc, NiPc films can also be used to fabricate humidity sensors for ambient evaluation.

(iii) As a third part, the effect of illumination on the impedance and capacitance of the NiPc-CoPc composite (bulk heterojunction) sensors have been investigated. In this part, the photo sensors have been fabricated by drop casting and under centrifugal force. Samples fabricated under centrifugal force showed better sensitivity compared to the samples made by drop casting. Impedance sensitivity (S_Z) of the samples fabricated by drop casting and under centrifugal force was equal to -1.83 MΩ cm^2(mW)$^{-1}$ and -5.365 MΩ cm^2(mW)$^{-1}$, respectively. Likewise, the capacitance sensitivity (S_C)

was equal to 0.083 pF cm^2(mW)$^{-1}$ and 0.185 pF cm^2(mW)$^{-1}$ for the samples fabricated by drop casting and under centrifugal force. It is, therefore, established that a composite of NiPc and CoPc can be employed to fabricate optical sensors for industrial applications.

(iv) As a fourth part, effects of humid environment on a surface type humidity sensor based on VOPcPhO, Alq$_3$, and their composite thin film prepared by spin coating were investigated. Compared to VOPcPhO and Alq$_3$ stand-alone sensors, VOPcPhO:Alq$_3$ composite-based sensor demonstrated superior performance with significantly improved sensing parameters, highlighting unique advantages of the low-molecular composite-based thin film organic humidity sensor. It has been established that low-molecular weight complex can be employed to develop cheap and reliable sensing elements for assessing humidity in the surrounding environment.

(v) The fifth part of the research demonstrates the visible wavelength photodiode (ITO/ PEDOT: PSS/ ZnPc:PC$_{71}$BM/ LiF/Al), which was successfully fabricated and characterized by an economical fabrication technique. The motivation to choose ZnPc:PC$_{71}$BM as photosensitive donor and acceptor dyad has been dictated by complementary absorption profiles of pristine thin films of ZnPc and PC$_{71}$BM. The absorption curve of ZnPc:PC$_{71}$BM dyad is observed to trace the summation of the individual absorption curves of donor and acceptor pristine thin films; thereby leading to strong and wide absorption bandwidth (350-800 nm) of the optical photo diode (OPD). The electrical characterization of the OPD is performed by measuring the photocurrent density-voltage relationship in response to varied illumination levels (0-150 mWcm^{-2}) of incident light. At higher intensity of light, more excitons are assumed to be generated and eventually disintegrated in the photoactive film, therefore, a pronounced photocurrent has been observed in the OPD with increase in incident photon density. Resultantly, improved sensing parameters; such as responsivity, J_{ph}/J_d and switching time between stable dark and illuminated states are observed. The reason for the improved sensing performance of the OPD was attributed to judicious selection

of donor and acceptor components on the basis of their synergic absorption profiles and desirable energy levels alignment.

(vi) In the sixth part, orange dye (OD) based organic field effect transistors with Schottky junction gate were fabricated at different gravity conditions by employing a simple drop-casting technology. The channel of fabricated FETs was made either by OD or OD composite with sugar. Effects of humidity and temperature on source-drain impedance and capacitance were investigated. Both types of FETs (OD and OD:Sugar) showed good response as humidity and temperature sensors. By evaluating their response as a function of ambient conditions, it has been demonstrated that OD and OD:Sugar based organic transistors can be used as multi-functional sensors to measure humidity and temperature in environmental monitoring and assessment instruments.

(vii) In the seventh and last part of this research, Nickle phthalocyanines (NiPc) based OFETs with Al-NiPc Schottky junctions were fabricated and their electrical characteristics were investigated under white light illumination. By examining $I-V$ characteristics under varying radiation intensity, it was observed that the transistors are sensitive to light and a 22 nm thick Al-NiPc Schottky barrier behaves as a semi-transparent barrier for incident radiation. It was further noted that the device current increases by increasing the intensity of radiation, and a plausible explanation of the observed behavior was given by assuming that photoconductive and photovoltaic effects were responsible for the increased drain current. An equivalent circuit of the OFET was developed where gate-source and gate-drain junctions were represented by independent current sources, and source-drain channel by a dependent current source. It was also shown that NiPc OFET's performance depends upon channel thickness, and the devices having 200 nm thick channel offered better characteristics compared to those having channel thickness of 100 nm and 300 nm. Effects of heating on the impedance of NiPc OFETs were investigated, and it was observed that the fabricated transistors showed high temperature dependent responses. As NiPc is known to be a good light

and humidity sensing material, therefore, it was demonstrated that the transistors fabricated using NiPc films can be used as multi-functional sensors to evaluate light, humidity and temperature variations. It was further established that NiPc based OFETs can potentially be used in environmental monitoring equipment to assess light, humidity and temperature changes.

11.1   Future Work

Although, this thesis covers numerous aspects pertaining to sensors fabrication using dyes and their composite, there are lot of avenues to which this work can be extended, and a few of those are explained below:

(i) Organic dye materials having higher sensitivity and wider spectrum may be explored to achieve optical sensors for wider industrial applications.

(ii) Organic dye materials with relatively increased carriers mobility can be explored for improved switching.

(iii) Transistors having high transconductance (g_m) for high frequency operations can be designed by improving channel and contact properties.

(iv) Flexible as well as brittle substrates can be used for fabrication of sensors at different gravity conditions to explore the effect of gravity.

(v) By at large, the observed sensors output was quasi-linear, which can potentially restrict their use as a sensor. To make them commercially viable, further research is needed to have their responses either linear or to convert them into a linear response by adding a linearization circuit immediately after their output.

(vi) The research can also be extended to improve detectivity, linearity, and optical characterization of light sensors.

(vii) New dyes and their composite can be explored for achieving multi-functional devices, i.e. temperature, light and humidity sensitive devices such that one sensor can measure the changes in the three listed variables simultaneously.

(viii) To develop an improved understanding of $I - V$ characteristics of organic devices, a mathematical model may be developed by envisioning equivalent circuit of the device.

Bibliography

[1] B. Lucas, T. Trigaud, and C. Videlot-Ackermann, "Organic transistors and phototransistors based on small molecules," *Polymer International*, vol. 61, no. 3, pp. 374–389, 2012.

[2] K. Baeg, M. Binda, D. Natali, M. Caironi, and Y. Noh, "Organic light detectors: photodiodes and phototransistors," *Advanced Materials*, vol. 25, no. 31, pp. 4267–4295, 2013.

[3] J. Shaw and P. Seidler, "Organic electronics: introduction," *IBM Journal of Research and Development*, vol. 45, no. 1, pp. 3–9, 2001.

[4] M. Shur, "GaAs devices and circuits, 1987."

[5] S. Sze, "Semiconductor devices: Physics and technology," *John Wiley & Sons, New York*, p. 413, 1985.

[6] K. Karimov, I. Ibrahim, M. Tahir, T. Khan, and U. Shafique, "Photo organic field effect transistor's properties," *Turkish Journal of Physics*, vol. 32, no. 1, pp. 13–19, 2008.

[7] Z. Li, *Organic light-emitting materials and devices.* CRC press, 2015.

[8] A. Nardes, "On the conductivity of PEDOT:PSS thin films," *Technische Universiteit Eindhoven. Eindhoven*, p. 132, 2007.

[9] D. Prentice, "Simulation of pentacene organic metal-oxide field effect transistors," Ph.D. dissertation, University of Cincinnati, 2003.

[10] H. Wang, J. Wang, H. Huang, X. Yan, and D. Yan, "Organic heterojunction with reverse rectifying characteristics and its application in field-effect transistors," *Organic Electronics*, vol. 7, no. 5, pp. 369–374, 2006.

[11] M. Fedorov, "Heterojunctions based organic semiconductor devices," Ph.D. dissertation, D. Sc. Thesis, State University, Ryazan, Russia, 2004.

[12] C. Chen and I. Shih, "Hybrid organic on inorganic semiconductor heterojunction," *Journal of Materials Science: Materials in Electronics*, vol. 17, no. 12, pp. 1047–1053, 2006.

[13] P. Mudimela, K. Grigoras, I. Anoshkin, A. Varpula, V. Ermolov, A. S. Anisimov, A. Nasibulin, S. Novikov, and E. Kauppinen, "Single-walled carbon nanotube network field effect transistor as a humidity sensor," *Journal of Sensors*, vol. 2012, 2012.

[14] S. Cho, L. Piper, A. DeMasi, A. Preston, K. Smith, K. Chauhan, P. Sullivan, R. Hatton, and T. Jones, "Electronic structure of C_{60}/phthalocyanine/ITO interfaces studied using soft X-ray spectroscopies," *The Journal of Physical Chemistry C*, vol. 114, no. 4, pp. 1928–1933, 2010.

[15] K. S. Karimov and T. Qasuria, "The use of displacement sensitive organic field effect transistor for telemetry system applications," *Measurement*, vol. 45, no. 1, pp. 41–46, 2012.

[16] *Stabilization of organic materials for sensors.* IEEE, 2010.

[17] Y. Wang, J. Ren, X. Yuan, Z. Dou, and G. Hu, "Effects of electric field and magnetic induction on spin injection into organic semiconductors," *Physica B: Condensed Matter*, vol. 406, no. 4, pp. 926–929, 2011.

[18] J. Zhang, Y. Nan, H. Li, W. Qiu, X. Yang, G. Wu, H. Chen, and M. Wang, "A new wide bandgap organic semiconductor and its application in organic uv sensors with tunable response wavelength," *Sensors and Actuators B: Chemical*, vol. 162, no. 1, pp. 321–326, 2012.

[19] G. Horowitz, "Organic semiconductors for new electronic devices," *Advanced Materials*, vol. 2, no. 6-7, pp. 287–292, 1990.

[20] H. Yao, J. Ge, C. Wang, X. Wang, W. Hu, Z. Zheng, Y. Ni, and S. Yu, "A flexible and highly pressure-sensitive graphene–polyurethane sponge based on fractured microstructure design," *Advanced Materials*, vol. 25, no. 46, pp. 6692–6698, 2013.

[21] W. Brutting, *Introduction to the physics of organic semiconductors.* Wiley Online Library, 2006.

[22] M. Grundmann, H. Alloul, H. Fuchs, W. Demtröder, R. Dreizler, C. Lüdde, K. Thyagarajan, and A. Ghatak, "Graduate texts in physics," 2010.

[23] E. Umbach, M. Sokolowski, and R. Fink, "Substrate-interaction, long-range order, and epitaxy of large organic adsorbates," *Applied Physics A*, vol. 63, no. 6, pp. 565–576, 1996.

[24] A. Koma, "Molecular beam epitaxial growth of organic thin films," *Progress in Crystal Growth and Characterization of Materials*, vol. 30, no. 2-3, pp. 129–152, 1995.

[25] S. Forrest, "Ultrathin organic films grown by organic molecular beam deposition and related techniques," *Chemical Reviews*, vol. 97, no. 6, pp. 1793–1896, 1997.

[26] X. Lu, W. Zhang, C. Wang, T. Wen, and Y. Wei, "One-dimensional conducting polymer nanocomposites: synthesis, properties and applications," *Progress in Polymer Science*, vol. 36, no. 5, pp. 671–712, 2011.

[27] A. Pron and P. Rannou, "Processible conjugated polymers: from organic semiconductors to organic metals and superconductors," *Progress in Polymer Science*, vol. 27, no. 1, pp. 135–190, 2002.

[28] A. Larbi, B. Djedou, L. Bennacer, and M. Bousbia-salah, "Towards a new gas sensor microsystem using electroactive polymers thin films," *International*

Journal on Smart Sensing and Intelligent Systems, vol. 2, no. 3, pp. 448–462, 2009.

[29] C. Chiang, C. Fincher Jr, Y. W. Park, A. J. Heeger, H. Shirakawa, E. Louis, S. Gau, and A. MacDiarmid, "Electrical conductivity in doped polyacetylene," *Physical Review Letters*, vol. 39, no. 17, p. 1098, 1977.

[30] V. Gonçalves and D. Balogh, "Optical chemical sensors using polythiophene derivatives as active layer for detection of volatile organic compounds," *Sensors and Actuators B: Chemical*, vol. 162, no. 1, pp. 307–312, 2012.

[31] A. Szent-Gyorgyi, "Internal photo-electric effect and band spectra in proteins," *Nature*, vol. 157, no. 4000, pp. 875–875, 1946.

[32] D. Eley, "Phthalocyanines as semiconductors," *Nature*, vol. 162, no. 4125, pp. 819–819, 1948.

[33] H. Akamatu and H. Inokuchi, "On the electrical conductivity of violanthrone, iso-violanthrone, and pyranthrone," *The Journal of Chemical Physics*, vol. 18, no. 6, pp. 810–811, 1950.

[34] A. Bernanose, "Electroluminescence of organic compounds," *British Journal of Applied Physics*, vol. 6, no. S4, p. S54, 1955.

[35] D. Williams and M. Schadt, "A simple organic electroluminescent diode," *Proceedings of the IEEE*, vol. 58, no. 3, pp. 476–476, 1970.

[36] D. Barbe and C. Westgate, "Surface state parameters of metal-free phthalocyanine single crystals," *Journal of Physics and Chemistry of Solids*, vol. 31, no. 12, pp. 2679–2687, 1970.

[37] F. Ebisawa, T. Kurokawa, and S. Nara, "Electrical properties of polyacetylene-polysiloxane interface," *Journal of Applied Physics*, vol. 54, no. 6, pp. 3255–3259, 1983.

[38] G. Chamberlain, "Organic solar cells: A review," *Solar Cells*, vol. 8, no. 1, pp. 47–83, 1983.

[39] H. Koezuka, A. Tsumura, and T. Ando, "Field-effect transistor with poly-thiophene thin film," *Synthetic Metals*, vol. 18, no. 1-3, pp. 699–704, 1987.

[40] C. Tang and S. VanSlyke, "Organic electroluminescent diodes," *Applied Physics Letters*, vol. 51, no. 12, pp. 913–915, 1987.

[41] C. Dimitrakopoulos and P. Malenfant, "Organic thin film transistors for large area electronics," *Advanced Materials*, vol. 14, no. 2, pp. 99–117, 2002.

[42] T. Frängsmyr, *Les Prix Nobel*, 2000.

[43] R. Zhang and T. Conductive, "CNT composites for strain sensing," *School of Engineering and Materials Science, Queen Mary, University of London, London*, 2009.

[44] *RFCPUs on glass and plastic substrates fabricated by TFT transfer technology.* IEEE, 2005.

[45] *A CPU on a plastic film substrate.* IEEE, 2004.

[46] T. Sekitani, U. Zschieschang, H. Klauk, and T. Someya, "Flexible organic transistors and circuits with extreme bending stability," *Nature Materials*, vol. 9, no. 12, p. 1015, 2010.

[47] J. Noh, M. Jung, Y. Jung, C. Yeom, M. Pyo, and G. Cho, "Key issues with printed flexible thin film transistors and their application in disposable RF sensors," *Proceedings of the IEEE*, vol. 103, no. 4, pp. 554–566, 2015.

[48] S. Fluxman, "Design and performance of digital polysilicon thin-film-transistor circuits on glass," *IEE Proceedings-Circuits, Devices and Systems*, vol. 141, no. 1, pp. 56–59, 1994.

[49] Y. Rim, S. Bae, H. Chen, N. De-Marco, and Y. Yang, "Recent progress in materials and devices toward printable and flexible sensors," *Advanced Materials*, vol. 28, no. 22, pp. 4415–4440, 2016.

[50] *Differential amplifier using polysilicon TFTs processed at low temperature to be integrated with TFT Hall sensor.* IEEE, 2006.

[51] K. Fukuda, T. Minamiki, T. Minami, M. Watanabe, T. Fukuda, D. Kumaki, and S. Tokito, "Printed organic transistors with uniform electrical performance and their application to amplifiers in biosensors," *Advanced Electronic Materials*, vol. 1, no. 7, 2015.

[52] K. Myny, S. Smout, M. Rockelé, A. Bhoolokam, T. Ke, S. Steudel, B. Cobb, A. Gulati, F. Rodriguez, and K. Obata, "A thin-film microprocessor with inkjet print-programmable memory," *Scientific Reports*, vol. 4, 2014.

[53] *A flexible 8b asynchronous microprocessor based on low-temperature poly-silicon TFT technology.* IEEE, 2005.

[54] T. Moy, L. Huang, W. Rieutort-Louis, C. Wu, P. Cuff, S. Wagner, J. Sturm, and N. Verma, "An EEG acquisition and biomarker-extraction system using low-noise-amplifier and compressive-sensing circuits based on flexible, thin-film electronics," *IEEE Journal of Solid-State Circuits*, vol. 52, no. 1, pp. 309–321, 2017.

[55] *Low temperature polycrystalline silicon TFT fingerprint sensor with integrated comparator circuit.* IEEE, 2004.

[56] J. Zhou, T. Ge, and J. Chang, "Printed electronics: Effects of bending and a self-compensation means," *IEEE Transactions on Circuits and Systems I: Regular Papers*, vol. 64, no. 3, pp. 505–515, 2017.

[57] R. Pierret, "Semiconductor deviceffundamentals, Addision-Wesley," *Reading, Massachusetts*, 1996.

[58] F. Braun, "Ueber die Stromleitung durch schwefelmetalle," *Annalen der Physik*, vol. 229, no. 12, pp. 556–563, 1875.

[59] W. Schottky, "Halbleitertheorie der sperrschicht," *Naturwissenschaften*, vol. 26, no. 52, pp. 843–843, 1938.

[60] R. Muller, T. Kamins, and M. Chan, "Device electronics for integrated circuits," *John Wiley & Sons, New York*, 1986.

[61] D. Neaman, *Semiconductor physics and devices.* Irwin Chicago, 1992.

[62] R. Noyce and J. Kilby, "The origins of the integrated circuit," 1904.

[63] G. W. Pierce, "Crystal rectifiers for electric currents and electric oscillations. Part I. carborundum," *Physical Review (Series I)*, vol. 25, no. 1, p. 31, 1907.

[64] W. R. Shockley, "About William Shockley," 1926.

[65] J. Bardeen, "Surface states and rectification at a metal semi-conductor contact," *Physical Review*, vol. 71, no. 10, p. 717, 1947.

[66] C. Crowell, J. Sarace, and S. Sze, "Tungsten-semiconductor Schottky-barrier diodes," *Transactions of the Metallurgical Society of Aime*, vol. 233, no. 3, p. 478, 1965.

[67] S. S. Li, "Theoretical analysis of a novel MPN gallium arsenide Schottky barrier solar cell," *Solid-State Electronics*, vol. 21, no. 2, pp. 435–438, 1978.

[68] C. Wu, "Interfacial layer theory of the Schottky barrier diodes," *Journal of Applied Physics*, vol. 51, no. 7, pp. 3786–3789, 1980.

[69] A. Piotrowska, "Ohmic contacts to GaAs: Fundamentals and practice," *ACTA Physica Polonica Series A*, vol. 84, pp. 491–491, 1993.

[70] F. Léonard and J. Tersoff, "Role of Fermi-level pinning in nanotube Schottky diodes," *Physical Review Letters*, vol. 84, no. 20, p. 4693, 2000.

[71] *Spectral absorption analysis in AlGaAs/GaAs photodetectors*, vol. 1. IEEE, 2001.

[72] W. Park, G.-C. Yi, J.-W. Kim, and S.-M. Park, "Schottky nanocontacts on ZnO nanorod arrays," *Applied Physics Letters*, vol. 82, no. 24, pp. 4358–4360, 2003.

[73] A. Saxler and R. Smith, "Methods of fabricating nitride-based transistors having regrown ohmic contact regions," Oct. 2008.

[74] J. Moon, M. Antcliffe, H. Seo, D. Curtis, S. Lin, A. Schmitz, I. Milosavljevic, A. Kiselev, R. Ross, and D. Gaskill, "Ultra-low resistance ohmic contacts in graphene field effect transistors," *Applied Physics Letters*, vol. 100, no. 20, p. 203512, 2012.

[75] W. Jin, K. Zhang, Z. Gao, Y. Li, L. Yao, Y. Wang, and L. Dai, "CdSe nanowire-based flexible devices: Schottky diodes, metal–semiconductor field-effect transistors, and inverters," *ACS Applied Materials & Interfaces*, vol. 7, no. 24, pp. 13 131–13 136, 2015.

[76] S. Jang, P. Son, J. Kim, S.-N. Lee, and K. Baik, "Hydrogen sensitive Schottky diode using semipolar AlGaN/GaN heterostructures," *Sensors and Actuators B: Chemical*, vol. 222, pp. 43–47, 2016.

[77] S. Sze, "Physics of semiconductor devices. New York: J," *Whiley and Sons*, 1981.

[78] J. Sparkes, *Semiconductor devices*. CRC Press, 1994.

[79] M. Pope and C. Swenberg, *Electronic processes in organic crystals and polymers*. Oxford University Press on Demand, 1999.

[80] J. Tang, J. Zhou, J. Fan, X. Li, Y. Shi, N. Gu, G. Feng, Y. Xing, J. Shi, and L. He, "Family-based association study of DTNBP1 in 6p22. 3 and schizophrenia," *Molecular Psychiatry*, vol. 8, no. 8, pp. 717–717, 2003.

[81] S. Lee, Z. Gao, and L. Hung, "Metal diffusion from electrodes in organic light-emitting diodes," *Applied Physics Letters*, vol. 75, no. 10, pp. 1404–1406, 1999.

[82] J. Tang, Y. Li, X. Dong, S. Wang, C. Lee, L. Hung, and S. Lee, "Photoemission and vibrational studies of metal/organic interfaces modified by plasma-polymerized fluorocarbon films," *Applied Surface Science*, vol. 239, no. 1, pp. 117–124, 2004.

[83] I. Parker, "Carrier tunneling and device characteristics in polymer light-emitting diodes," *Journal of Applied Physics*, vol. 75, no. 3, pp. 1656–1666, 1994.

[84] V. Arkhipov, E. Emelianova, Y. Tak, and H. Bässler, "Charge injection into light-emitting diodes: Theory and experiment," *Journal of Applied Physics*, vol. 84, no. 2, pp. 848–856, 1998.

[85] U. Wolf, V. Arkhipov, and H. Bässler, "Current injection from a metal to a disordered hopping system," *Physical Review B*, vol. 59, no. 11, p. 7507, 1999.

[86] Y. Gartstein and E. Conwell, "Field-dependent thermal injection into a disordered molecular insulator," *Chemical Physics Letters*, vol. 255, no. 1-3, pp. 93–98, 1996.

[87] A. Miller and E. Abrahams, "Impurity conduction at low concentrations," *Physical Review*, vol. 120, no. 3, p. 745, 1960.

[88] A. Lösche, "Electronic processes in non-crystalline materials," *Crystal Research and Technology*, vol. 7, no. 4, 1972.

[89] A. Campbell, D. Bradley, and D. Lidzey, "Space-charge limited conduction with traps in poly (phenylene vinylene) light emitting diodes," *Journal of Applied Physics*, vol. 82, no. 12, pp. 6326–6342, 1997.

[90] N. Karl and J. Marktanner, "Electron and hole mobilities in high purity anthracene single crystals," *Molecular Crystals and Liquid Crystals*, vol. 355, no. 1, pp. 149–173, 2001.

[91] W. Ford and P. Kamat, "Photochemistry of 3, 4, 9, 10-perylenetetracarboxylic dianhydride dyes. 3. Singlet and triplet excited-state properties of the bis (2, 5-di-tert-butylphenyl) imide derivative," *Journal of Physical Chemistry*, vol. 91, no. 25, pp. 6373–6380, 1987.

[92] H. Bässler, "Charge transport in disordered organic photoconductors a Monte Carlo simulation study," *Physica Status Solidi (b)*, vol. 175, no. 1, pp. 15–56, 1993.

[93] A. McEvoy, C. McDonagh, and B. MacCraith, "Dissolved oxygen sensor based on fluorescence quenching of oxygen-sensitive ruthenium complexes immobilized in sol–gel-derived porous silica coatings," *Analyst*, vol. 121, no. 6, pp. 785–788, 1996.

[94] P. Burrows, Z. Shen, V. Bulovic, D. McCarty, S. Forrest, J. Cronin, and M. Thompson, "Relationship between electroluminescence and current transport in organic heterojunction light-emitting devices," *Journal of Applied Physics*, vol. 79, no. 10, pp. 7991–8006, 1996.

[95] R. Schmechel and H. Von-Seggern, "Electronic traps in organic transport layers," *Physica Status Solidi (a)*, vol. 201, no. 6, pp. 1215–1235, 2004.

[96] A. Hepp, N. Von Malm, R. Schmechel, and H. Von Seggern, "Effects of process parameters on trap distributions in organic semiconductors," *Synthetic Metals*, vol. 138, no. 1, pp. 201–207, 2003.

[97] V. Savvateev, J. Friedl, L. Zou, J. Shinar, K. Christensen, W. Oldham, L. Rothberg, Z. Chen-Esterlit, and R. Kopelman, "Nanosecond transients in the electroluminescence from multilayer blue organic light-emitting devices based on 4, 4-bis (2, 2 diphenyl vinyl)-1, 1-biphenyl," *Applied Physics Letters*, vol. 76, no. 12, pp. 1501–1503, 2000.

[98] C. Giebeler, S. Whitelegg, A. Campbell, M. Liess, S. Martin, P. Lane, D. Bradley, G. Webster, and P. Burn, "Optical studies of electric fields in poly (2-methoxy-5-ethyl (2-hexyloxy) para-phenylene vinylene) light-emitting diodes," *Applied Physics Letters*, vol. 74, no. 24, pp. 3714–3716, 1999.

[99] H. Antoniadis, M. Abkowitz, and B. Hsieh, "Carrier deep-trapping mobility-lifetime products in poly (p-phenylene vinylene)," *Applied Physics Letters*, vol. 65, no. 16, pp. 2030–2032, 1994.

[100] S. Berleb, A. Mückl, W. Brütting, and M. Schwoerer, "Temperature dependent device characteristics of organic light-emitting devices," *Synthetic Metals*, vol. 111, pp. 341–344, 2000.

[101] A. Rose, "Space-charge-limited currents in solids," *Physical Review*, vol. 97, no. 6, p. 1538, 1955.

[102] M. Lampert, "Simplified theory of space-charge-limited currents in an insulator with traps," *Physical Review*, vol. 103, no. 6, p. 1648, 1956.

[103] S. El-Sayed, H. A. Hamid, and R. Radwan, "Effect of electron beam irradiation on the conduction phenomena of unplasticized PVC/PVA copolymer," *Radiation Physics and Chemistry*, vol. 69, no. 4, pp. 339–345, 2004.

[104] A. Böhler, P. Urbach, J. Schöbel, S. Dirr, H.-H. Johannes, S. Wiese, D. Ammermann, and W. Kowalsky, "Organic heterostructures for electronic and photonic devices," *Physica E: Low-dimensional Systems and Nanostructures*, vol. 2, no. 1, pp. 562–572, 1998.

[105] A. Rose, "Recombination processes in insulators and semiconductors," *Physical Review*, vol. 97, no. 2, p. 322, 1955.

[106] M. Lampert and P. Mark, "Current injection in solids," 1970.

[107] N. Mott and R. Gurney, "Electronic processes in ionic crystals," 1940.

[108] P. Marks, J. Banks, and R. gross, "Genetic heterogeneity of glucose-6-phosphate dehydrogenase deficiency," *Nature*, vol. 194, no. 4827, pp. 454–456, 1962.

[109] A. Riad, "Influence of dioxygen and annealing process on the transport properties of nickel phthalocyanine Schottky-barrier devices," *Physica B: Condensed Matter*, vol. 270, no. 1, pp. 148–156, 1999.

[110] M. Chani, K. Karimov, S. Khan, A. Asiri, M. Saleem, and M. Bashir, "Fe_2O_3–silicone adhesive composite based humidity sensors," *Optoelectron Adv Mater Rapid Commun*, vol. 7, pp. 861–865, 2013.

[111] A. Braun and J. Tcherniac, "Über die produkte der einwirkung von acetan-hydrid auf phthalamid," *European Journal of Inorganic Chemistry*, vol. 40, no. 2, pp. 2709–2714, 1907.

[112] A. P. Lever, "The phthalocyanines," *Advances in Inorganic Chemistry and Radiochemistry*, vol. 7, pp. 27–114, 1965.

[113] G. Byrne, R. Linstead, and A. Lowe, "The preparation of phthalocyanine and some metallic derivatives from o-cyanobenzamide and phthalimide," *Journal of the Chemical Society (Resumed)*, pp. 1017–1022, 1934.

[114] J. Jiang, *Functional phthalocyanine molecular materials.* Springer, 2010, vol. 135.

[115] R. Gould and R. Blyth, "Conductivity and absorption measurements in nickel phthalocyanine thin films," *Physica Status Solidi (a)*, vol. 120, no. 1, 1990.

[116] N. McKeown, *Phthalocyanine materials: synthesis, structure and function.* Cambridge University Press, 1998, no. 6.

[117] F. So and Y. Gao, "Aluminum phthalocyanine chloride/C_{60} organic photo-voltaic cells with high open-circuit voltages," *Solar Energy Materials and Solar Cells*, vol. 93, no. 9, pp. 1688–1691, 2009.

[118] Y. Sadaoka, T. Jones, and W. Göpel, "Fast NO_2 detection at room temper-ature with optimized lead phthalocyanine thin-film structures," *Sensors and Actuators B: Chemical*, vol. 1, no. 1-6, pp. 148–153, 1990.

[119] J. Simon and C. Sirlin, "Mesomorphic molecular materials for electron-ics, opto-electronics, iono-electronics: octaalkyl-phthalocyanine derivatives," *Pure and Applied Chemistry*, vol. 61, no. 9, pp. 1625–1629, 1989.

[120] K. Abe, H. Saito, T. Kimura, Y. Ohkatsu, and T. Kusano, "Characteristics of rectifying devices with thin films of polyphthalocyanine," *Macromolecular Chemistry and Physics*, vol. 190, no. 11, pp. 2693–2701, 1989.

[121] J. Simon and J. Andre, *Molecular semiconductors: photoelectrical properties and solar cells.* Springer Science & Business Media, 2012.

[122] A. Lever, M. Hempstead, C. Leznoff, W. Liu, M. Melnik, W. Nevin, and P. Seymour, "Recent studies in phthalocyanine chemistry," *Pure and Applied Chemistry*, vol. 58, no. 11, pp. 1467–1476, 1986.

[123] T. Komori and Y. Amao, "Near-infrared sensitization solar cell with the electrode of aluminium phthalocyanine adsorbed on nanocrystalline titanium dioxide film," *Journal of Porphyrins and Phthalocyanines*, vol. 6, no. 03, pp. 211–216, 2002.

[124] J. Fabian, H. Nakazumi, and M. Matsuoka, "Near-infrared absorbing dyes," *Chemical Reviews*, vol. 92, no. 6, pp. 1197–1226, 1992.

[125] E. Lukyanets, "Phthalocyanines as photosensitizers in the photodynamic therapy of cancer," *Journal of Porphyrins and Phthalocyanines*, vol. 3, no. 67, pp. 424–432, 1999.

[126] I. Rosenthal, "Phthalocyanines as photodynamic sensitizers," *Photochemistry and Photobiology*, vol. 53, no. 6, pp. 859–870, 1991.

[127] K. Kadish, K. Smith, and R. Guilard, "The porphyrin handbook, vol 19: Applications of phthalocyanines," 2003.

[128] H. Nalwa, M. Engel, M. Hanack, and H. Schultz, "Third-order nonlinear optical properties of octa-substituted metal-free phthalocyanine thin films," *Applied Organometallic Chemistry*, vol. 10, no. 8, pp. 661–664, 1996.

[129] S. Griveau, M. Gulppi, F. Bedioui, and J. Zagal, "Electropolymerized cobalt macrocomplex-based films for thiols electro-oxidation: effect of the film formation conditions and the nature of the macrocyclic ligand," *Solid State Ionics*, vol. 169, no. 1, pp. 59–63, 2004.

[130] K. Kasuga, K. Mori, T. Sugimori, and M. Handa, "Kinetic study on the oxidation of trichlorophenol using hydrogen peroxide and an iron (iii) complex

of tetrasulfonatophthalocyanine catalyst," *Bulletin of the Chemical Society of Japan*, vol. 73, no. 4, pp. 939–940, 2000.

[131] J. Spikes, "New trends in photobiology: Chlorins as photosensitizers in biology and medicine," *Journal of Photochemistry and Photobiology B: Biology*, vol. 6, no. 3, pp. 259–274, 1990.

[132] R. Hagen and T. Bieringer, "Photoaddressable polymers for optical data storage," *Advanced Materials*, vol. 13, no. 23, pp. 1805–1810, 2001.

[133] R. Collins and A. Belghachi, "Structural properties of lead phthalocyanine thin films," *Materials Letters*, vol. 8, no. 9, pp. 349–352, 1989.

[134] R. Collins, K. Strickland, M. Jeffery, K. Davidson, and T. Jones, "The effects of impurities on the microtopography of lead phthalocyanine thin films," *Materials Letters*, vol. 10, no. 4-5, pp. 170–174, 1990.

[135] T. Taima, J. Sakai, T. Yamanari, and K. Saito, "Doping effects for organic photovoltaic cells based on small-molecular-weight semiconductors," *Solar Energy Materials and Solar Cells*, vol. 93, no. 6, pp. 742–745, 2009.

[136] H. Heli, A. Jabbari, M. Zarghan, and A. Moosavi-Movahedi, "Copper nanoparticles–carbon microparticles nanocomposite for electrooxidation and sensitive detection of sotalol," *Sensors and Actuators B: Chemical*, vol. 140, no. 1, pp. 245–251, 2009.

[137] U. Kürüm, T. Ceyhan, A. Elmali, and Ö. Bekaroğlu, "Optical limiting response by embedding copper phthalocyanine into polymer host," *Optics Communications*, vol. 282, no. 12, pp. 2426–2430, 2009.

[138] S. Kment, P. Kluson, M. Drobek, R. Kuzel, I. Gregora, M. Kohout, and Z. Hubicka, "Preparation of thin phthalocyanine layers and their structural and absorption properties," *Thin Solid Films*, vol. 517, no. 17, pp. 5274–5279, 2009.

[139] A. Atta, "AC conductivity and dielectric measurements of bulk magnesium phthalocyanine (MgPc)," *Journal of Alloys and Compounds*, vol. 480, no. 2, pp. 564–567, 2009.

[140] Y. Abe, G. Maizza, N. Sone, Y. Nagasaka, and T. Suzuki, "A high gravity chemical vapor deposition apparatus," *Review of Scientific Instruments*, vol. 68, no. 11, pp. 4225–4231, 1997.

[141] G. Müller and G. Neumann, "Suppression of doping striations in zone melting of InSb by enhanced convection on a centrifuge," *Journal of Crystal Growth*, vol. 59, no. 3, pp. 548–556, 1982.

[142] H. Rodot, L. Regel, G. Sarafanov, M. Hamidi, I. Videskii, and A. Turtchaninov, "Cristaux de rellurure de plomb élaborés en centrifugeuse," *Journal of Crystal Growth*, vol. 79, no. 1-3, pp. 77–83, 1986.

[143] R. Parfeniev and L. Regel, "Gravity application to anisotropic semiconductor materials: from high-to microgravity conditions," *Acta Astronautica*, vol. 48, no. 2, pp. 163–168, 2001.

[144] Y. Park, T. Kanki, H. Lee, H. Tanaka, and T. Kawai, "CuPc/PbZr$_{0.2}$Ti$_{0.8}$O$_3$/(La, Ba)MnO$_3$ field effect transistor heterojunction photomemory," *Solid-State Electronics*, vol. 47, no. 12, pp. 2221–2224, 2003.

[145] M. Ahmed, K. S. Karimov, and S. Moiz, "Temperature-dependent I-V characteristics of organic-inorganic heterojunction diodes," *IEEE Transactions on Electron Devices*, vol. 51, no. 1, pp. 121–126, 2004.

[146] S. Moiz, "Temperature-dependent electrical characterization of novel organic semiconductor based diodes for sensor technology," *Faculty of Electronic Engineering, vol. Ph. D.: Ghulam Ishaq Khan Institute of Engineering Sciences and Technology, Topi, Pakistan*, 2005.

[147] K. S. Karimov, I. Qazi, T. Khan, P. Draper, F. Khalid, and M. Mahroof-Tahir, "Humidity and illumination organic semiconductor copper phthalocyanine sensor for environmental monitoring," *Environmental Monitoring and Assessment*, vol. 141, no. 1, pp. 323–328, 2008.

[148] M. Mahroof-Tahir and K. S. Karimov, "Fabrication of heterojunctions and current-voltage characteristics of vanadium coordination compounds," *Journal of Optoelectronics and Advanced Materials*, vol. 11, no. 1, pp. 83–88, 2009.

[149] T. Plookphol, S. Wisutmethangoon, and S. Gonsrang, "Influence of process parameters on SAC-305 lead-free solder powder produced by centrifugal atomization," *Powder Technology*, vol. 214, no. 3, pp. 506–512, 2011.

[150] F. Meng, X. Di, H. Dong, Y. Zhang, C. Zhu, C. Li, and Y. Chen, "PpbH$_2$S gas sensing characteristics of Cu$_2$O/CuO sub-microspheres at low-temperature," *Sensors and Actuators B: Chemical*, vol. 182, pp. 197–204, 2013.

[151] Z. Ahmad, Q. Zafar, K. Sulaiman, R. Akram, and K. Karimov, "A humidity sensing organic-inorganic composite for environmental monitoring," *Sensors*, vol. 13, no. 3, pp. 3615–3624, 2013.

[152] X. Huang, Z. Zhao, L. Zhang, C. Yin, and J. Wu, "Microstructure modification and fracture behavior of solidified TiC–TiB$_2$ ceramic prepared by combustion synthesis in ultra-high gravity field," *Journal of Asian Ceramic Societies*, vol. 2, no. 2, pp. 144–149, 2014.

[153] A. Markelonis, J. Wang, B. Ullrich, C. Wai, and G. Brown, "Nanoparticle film deposition using a simple and fast centrifuge sedimentation method," *Applied Nanoscience*, vol. 5, no. 4, pp. 457–468, 2015.

[154] S. Moiz, K. S. Karimov, and N. Gohar, "Orange dye thin film resistive hygrometers," *Eurasian Chemico-Technological Journal*, vol. 6, no. 3, pp. 179–183, 2017.

[155] X. Yin, Y. Li, W. Wu, G. Chu, Y. Luo, and H. Meng, "Preparation of two-dimensional molybdenum disulfide nanosheets by high-gravity technology," *Industrial & Engineering Chemistry Research*, vol. 56, no. 16, pp. 4736–4742, 2017.

[156] M. Chani, K. S. Karimov, and A. Asiri, "Fabrication and characterization of organic-inorganic (orange dye-vanadium oxide) composite based humidity sensors," *Int. J. Electrochem. Sci*, vol. 12, pp. 1434–1444, 2017.

[157] B. Adhikari and S. Majumdar, "Polymers in sensor applications," *Progress in polymer science*, vol. 29, no. 7, pp. 699–766, 2004.

[158] Z. Chen and C. Lu, "Humidity sensors: a review of materials and mechanisms," *Sensor Letters*, vol. 3, no. 4, pp. 274–295, 2005.

[159] J. Lovell-Smith, R. Feistel, A. Harvey, O. Hellmuth, S. Bell, M. Heinonen, and J. Cooper, "Metrological challenges for measurements of key climatological observables. part 4: atmospheric relative humidity," *Metrologia*, vol. 53, no. 1, p. R40, 2015.

[160] J. Wilson, "Sensor technology handbook. 2005."

[161] R. Pode, "On the problem of open circuit voltage in metal phthalocyanine/C_{60} organic solar cells," *Advanced Materials Letters*, vol. 2, pp. 3–11, 2011.

[162] M. El-Khouly, O. Ito, P. Smith, and F. D-Souza, "Intermolecular and supramolecular photoinduced electron transfer processes of fullerene–porphyrin/phthalocyanine systems," *Journal of Photochemistry and Photobiology C: Photochemistry Reviews*, vol. 5, no. 1, pp. 79–104, 2004.

[163] L. Zhu, T. Zhao, K. Li, W. Sun, and Y. Xing, "Bulk heterojunction organic solar cells fabricated by oblique angle deposition," *Physical Chemistry Chemical Physics*, vol. 17, no. 43, pp. 28 765–28 769, 2015.

[164] L. Holland, "Vacuum deposition of thin films," *London: Chapman & Hall, 1970*, 1970.

[165] A. Farag and I. Yahia, "Structural, absorption and optical dispersion characteristics of rhodamine B thin films prepared by drop casting technique," *Optics Communications*, vol. 283, no. 21, pp. 4310–4317, 2010.

[166] F. Krebs, "Fabrication and processing of polymer solar cells: a review of printing and coating techniques," *Solar Energy Materials and Solar Cells*, vol. 93, no. 4, pp. 394–412, 2009.

[167] N. Azarova, J. Owen, C. McLellan, M. Grimminger, E. Chapman, J. Anthony, and O. Jurchescu, "Fabrication of organic thin-film transistors by spray-deposition for low-cost, large-area electronics," *Organic Electronics*, vol. 11, no. 12, pp. 1960–1965, 2010.

[168] R. H. Schmidt, K. Mosbach, and K. Haupt, "A simple method for spin-coating molecularly imprinted polymer films of controlled thickness and porosity," *Advanced Materials*, vol. 16, no. 8, pp. 719–722, 2004.

[169] D. C. Joy, *Scanning electron microscopy.* Wiley Online Library, 2006.

[170] D. Rugar and P. Hansma, "Atomic force microscopy," *Physics today*, vol. 43, no. 10, pp. 23–30, 1990.

[171] H. Hoshi, A. Dann, and Y. Maruyama, "The structure and properties of phthalocyanine films grown by the molecular-beam epitaxy technique. ii. Ultraviolet/visible spectroscopic study," *Journal of Applied Physics*, vol. 67, no. 4, pp. 1845–1849, 1990.

[172] F. Gutman and L. Lyons, "Organic semiconductors Part A, Robert E," *Publishing, Malabar, FL*, 1981.

[173] F. Gutman, H. Keyzer, L. Lyons, and R. Smoano, "Organic semiconductors, Part B, Kriger Robert E," *Publishing Company, Malabar Florida, USA*, vol. 35, 1983.

[174] L. Regel and W. Wilcox, *Processing by centrifugation.* Springer Science & Business Media, 2011.

[175] ——, "Centrifugal materials processing," in *Centrifugal Materials Processing.* Springer, 1997, pp. 1–15.

[176] C. Colesniuc, "Metallophthalocyanine thin films: structure and physical properties," 2011.

[177] *Device operation of organic semiconductor copper phthalocyanine thin film transistor*, vol. 1. IEEE, 2013.

[178] N. Touka, H. Benelmadjat, B. Boudine, O. Halimi, and M. Sebais, "Copper phthalocyanine nanocrystals embedded into polymer host: Preparation and structural characterization," *Journal of the Association of Arab Universities for Basic and Applied Sciences*, vol. 13, no. 1, pp. 52–56, 2013.

[179] W. Brutting, "Physics of organic semiconductors," 2007.

[180] L. Hu, X. Liu, S. Dalgleish, M. Matsushita, H. Yoshikawa, and K. Awaga, "Organic optoelectronic interfaces with anomalous transient photocurrent," *Journal of Materials Chemistry C*, vol. 3, no. 20, pp. 5122–5135, 2015.

[181] *Opto-electronic properties of ITO/CuPc/NiPc/Al and ITO/NiPc/CuPc/Al double junction cells*, 2008.

[182] K. S. Karimov, F. Khalid, M. Chani, A. Mateen, M. Hussain, A. Maqbool, and J. Ahn, "Carbon nanotubes based flexible temperature sensors," *Optoelectronics and Advanced Materials-Rapid Communication*, vol. 6, no. 1/2, pp. 194–196, 2012.

[183] A. Mahapatro and S. Ghosh, "Schottky energy barrier and charge injection in metal/copper–phthalocyanine/metal structures," *Applied Physics Letters*, vol. 80, no. 25, pp. 4840–4842, 2002.

[184] R. Hiesgen, M. Räbisch, H. Böttcher, and D. Meissner, "STM investigation of the growth structure of cu-phthalocyanine films with submolecular resolution," *Solar Energy Materials and Solar Cells*, vol. 61, no. 1, pp. 73–85, 2000.

[185] J. Xue and S. Forrest, "Carrier transport in multilayer organic photodetectors: I. Effects of layer structure on dark current and photoresponse," *Journal of Applied Physics*, vol. 95, no. 4, pp. 1859–1868, 2004.

[186] J. Dally, W. Riley, and K. McConnell, "Instruments for engineering measurements," 1993.

[187] M. Omar, *Elementary solid state physics: principles and applications*. Pearson Education India, 1975.

[188] S. Boguslavsky and V. Vannikov, "Organic semiconductors," *Nauka, Moscow*, 1968.

[189] M. Saeed, F. Khalid, K. S. Karimov, and M. Shah, "Organic cu/cellulose/pepc/cu humidity sensor," *Optoelectron. Adv. Mater. Rapid Commun*, vol. 4, pp. 888–892, 2010.

[190] M. Shah, M. Sayyad, and S. Karimov Kh, "Fabrication and study of nickel phthalocyanine based surface-type capacitive sensors," *World Academy of Science, Engineering and Technology*, vol. 43, no. 2008, pp. 392–394, 2008.

[191] Z. Ahmad, M. Sayyad, and K. Karimov, "Capacitive hygrometers based on natural organic compound," *J Optoelectron Adv Mater*, vol. 2, p. 507, 2008.

[192] D. Yan, H. Wang, and B. Du, *Introduction to organic semiconductor heterojunctions*. John Wiley & Sons, 2010.

[193] B. Patowary, "Review: use of organic semiconductor in gas sensing," *Int. J. Adv. Res. Elect. Electron. Instrum. Eng*, vol. 3, pp. 2278–8875, 2014.

[194] T. Dzugan, M. Kroupa, and J. Reboun, "Sensitivity of organic humidity sensor element on organic vapours," *Procedia Engineering*, vol. 69, pp. 962–967, 2014.

[195] M. Yang, C. Dai, and W. Lin, "Fabrication and characterization of polyaniline/PVA humidity microsensors," *Sensors*, vol. 11, no. 8, pp. 8143–8151, 2011.

[196] Q. Weng and S. Yang, "Urban air pollution patterns, land use, and thermal landscape: an examination of the linkage using GIS," *Environmental Monitoring and Assessment*, vol. 117, no. 1, pp. 463–489, 2006.

[197] Y. Anjaneyulu, I. Jayakumar, V. H. Bindu, P. V. M. Rao, G. Sagareswar, K. Ramani, and T. Rao, "Real time remote monitoring of air pollutants and their online transmission to the web using internet protocol," *Environmental Monitoring and Assessment*, vol. 124, no. 1, pp. 371–381, 2007.

[198] A. Joyce, J. Adamson, B. Huntley, T. Parr, and R. Baxter, "Standardisation of temperature observed by automatic weather stations," *Environmental Monitoring and Assessment*, vol. 68, no. 2, pp. 127–136, 2001.

[199] S. Park, J. Kang, J. Park, and S. Mun, "One-bodied humidity and temperature sensor having advanced linearity at low and high relative humidity range," *Sensors and Actuators B: Chemical*, vol. 76, no. 1, pp. 322–326, 2001.

[200] M. Rinkio, M. Zavodchikova, P. Torma, and A. Johansson, "Effect of humidity on the hysteresis of single walled carbon nanotube field-effect transistors," *Physica Status Solidi (B)*, vol. 245, no. 10, pp. 2315–2318, 2008.

[201] D. Tang, L. Ci, W. Zhou, and S. Xie, "Effect of H_2O adsorption on the electrical transport properties of double-walled carbon nanotubes," *Carbon*, vol. 44, no. 11, pp. 2155–2159, 2006.

[202] M. Anbia and S. Fard, "Humidity sensing properties of Ce-doped nanoporous ZnO thin film prepared by sol-gel method," *Journal of Rare Earths*, vol. 30, no. 1, pp. 38–42, 2012.

[203] M. Chani, K. Karimov, F. Khalid, and S. Moiz, "Polyaniline based impedance humidity sensors," *Solid State Sciences*, vol. 18, pp. 78–82, 2013.

[204] T. Shafai and T. Anthopoulos, "Junction properties of nickel phthalocyanine thin film devices utilising indium injecting electrodes," *Thin Solid Films*, vol. 398, pp. 361–367, 2001.

[205] T. Anthopoulos and T. Shafai, "Low frequency capacitance characterization of α-phase nickel phthalocyanine/lead interfaces: effects of temperature and oxygen doping," *Journal of Physics and Chemistry of Solids*, vol. 65, no. 7, pp. 1345–1348, 2004.

[206] R. Chaabane, A. Ltaief, C. Dridi, H. Rahmouni, A. Bouazizi, and H. Ouada, "Study of organic thin film transistors based on nickel phthalocyanine: effect of annealing," *Thin Solid Films*, vol. 427, no. 1, pp. 371–376, 2003.

[207] P. Binu, C. Joseph, K. Shreekrishnakumar, and C. Menon, "Electrical conductivity and optical absorption studies on nipc-substituted borate glass matrix," *Materials Chemistry and Physics*, vol. 80, no. 3, pp. 591–594, 2003.

[208] C. Liu, J. Shih, and Y. Ju, "Surface morphology and gas sensing characteristics of nickel phthalocyanine thin films," *Sensors and Actuators B: Chemical*, vol. 99, no. 2, pp. 344–349, 2004.

[209] M. El-Nahass, K. Abd-El-Rahman, A. Farag, and A. Darwish, "Photovoltaic properties of NiPc/p-Si (organic/inorganic) heterojunctions," *Organic Electronics*, vol. 6, no. 3, pp. 129–136, 2005.

[210] M. El-Nahass, A. El-Deeb, and F. Abd-El-Salam, "Influence of temperature and frequency on the electrical conductivity and the dielectric properties of nickel phthalocyanine," *Organic Electronics*, vol. 7, no. 5, pp. 261–270, 2006.

[211] M. El-Nahass, K. Abd-El-Rahman, and A. Darwish, "Fabrication and electrical characterization of p-NiPc/n-Si heterojunction," *Microelectronics Journal*, vol. 38, no. 1, pp. 91–95, 2007.

[212] T. Anthopoulos and T. Shafai, "Influence of oxygen doping on the electrical and photovoltaic properties of schottky type solar cells based on α-nickel phthalocyanine," *Thin Solid Films*, vol. 441, no. 1, pp. 207–213, 2003.

[213] M. El-Nahass and K. El-Rahman, "Investigation of electrical conductivity in Schottky-barrier devices based on nickel phthalocyanine thin films," *Journal of Alloys and Compounds*, vol. 430, no. 1, pp. 194–199, 2007.

[214] F. Petraki, V. Papaefthimiou, and S. Kennou, "The electronic structure of Ni-phthalocyanine/metal interfaces studied by X-ray and ultraviolet photoelectron spectroscopy," *Organic Electronics*, vol. 8, no. 5, pp. 522–528, 2007.

[215] M. Shah, M. Sayyad, K. S. Karimov, and M. Maroof-Tahir, "Investigation of the electrical properties of a surface-type Al/NiPc/Ag Schottky diode using I-V and C-V characteristics," *Physica B: Condensed Matter*, vol. 405, no. 4, pp. 1188–1192, 2010.

[216] M. Mahroof-Tahir and K. Karimov, "Fabrication of heterojunctions and current-voltage characteristics of vanadium coordination compounds," *Journal of Optoelectronics and Advanced Materials*, vol. 11, no. 1, pp. 83–88, 2009.

[217] R. Boylestad and L. Nashelsky, "Electronics i."

[218] S. Khan, M. Chani, K. S. Karimov, A. Asiri, M. Bashir, and R. Tariq, "Humidity and temperature sensing properties of copper oxide–Si-adhesive nanocomposite," *Talanta*, vol. 120, pp. 443–449, 2014.

[219] Z. Rittersma, "Recent achievements in miniaturised humidity sensors-a review of transduction techniques," *Sensors and Actuators A: Physical*, vol. 96, no. 2, pp. 196–210, 2002.

[220] M. Azmer, Z. Ahmad, K. Sulaiman, and F. Touati, "Morphological and structural properties of VoPcPhO: P$_3$HT composite thin films," *Materials Letters*, vol. 164, pp. 605–608, 2016.

[221] K. Park and M. Gong, "A water durable resistive humidity sensor based on rigid sulfonated polybenzimidazole and their properties," *Sensors and Actuators B: Chemical*, vol. 246, pp. 53–60, 2017.

[222] M. Eryürek, Z. Tasdemir, Y. Karadag, S. Anand, N. Kilinc, B. Alaca, and A. Kiraz, "Integrated humidity sensor based on SU-8 polymer microdisk microresonator," *Sensors and Actuators B: Chemical*, vol. 242, pp. 1115–1120, 2017.

[223] Z. Zhuang, Y. Li, D. Qi, C. Zhao, and H. Na, "Novel polymeric humidity sensors based on sulfonated poly (ether ether ketone) s: Influence of sulfonation degree on sensing properties," *Sensors and Actuators B: Chemical*, vol. 242, pp. 801–809, 2017.

[224] C. Kelb, M. Körner, O. Prucker, J. Rühe, E. Reithmeier, and B. Roth, "A planar low-cost full-polymer optical humidity sensor," *Procedia Technology*, vol. 26, pp. 530–536, 2016.

[225] D. Toloman, A. Popa, M. Stan, C. Socaci, A. Biris, G. Katona, F. Tudorache, I. Petrila, and F. Iacomi, "Reduced graphene oxide decorated with Fe doped SnO$_2$ nanoparticles for humidity sensor," *Applied Surface Science*, 2017.

[226] H. Zhao, T. Zhang, R. Qi, S. Dai, Jand Liu, T. Fei, and G. Lu, "Organic-inorganic hybrid materials based on mesoporous silica derivatives for humidity sensing," *Sensors and Actuators B: Chemical*, 2016.

[227] M. Chani, K. S. Karimov, F. Khalid, K. Raza, M. Farooq, and Q. Zafar, "Humidity sensors based on aluminum phthalocyanine chloride thin films," *Physica E: Low-dimensional Systems and Nanostructures*, vol. 45, pp. 77–81, 2012.

[228] Y. Sakai, Y. Sadaoka, and M. Matsuguchi, "Humidity sensors based on polymer thin films," *Sensors and Actuators B: Chemical*, vol. 35, no. 1-3, pp. 85–90, 1996.

[229] Z. Ahmad, M. Sayyad, M. Yaseen, K. Aw, M. M-Tahir, and M. Ali, "Potential of 5, 10, 15, 20-Tetrakis (3, 5-di-tertbutylphenyl) porphyrinatocopper (ii) for a multifunctional sensor," *Sensors and Actuators B: Chemical*, vol. 155, no. 1, pp. 81–85, 2011.

[230] X. Liao, Y. Wu, L. Chen, Y. Zhao, Y. Shen, F. Li, S.-y. Shen, and D.-y. Huang, "Steady-state photovoltaic and electroreflective spectra in al/-vanadyl phthalocyanine (VOPc, in phase ii)/indium–tin–oxide (ITO) sandwich cell," *Thin solid films*, vol. 324, no. 1, pp. 209–213, 1998.

[231] H. Wang, D. Song, J. Yang, B. Yu, Y. Geng, and D. Yan, "High mobility vanadyl-phthalocyanine polycrystalline films for organic field-effect transistors," *Applied Physics Letters*, vol. 90, no. 25, p. 253510, 2007.

[232] M. Azmer, Z. Ahmad, K. Sulaiman, F. Touati, T. Bawazeer, and M. Alsoufi, "VOPcPhO: P$_3$HT composite micro-structures with nano-porous surface morphology," *Applied Surface Science*, vol. 399, pp. 426–431, 2017.

[233] H. Malik, F. Aziz, M. Asif, E. Raza, M. Najeeb, Z. Ahmad, W. Swelm, Q. Zafar, F. Touati, and A. Kamboh, "Enhancement of optical features and sensitivity of MEH-PPV/VOPcPhO photodetector using CdSe quantum dots," *Journal of Luminescence*, vol. 180, pp. 209–213, 2016.

[234] M. Azmer, Q. Zafar, Z. Ahmad, K. Sulaiman, and K. Karimov, "VOPcPhO based organic pressure sensor and displacement transducer," *Synthetic Metals*, vol. 191, pp. 120–125, 2014.

[235] F. Aziz, M. Sayyad, K. Sulaiman, B. Majlis, K. Karimov, Z. Ahmad, and G. Sugandi, "Influence of humidity conditions on the capacitive and resistive response of an Al/VOPc/Pt co-planar humidity sensor," *Measurement Science and Technology*, vol. 23, no. 1, p. 014001, 2011.

[236] Z. Ahmad, M. Sayyad, F. Wahab, K. Sulaiman, M. Shahid, J. Chaudry, M. Munawar, and F. Aziz, "Enhancement of electronic and charge transport properties of NiPc by potassium-tetrasulpho group," *Physica B: Condensed Matter*, vol. 413, pp. 21–23, 2013.

[237] J. Shinar and V. Savvateev, "Introduction to organic light-emitting devices," in *Organic Light-Emitting Devices*. Springer, 2004, pp. 1–41.

[238] K. Barua, *Introduction to condensed matter physics*. Alpha Science International Limited, 2007.

[239] A. Croft, R. Davison, and M. Hargreaves, *Engineering mathematics: A modern foundation for electrical, electronic, and control engineers*. Addison-Wesley Longman Publishing Co., Inc., 1992.

[240] S. Kim, S. Ryu, J. Choi, S. Kang, S. Park, S. Im, C. Whang, and D. Choi, "Characterization and luminescence properties of Alq$_3$ films grown by ionized-cluster-beam deposition, neutral-cluster-beam deposition and thermal evaporation," *Thin Solid Films*, vol. 398, pp. 78–81, 2001.

[241] Y. Sakurai, Y. Hosoi, H. Ishii, Y. Ouchi, G. Salvan, A. Kobitski, T. Kampen, D. Zahn, and K. Seki, "Study of the interaction of tris-(8-hydroxyquinoline) aluminum (Alq$_3$) with potassium using vibrational spectroscopy: examination of possible isomerization upon K doping," *Journal of Applied Physics*, vol. 96, no. 10, pp. 5534–5542, 2004.

[242] F. Miller and L. R. Cousins, "Infrared and raman spectra of vanadium oxytrichloride," *The Journal of Chemical Physics*, vol. 26, no. 2, pp. 329–331, 1957.

[243] L. Frederickson Jr and D. Hausen, "Infrared spectra-structure correlation study of vanadium-oxygen compounds." *Analytical Chemistry*, vol. 35, no. 7, pp. 818–827, 1963.

[244] V. Kolotovska, M. Friedrich, D. Zahn, and G. Salvan, "Magnetic field influence on the molecular alignment of vanadyl phthalocyanine thin films," *Journal of Crystal Growth*, vol. 291, no. 1, pp. 166–174, 2006.

[245] Z. Zhao, J. Fan, M. Xie, and Z. Wang, "Photo-catalytic reduction of carbon dioxide with in-situ synthesized CoPc/TiO$_2$ under visible light irradiation," *Journal of Cleaner Production*, vol. 17, no. 11, pp. 1025–1029, 2009.

[246] C. Brabec, V. Dyakonov, J. Parisi, and N. Sariciftci, "Organic photovoltaics: Concepts and realization springer-verlag," *Berlin Heidelberg*, 2003.

[247] K. S. Karimov, K. Cheong, M. Saleem, I. Murtaza, M. Farooq, and A. Noor, "Ag/PEPC/NiPc/ZnO/Ag thin film capacitive and resistive humidity sensors," *Journal of Semiconductors*, vol. 31, no. 5, p. 054002, 2010.

[248] A. Farooq, K. S. Karimov, F. Wahab, T. Ali, and S. Abbas, "Copper phthalocyanine and metal free phthalocyanine bulk heterojunction for temperature

sensing," *Journal of Optoelectronics and Advanced Materials*, vol. 17, no. 5-6, pp. 822–826, 2015.

[249] I. Murtaza and K. Karimov, "Nickel phthalocyanine-based sandwich-type photocapacitive illumination sensors for environmental monitoring," *Arabian Journal for Science and Engineering*, vol. 37, no. 1, pp. 233–237, 2012.

[250] K. Rajesh and C. Menon, "Electrical and optical properties of vacuum deposited ZnPc and CoPc thin films and application of variable range hopping model," 2005.

[251] M. El-Nahass, Z. El-Gohary, and H. Soliman, "Structural and optical studies of thermally evaporated CoPc thin films," *Optics & Laser Technology*, vol. 35, no. 7, pp. 523–531, 2003.

[252] D. Bian, "Absorption and dispersion of visible light in CoPc thin film," *Acta Optica Sinica*, vol. 19, pp. 570–573, 1999.

[253] M. Neghabi, M. Zadsar, and S. Ghorashi, "Investigation of structural and optoelectronic properties of annealed nickel phthalocyanine thin films," *Materials Science in Semiconductor Processing*, vol. 17, pp. 13–20, 2014.

[254] M. Liao and S. Scheiner, "Electronic structure and bonding in metal phthalocyanines, metal= Fe, Co, Ni, Cu, Zn, Mg," *The Journal of Chemical Physics*, vol. 114, no. 22, pp. 9780–9791, 2001.

[255] R. Boylestad, *Introductory circuit analysis*. Pearson Education India, 1968.

[256] M. Shah, K. S. Karimov, and M. Sayyad, "Organic semiconductor nickel phthalocyanine-based photocapacitive and photoresistive detector," *Semiconductor Science and Technology*, vol. 25, no. 7, p. 075014, 2010.

[257] M. Omar, *Elementary solid state physics: principles and applications*. Pearson Education India, 1975.

[258] *Experimental evidence of surface polarization in organic films and control of current-voltage characteristics by the surface polarization*, vol. 6. Citeseer, 2005.

[259] F. Amy, C. Chan, and A. Kahn, "Polarization at the gold/pentacene inter-face," *Organic Electronics*, vol. 6, no. 2, pp. 85–91, 2005.

[260] A. Al-Sehemi, M. Al-Assiri, A. Kalam, Q. Zafar, M. Azmer, K. Sulaiman, and Z. Ahmad, "Sensing performance optimization by tuning surface mor-phology of organic (D-π-A) dye based humidity sensor," *Sensors and Actu-ators B: Chemical*, vol. 231, pp. 30–37, 2016.

[261] Q. Zafar, M. Najeeb, Z. Ahmad, and K. Sulaiman, "Organic–inorganic hy-brid nanocomposite for enhanced photo-sensing of PFO-DBT: MEH-PPV: PC$_{71}$BM blend-based photodetector," *Journal of Nanoparticle Research*, vol. 17, no. 9, pp. 1–10, 2015.

[262] K. Qadir, Z. Ahmad, K. Sulaiman, C. Yap, and F. Touati, "Binary blend based dye sensitized photo sensor using PCPDTBT and MEH-PPV com-posite as a light sensitizer," *Synthetic Metals*, vol. 210, pp. 392–397, 2015.

[263] Z. Ahmad, Q. Zafar, F. Touati, R. Shakoor, and N. Al-Thani, "Study of π-conjugation effect of organic semiconductors on their optical parameters," *Optical Materials*, vol. 54, pp. 94–97, 2016.

[264] K. Karimov, S. Moiz, M. Tahir, N. Ahmed, R. Tariq, S. Abbas, and Q. Zafar, "Nickel phthalocynanine-metal Schottky diode as photodetector," *J. Opto-electron. Adv. Mater*, vol. 16, pp. 1430–1435, 2014.

[265] R. Bonnett, "Photosensitizers of the porphyrin and phthalocyanine series for photodynamic therapy," *Chemical Society Reviews*, vol. 24, no. 1, pp. 19–33, 1995.

[266] N. Oleinick, A. Antunez, M. Clay, B. Rihter, and M. Kenney, "New ph-thalocyanine photosensitizers for photodynamic therapy," *Photochemistry and Photobiology*, vol. 57, no. 2, pp. 242–247, 1993.

[267] W. Wu, Y. Liu, and D. Zhu, "π-conjugated molecules with fused rings for organic field-effect transistors: design, synthesis and applications," *Chemical Society Reviews*, vol. 39, no. 5, pp. 1489–1502, 2010.

[268] *Enhanced efficiency in ZnPc/C$_{60}$ organic photovoltaic cells incorporating organic interlayers on anode.* IEEE, 2013.

[269] Q. Zafar, R. Akram, K. S. Karimov, T. Khan, M. Farooq, and M. Tahir, "Temperature variation effects on I-V characteristics of CuPc based OFET," *World Academy of Science, Engineering and Technology, International Journal of Mathematical, Computational, Physical, Electrical and Computer Engineering*, vol. 5, no. 10, pp. 1593–1597, 2011.

[270] S. Senthilarasu, S. Velumani, R. Sathyamoorthy, A. Subbarayan, J. Ascencio, G. Canizal, P. Sebastian, J. Chavez, and R. Perez, "Characterization of zinc phthalocyanine for photovoltaic applications," *Applied Physics A*, vol. 77, no. 3-4, pp. 383–389, 2003.

[271] R. Koeppe, P. Troshin, A. Fuchsbauer, R. Lyubovskaya, and N. Sariciftci, "Photoluminescence studies on the supramolecular interactions between a pyrollidinofullerene and zinc-phthalocyanine used in organic solar cells," *Fullerenes, Nanotubes, and Carbon Nonstructures*, vol. 14, no. 2-3, pp. 441–446, 2006.

[272] *Fabrication and characterization of P$_3$HT: PCBM-based thin film organic solar cells with zinc phthalocyanine*, vol. 1649, 2015.

[273] R. Koeppe and N. Sariciftci, "Photoinduced charge and energy transfer involving fullerene derivatives," *Photochemical & Photobiological Sciences*, vol. 5, no. 12, pp. 1122–1131, 2006.

[274] G. Tregnago, M. Wykes, G. Paterno, D. Beljonne, and F. Cacialli, "Low-temperature photoluminescence spectroscopy of solvent-free PCBM single-crystals," *The Journal of Physical Chemistry C*, vol. 119, no. 21, pp. 11 846–11 851, 2015.

[275] J. Poortmans and V. Arkhipov, *Thin film solar cells: fabrication, characterization and applications.* John Wiley & Sons, 2006, vol. 5.

[276] *Visible light communication*, 2010.

[277] T. Ng, W. Wong, M. Chabinyc, S. Sambandan, and R. Street, "Flexible image sensor array with bulk heterojunction organic photodiode," *Applied Physics Letters*, vol. 92, no. 21, p. 213303, 2008.

[278] X. Yang, *Semiconducting Polymer Composites: Principles, Morphologies, Properties and Applications.* John Wiley & Sons, 2012.

[279] K. Lee, D. Leem, J. Castrucci, K. Park, X. Bulliard, K. Kim, Y. W. Jin, S. Lee, T. Bender, and S. Park, "Green-sensitive organic photodetectors with high sensitivity and spectral selectivity using subphthalocyanine derivatives," *ACS Applied Materials & Interfaces*, vol. 5, no. 24, pp. 13 089–13 095, 2013.

[280] F. Aziz, M. Sayyad, Z. Ahmad, K. Sulaiman, M. Muhammad, and K. S. Karimov, "Spectroscopic and microscopic studies of thermally treated vanadyl 2, 9, 16, 23-tetraphenoxy-29H, 31H-phthalocyanine thin films," *Physica E: Low-dimensional Systems and Nanostructures*, vol. 44, no. 9, pp. 1815–1819, 2012.

[281] W. Bala, M. Wojdya, M. Rebarz, M. Szybowic, M. Drozdowski, A. Grodzicki, and P. Piszczek, "Influence of central metal atom in MPc (M= Cu, Zn, Mg, Co) on Raman, FT-IR, absorbance, reflectance, and photoluminescence spectra," *Journal of Optoelectronics and Advanced Materials*, vol. 11, no. 3, pp. 264–269, 2009.

[282] Z. Horvolgyi and E. Kiss, *Colloids for nano-and biotechnology.* Springer, 2008, vol. 135.

[283] J. Dittmer, R. Lazzaroni, P. Leclere, P. Moretti, M. Granstrom, K. Petritsch, E. Marseglia, R. Friend, J. Bredas, and H. Rost, "Crystal network formation in organic solar cells," *Solar Energy Materials and Solar Cells*, vol. 61, no. 1, pp. 53–61, 2000.

[284] H. Dunn, J. Feckl, A. Muller, D. Fattakhova-Rohlfing, S. Morehead, J. Roos, L. Peter, C. Scheu, and T. Bein, "Tin doping speeds up hole transfer during

light-driven water oxidation at hematite photoanodes," *Physical Chemistry Chemical Physics*, vol. 16, no. 44, pp. 24 610–24 620, 2014.

[285] P. Aruna and C. Joseph, "Photoelectrical properties of fullerene doped P$_3$HT blends for photo sensing applications," *Materials Today: Proceedings*, vol. 2, no. 4-5, pp. 1309–1315, 2015.

[286] F. Yakuphanoglu, M. Kandaz, and B. Senkal, "Inorganic–organic photodiodes based on polyaniline doped boric acid and polyaniline doped boric acid: nickel (ii) phthalocyanine composite," *Sensors and Actuators A: Physical*, vol. 153, no. 2, pp. 191–196, 2009.

[287] Z. Zhang, Q. Liao, Y. Yu, X. Wang, and Y. Zhang, "Enhanced photoresponse of ZnO nanorods-based self-powered photodetector by piezotronic interface engineering," *Nano Energy*, vol. 9, pp. 237–244, 2014.

[288] H. Xia, J. Li, W. Sun, and L. Peng, "Organohalide lead perovskite based photodetectors with much enhanced performance," *Chemical Communications*, vol. 50, no. 89, pp. 13 695–13 697, 2014.

[289] Q. Zafar, Z. Ahmad, K. Sulaiman, A. Hamzah, and Z. Rahman, "A MEH-PPV/VOPcPhO composite based diode as a photodetector," *Sensors and Actuators A: Physical*, vol. 206, pp. 138–143, 2014.

[290] Q. Zafar, F. Aziz, and K. Sulaiman, "Eco-benign visible wavelength photodetector based on phthalocyanine-low bandgap copolymer composite blend," *RSC Advances*, vol. 6, no. 16, pp. 13 101–13 109, 2016.

[291] H. Sirringhaus, "25th Anniversary article: Organic field-effect transistors: the path beyond amorphous silicon," *Advanced Materials*, vol. 26, no. 9, pp. 1319–1335, 2014.

[292] K. Karimov, N. Ibrahim, and S. Tahir, Moiz, "Photo organic field effect transistor's properties," *Proceedings of the Int. Conf. on Computer and Communication Engineering, ICCCE-06*, vol. 11, no. 1, pp. 1173–1178, 2006.

[293] S. Nelson, Y.-Y. Lin, D. Gundlach, and T. Jackson, "Temperature-independent transport in high-mobility pentacene transistors," *Applied Physics Letters*, vol. 72, no. 15, pp. 1854–1856, 1998.

[294] M. Chani, A. Asiri, K. S. Karimov, M. Bashir, S. Khan, and M. Rahman, "Carbon nanotubes-silicon nanocomposites based resistive temperature sensors," *Int. J. Electrochem. Sci*, vol. 10, pp. 3784–3791, 2015.

[295] N. Fatima, M. Ahmed, and K. Karimov, "Effect of heating on the impedance of nipc based organic field effect transistor."

[296] M. Ahmed, H. Ahmed, and P. Ladbrooke, "Effects of interface states on submicron GaAs metal–semiconductor field-effect transistors assessed by gate leakage current," *Journal of Vacuum Science & Technology B: Microelectronics and Nanometer Structures Processing, Measurement, and Phenomena*, vol. 13, no. 4, pp. 1519–1525, 1995.

[297] I. Murtaza, K. S. Karimov, Z. Ahmad, I. Qazi, M. Mahroof-Tahir, T. Khan, and T. Amin, "Humidity sensitive organic field effect transistor," *Journal of Semiconductors*, vol. 31, no. 5, p. 054001, 2010.

[298] R. Nahar and V. Khanna, "A study of capacitance and resistance characteristics of an Al_2O_3 humidity sensor," *International Journal of Electronics Theoretical and Experimental*, vol. 52, no. 6, pp. 557–567, 1982.

[299] M. Ahmed, "Schottky barrier depletion modification-a source of output conductance in submicron GaAs MESFETs," *IEEE Transactions on Electron Devices*, vol. 48, no. 5, pp. 830–834, 2001.

[300] O. Abanoz and C. Dimitrakopoulos, "Recent advances in organic field effect transistors," *Turkish Journal of Physics*, vol. 38, no. 3, pp. 497–508, 2014.

[301] H. Gomes, P. Stallinga, F. Dinelli, M. Murgia, F. Biscarini, D. De Leeuw, T. Muck, J. Geurts, L. Molenkamp, and V. Wagner, "Bias-induced threshold voltages shifts in thin-film organic transistors," *Applied Physics Letters*, vol. 84, no. 16, pp. 3184–3186, 2004.

[302] P. Stallinga, H. Gomes, F. Biscarini, M. Murgia, and D. Leeuw, "Electronic transport in field-effect transistors of sexithiophene," *Journal of Applied Physics*, vol. 96, no. 9, pp. 5277–5283, 2004.

[303] H. Gomes, P. Stallinga, F. Dinelli, M. Murgia, F. Biscarini, D. de Leeuw, M. Muccini, and K. Mullen, "Electrical characterization of organic based transistors: stability issues," *Polymers for Advanced Technologies*, vol. 16, no. 2-3, pp. 227–231, 2005.

[304] Y. Wakayama, R. Hayakawa, and H. Seo, "Recent progress in photoactive organic field-effect transistors," *Science and Technology of Advanced Materials*, vol. 15, no. 2, p. 024202, 2014.

[305] H. Wang and D. Yan, "Organic heterostructures in organic field-effect transistors," *NPG Asia Materials*, vol. 2, no. 2, pp. 69–78, 2010.

[306] C. Bartic, A. Campitelli, and S. Borghs, "Field-effect detection of chemical species with hybrid organic/inorganic transistors," *Applied Physics Letters*, vol. 82, no. 3, pp. 475–477, 2003.

[307] J. Jakabovic, M. Weis, J. Kovac, D. Donoval, M. Donoval, M. Daricek, P. Telek, J. Cirak, Y. Peng, and J. Xie, "Photogenerated charge carriers in double-layer organic field-effect transistor," *Synthetic Metals*, vol. 175, pp. 47–51, 2013.

[308] Y. Noh, J. Ghim, S. Kang, K. Baeg, D. Kim, and K. Yase, "Effect of light irradiation on the characteristics of organic field-effect transistors," *Journal of Applied Physics*, vol. 100, no. 9, p. 094501, 2006.

[309] M. Hamilton, S. Martin, and J. Kanicki, "Thin-film organic polymer phototransistors," *IEEE Transactions on Electron Devices*, vol. 51, no. 6, pp. 877–885, 2004.

[310] B. Mukherjee, K. Sim, T. Shin, J. Lee, M. Mukherjee, M. Ree, and S. Pyo, "Organic phototransistors based on solution grown, ordered single crystalline

arrays of a π-conjugated molecule," *Journal of Materials Chemistry*, vol. 22, no. 7, pp. 3192–3200, 2012.

[311] Z. Bao, "Organic thin film transistor having a phthalocyanine semiconductor layer," Oct. 19 1999, uS Patent 5,969,376.

[312] M. El-Nahass, K. Abd-El-Rahman, and A. Darwish, "Fourier-transform infrared and UV–vis spectroscopes of nickel phthalocyanine thin films," *Materials Chemistry and Physics*, vol. 92, no. 1, pp. 185–189, 2005.

[313] M. Yasin, T. Tauqeer, K. Karimov, S. San, A. Kosemen, Y. Yerli, and A. Tunc, "P$_3$HT: PCBM blend based photo organic field effect transistor," *Microelectronic Engineering*, vol. 130, pp. 13–17, 2014.

[314] K. S. Karimov, M. Saleem, M. Mahroof-Tahir, T. Qasuria, A. Khan, and T. Khan, "Displacement-sensitive organic field effect transistor," *International Journal of Electronics*, vol. 99, no. 1, pp. 91–101, 2012.

[315] D. Neamen, "Semiconductor physics and devices: Basic principles, Richard D. Irwin Inc," ISBN 0-256-0B405-X, 1992, Homewood IL 60430, Tech. Rep., 1992.

[316] N. Chaure, A. Cammidge, I. Chambrier, M. Cook, and A. Ray, "A tetra-benzotriazaporphyrin based organic thin film transistor: Comparison with a device of the phthalocyanine analogue," *ECS Journal of Solid State Science and Technology*, vol. 4, no. 4, pp. P3086–P3090, 2015.

[317] V. Reddy, "Electrical properties and conduction mechanism of an organic-modified Au/NiPc/n-InP Schottky barrier diode," *Applied Physics A*, vol. 116, no. 3, pp. 1379–1387, 2014.

[318] K. Karimov, M. Ahmed, F. Noshin, M. Saleem, M. Mahroof-Tahir, S. Moiz, K. Akhmedov, M. Zahid, S. Abbas, and A. Rashid, "Nickel phthalocyanine based organic photo transistor: effect of semiconductor film thickness," *The European Physical Journal Applied Physics*, vol. 72, no. 2, p. 20202, 2015.

[319] L. Boguslavskii and L. Stilbans, "Conductivity of polymer films at high frequencies," *Polymer Science USSR*, vol. 6, no. 10, pp. 1996–2000, 1964.